A DSC-study on the demixing of binary polymer solutions

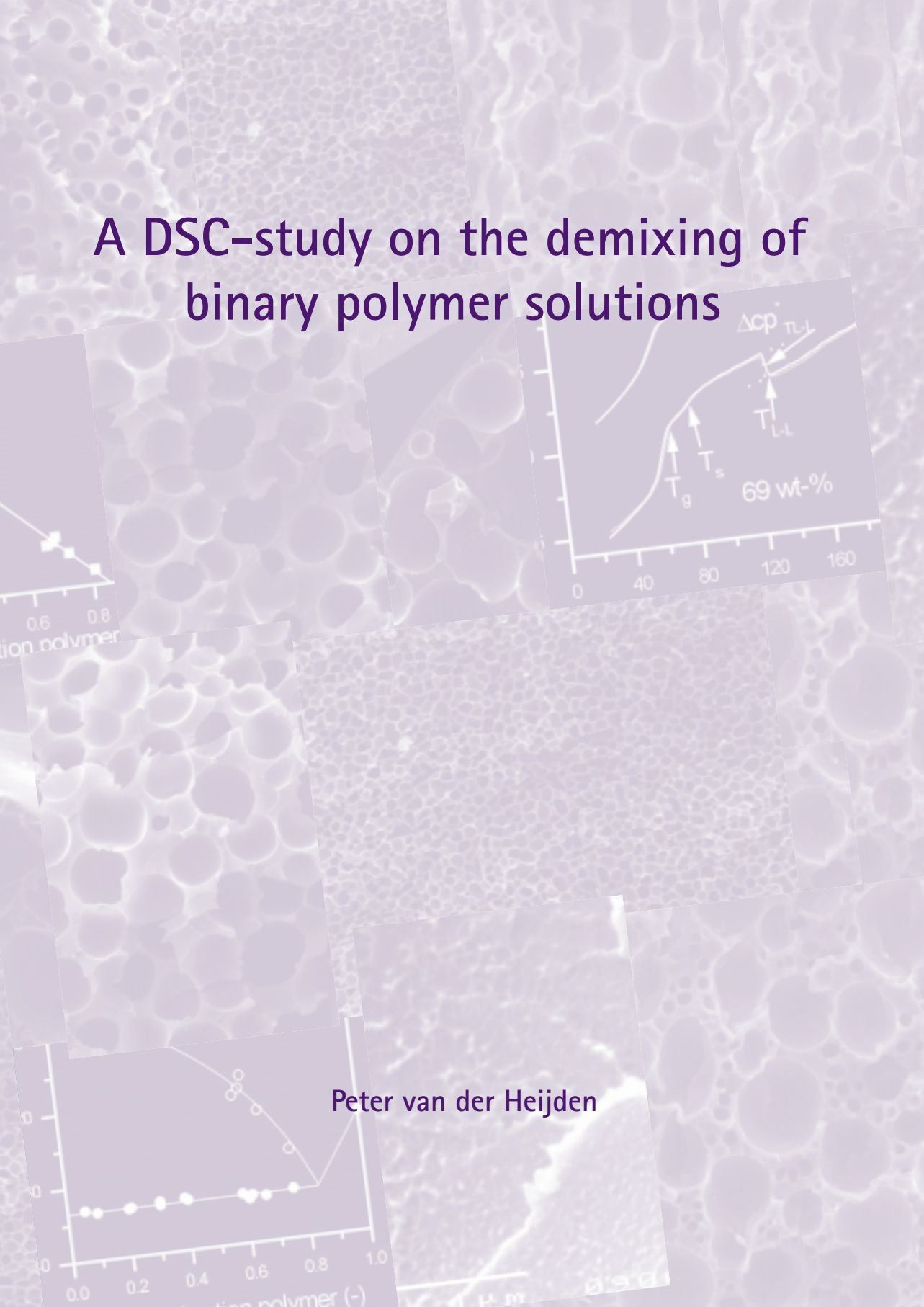

Peter van der Heijden

A DSC-STUDY ON THE DEMIXING OF BINARY POLYMER SOLUTIONS

PROEFSCHRIFT

ter verkrijging van
de graad van doctor aan de Universiteit Twente,
op gezag van de rector magnificus,
prof. dr. F.A. van Vught,
volgens het besluit van het College voor Promoties
in het openbaar te verdedigen
op vrijdag 12 oktober te 15.00 uur

door

Petrus Cornelis van der Heijden
geboren op 16 augustus 1973
te Hoogland

Dit proefschrift is goedgekeurd door de promotoren:

prof.dr.-ing M. Wessling

en

prof.dr.ing M.H.V.Mulder

This research was financially supported by the Nederlandse organisatie voor Wetenschappelijk Onderzoek (NWO)

ISBN: 90 365 1646 3

Printed by PrintPartners Ipskamp, Enschede

Cover design: Carolien van der Heijden

Contents

Chapter 1

Introduction

1.1 The formation of porous structures by thermally-induced phase-separation

Porous polymer membranes can be prepared by different techniques: track-etching, stretching and phase-separation [1]. The phase-separation method is very common to prepare polymeric membranes and a lot of attention has been paid to prepare membranes from various polymers and diluents [1, 2]. The preparation of a porous structure via phase-separation consists of two steps. First, the homogeneous polymer solution has to undergo liquid-liquid demixing to obtain a polymer-rich continuous matrix and a dispersed polymer-lean phase of almost pure solvent. The second step is a fixation step to give the structure mechanical stability.

Liquid-liquid demixing takes place when the solvent power is not sufficient anymore to dissolve the polymer. Two major methods can be distinguished to decrease the solvent power, either by adding a non-solvent which is called diffusion-induced phase-separation (DIPS) or by changing the temperature, defined as thermally-induced phase-separation (TIPS). The TIPS method will be studied in this thesis. Fig. 1 shows a schematic representation of the formation process of a porous structure with the TIPS method. The long black arrow represents a typical cooling route. When passing the binodal, the homogenous polymer solution will liquid-liquid demix in a polymer-rich phase with a polymer concentration given by the binodal and a polymer-lean phase of almost pure diluent. To avoid confusion, the term diluent will be used instead of solvent. The diluent acts as a solvent only when it can dissolve all the polymer. When the solvent power decreases that sufficiently so that liquid-liquid demixing takes place, the term solvent is not appropriate anymore.

After liquid-liquid demixing of the binary polymer-diluent system, the structure has to be fixed. This can be achieved by crystallization, vitrification, or gelation of the polymer-rich phase. After the structure fixation, it is possible to remove the polymer-lean phase with for example evaporation or extraction.

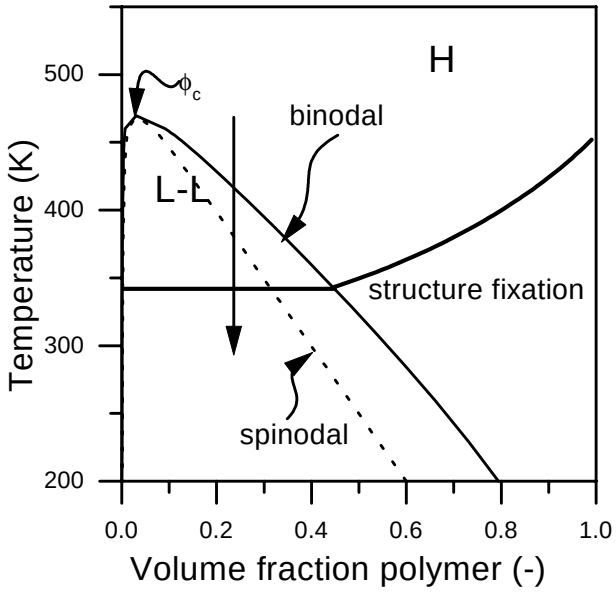

Figure 1. *Example of a phase diagram of a binary polymer- diluent solution. The black arrow represents a cooling trajectory to obtain a porous structure with the TIPS method. It goes from the homogeneous solution (H) via the liquid-liquid demixing gap (L-L) to below the structure fixation temperature.* ϕ_c *is the critical concentration of the solution.*

An advantage of the TIPS method over the DIPS method is the ability to form porous structures with polymers which do not form a solution at room temperature, for example polyethylene and polypropylene. Furthermore, symmetric structures can be obtained easier with TIPS than with DIPS because of the fast heat transfer involved in TIPS in comparison with the relatively slow mass transfer in the DIPS method.

The porous structures obtained with TIPS can be used for more applications then membranes, for example: separators in electrochemical cells, synthetic leather, ‘breathable’ rainwear, diapers, surgical dressings and bandages [3], inertial confined fusion targets [4, 5], biodegradable implants for cell transplantation [6], and scaffolds for tissue engineering [7]. Typical cell sizes obtained with this method are in the order of microns.

Table 1. *Crystalline polymer-diluent systems which have been used to form a porous structure with TIPS.*

Polymer	**Diluent**
Isotactic polypropylene (iPP)	Diphenyl ether [11-13] n,n-bis(2-hydroxylethyl)tallowamine [14-18]
Polyvinylidene fluoride (PVDF)	Cyclohexanone [14] Butrolactone Propylene carbonate Carbitol acetate
Isotactic polystyrene (iPS)	Nitrobenzene [19] Cyclohexane [20] Dioxane/isopropanol
Poly(tetrafluorethylene-co-per-fluoro-(propyl vinylether)) (Teflon®PFA, Neoflon™PFA)	Chlorotrifluorethylene [21]
Poly(2,6-dimethyl-1,4-phenylene ether) (PPE)	Cyclohexanol [22]
Nylon 12	Poly(ethylene glycol) [23]
Poly(γ-benzyl-l-glutamate) (PBIG)	Dioxane/ water [24] Benzene Dichloroethane
Polyethylene (HDPE)	Diphenylether [25] 1,2 ditrydecylphtalate/hexadecane[26]
Polysilastyrene (PSS)	Cyclohexane [27] Benzene
4-methyl-1-pentene (PMP)	Diisopropylbenzene [5]
Polylactide	1,4-dioxane [6]

Table 2. *Amorphous polymer-diluent systems which have been used to form a porous structure with TIPS.*

Polymer	**Diluent**
Atactic poly(methyl methacrylate) (aPMMA)	Cyclohexanol [28, 29] Tetramethylene sulfone (sulfolane) [30, 31] 1-butanol [28] Tert-butyl alcohol [32]
Atactic polystyrene (aPS)	Cylohexane [33] Diethyl malonate Cyclohexanol [34-37] Trans decahydronaphtalene (decalin) [38]

The formation of porous structures via TIPS started in the patent literature with a patent of Castro [8] in which he examined hundreds of polymer-diluent systems, both amorphous and crystalline polymers, on their ability to form a porous structure. Later on, Shipman [9] described a procedure to prepare porous structures with a certain shape, and Josefiak *et al.* [10] introduced a second liquid prior to the cooling step to adjust the morphology of the porous structure.

The first papers on the TIPS method were published in 1984 [14]. Since then the attention to study the formation of porous structures of various polymer-diluent systems with the TIPS method has increased rapidly. Table 1 gives a summary of crystalline polymer-diluent systems used in the TIPS method and Table 2 gives an overview of the formation of amorphous porous structures via TIPS. Besides the studies on new polymer-diluent systems, studies were performed on variations of the TIPS method by introducing, for example, an evaporation step to get a asymmetric structure [22, 39-42].

As mentioned before, the formation of a porous structure with the TIPS method consists of two steps: liquid-liquid demixing to obtain a porous structure and the fixation step to obtain mechanical stability of the structure. Both steps have been studied separately for quite a time. The first papers on liquid-liquid demixing of polymer solutions were already published in 1950's (for references see [43, 44]). The existence of crystalline polymers has been known from the mid 1940's (a historic overview can be found in [45]) and the vitrification temperature (= glass transition temperature) depression, for example, was already quantified in 1961 [46].

This thesis emphasizes the formation process of porous structures with amorphous polymers. The final morphology of these structures is completely determined by liquid-liquid demixing of the polymer solution whereas the vitrification process gives the mechanical strength. Therefore, the attention is focussed on liquid-liquid demixing.

1.2 Differential scanning calorimetry

Conventional experimental studies dealing with liquid-liquid demixing are frequently based on light based techniques, for example light scattering and optical microscopy. In this research, differential scanning calorimetry (DSC) will be used to

study the thermodynamics, kinetics and morphology development of the formation process of porous structures with the TIPS method.

After the introduction of the first differential scanning calorimetry (DSC) apparatus (see [47, 48] for a historical overview about the development of thermal analysis devices in general and for polymers in particular), polymers have been studied extensively, especially crystallization and vitrification phenomena. With DSC, the heat flow is measured as a function of time or temperature to observe physical transitions. With the introduction of temperature modulated differential scanning calorimetry (TMDSC) [49], an extra tool became available to study physical transitions with small heat effects, like liquid-liquid demixing.

The main reason for using the DSC to follow the formation process is that I expect that a different experimental method will give new insights. However, practical reasons are available to use DSC instead of light based techniques as well. For example, with light based techniques the refractive index has to differ significantly between both the diluent and polymer, and transparency of the experimental setup is required to observe a signal. Furthermore, high temperatures are involved in the TIPS process, and to exclude evaporation of diluent, closed sample holders are necessary to use, and this is very easy to achieve with closed DSC-pans.

1.3 Scope of the thesis

This PhD-project is part of a larger project, entitled ‘Phase separation phenomena in multicomponent polymer solutions and blends’ together with the PhD-project of Bastiaan de Geeter. In his PhD-project computer simulations are carried out to follow the formation process of porous structures with the TIPS method. This thesis describes the TIPS method in an experimental way. To relate computer simulations with experimental work, knowledge about time scales of liquid-liquid demixing has to be known. Therefore, Chapter 2 summarizes and quantifies existing models describing liquid-liquid demixing to get an indication about time scales and growth rates involved in the liquid-liquid demixing process. In the next chapters, (TM)DSC experiments will be used to examine the cooling trajectory of binary polymer solutions in the concentrated region (at the right side of the critical point in Fig.1).

Most experimental work described in this thesis will be carried out with the polymer-diluent system atactic polystyrene in 1-dodecanol. The reasons to chose this system are as follows: it is known that this system forms a porous polymer structure with TIPS at room temperature [8], 1-dodecanol is a non-toxic solvent, polystyrene has solvents at room temperature and therefore easy to use, and a lot of physical data is available for both components. Chapter 3 will discuss the experimentally observed transitions observed with TMDSC during cooling and heating of a binary polymer solution, in particular the liquid-liquid demixing signal. In Chapter 4, the TMDSC signal caused by liquid-liquid demixing will be quantified with the help of the Flory-Huggins theory. Furthermore by comparing theoretical results with experimental data, conclusions will be drawn with respect to an early stop of liquid-liquid demixing. In Chapter 5, the crystallization and melting behavior of the diluent (solid-liquid demixing) will be studied to relate observed DSC signals to the morphology of the porous structure. In Chapter 6, an application will be given by using the concepts obtained from Chapter 3 to 5. Data obtained from one single TMDSC experiment appeared to be sufficient to predict the binodal and the intersection between the binodal and the glass temperature depression curve (the Berghmans point). In Chapter 7 the main conclusions of this thesis will be summarized and suggestions for future work will be given.

1.4 References

1. Mulder, M., *Basic principles of membrane technology*. 2. ed, Dordrecht: Kluwer Acedemic Publishers (1996)
2. Zeman, L.J., and Zydney, A.L., *Microfiltration and Ultrafiltration*. 1. ed, New York: Marcel Dekker, Inc. (1996)
3. Lloyd, D.R., Kinzer, K.E., and Tseng, H.S., *Microporous membrane formation via thermally-induced phase separation. I. Solid-liquid phase separation*, Journal of Membrane Science, 52, p. 239-261 (1990)
4. Young, A.T., *Microcellular foams via phase separation*, Journal of Vacuum Science Technology, A 4, p. 1128-1133 (1985)
5. Williams, J.M., and Moore, J.E., *Microcellular foams: phase behaviour of poly (4-methyl-1-pentene) in diisopropylbenzene*, Polymer, 28, p. 1950-1958 (1987)
6. Schugens, C., Maquet, V., Grandfils, C., Jerome, R., and Teyssie, P., *Biodegradable and macroporous polylactide implants for cell transplantation: 1. Preparation of macroporous polylactide supports by solid-liquid phase separation*, Polymer, 37, p. 1027-1038 (1996)
7. Nam, Y.S., and Park, T.G., *Porous biodegradable polymeric scaffold prepared by thermally induced phase separation*, Journal of Biomedical Materials Research, 47, p. 8-17 (1999)
8. Castro, A.J., *Methods for making microporous products*, US-patent 4247498 (1981)
9. Shipman, G.H., *Microporous sheet material, method of making and articles made therewith*,US-patent 4539256 (1985)

10. Josefiak, C., and Wechs, F., *Process for the production of porous bodies having an adjustable total pore volume an adjustable pore size and an adjustable pore wall thickness*,GB-patent 2115425B (1985)
11. Laxminarayan, A., McGuire, K.S., Kim, S.S., and Lloyd, D.R., *Effect of initial composition, phase separation temperature and polymer crystallization on the formation of microcellular structures via thermally induced phase separation*, Polymer, 35, p. 3060-3068 (1994)
12. McGuire, K.S., Laxminarayan, A., and Lloyd, D.R., *A simple method of extrapolating the coexistence curve and predicting the melting point depression curve from cloud point data for polymer-diluent systems*, Polymer, 35, p. 4404-4407 (1994)
13. McGuire, K.S., Lawson, K.W., and Lloyd, D.R., *Pore size distribution determination from liquid permeation through microporous membranes*, Journal of Membrane Science, 99, p. 127-137 (1995)
14. Hiatt, W.C., Vitzthum, G.H., B., W.K., Gerlach, K., and Josefiak, C., *Microporous membranes via upper critical temperature phase separation*, in *Material science of synthetic membranes*, Editor: Lloyd, D.R., Missouri: American Chemical Society: p. 229-244 (1984)
15. Kinzer, K.E., and Lloyd, D.R., *Thermally induced phase separation mechanisms for microporous membrane formation*, Polymer Materials Science Engineering, 61, p. 794-798 (1989)
16. Lloyd, D.R., Kim, S.S., and Kinzer, K.E., *Microporous membrane formation via thermally-induced phase separation. II. Liquid-liquid phase separation*, Journal of Membrane Science, 64, p. 1-11 (1991)
17. Kim, S.S., and Lloyd, D.R., *Microporous membrane formation via thermally-induced phase separation. III. Effect of thermodynamic interactions on the structure of isotactic polypropylen membranes*, Journal of Membrane Science, 64, p. 13-29 (1991)
18. Kim, S.S., and Lloyd, D.R., *Thermodynamics of polymer/diluent systems for thermally induced phase separation: 3. Liquid-liquid phase separation systems.*, Polymer, 33, p. 1047-1057 (1992)
19. Aubert, J.H., *Isotactic polystyrene diagrams and physical gelation*, Macromolecules, 21, p. 3468-3473 (1988)
20. Aubert, J.H., and L., C.R., *Low-density, microcellular polystyrene foams*, Polymer, 26, p. 2047-2054 (1985)
21. Caplan, M.R., Chiang, C.-Y., Lloyd, D.R., and Yen, L.Y., *Formation of microporous Teflon.RTM. PFA membranes via thermally induced phase separation*, Journal of Membrane Science, 130, p. 219-237 (1997)
22. Berghmans, S., Berghmans, H., and Meijer, H.E.H., *Spinning of hollow porous fibers via the TIPS mechanism*, Journal of Membrane Science, 116, p. 171-189 (1996)
23. Cha, B.J., Char, K., Kim, J.-J., Kim, S.S., and Kim, C.K., *The effects of diluent molecular weight on the structure of thermally-induced phase separation membrane*, Journal of Membrane Science, 108, p. 219-229 (1995)
24. Jackson, C.L., and Shaw, M.T., *The phase behavior and gelation of a rodlike polymer in solution and implications for microcellular foam morphology*, Polymer, 31, p. 1070-1084 (1990)
25. Aerts, L., Kunz, M., Berghmans, H., and Koningsveld, R., *Relation between phase behaviour and morphology in polyethylen/diphenyl ether systems*, Macromolekulare Chemie, 194, p. 2697-2712 (1993)
26. Vadalia, H.C., Lee, H.K., Myerson, A.S., and Levon, K., *Thermally induced phase separation in ternary crystallizable polymer solutions*, Journal of Membrane Science, 89, p. 37-50 (1994)
27. Whinnery, L.L., Even, W.R., Beach, J.V., and Loy, D.A., *Engineering the macrostructure of thermally induced phase separated polysilane foams*, Journal of Polymer Science., Part A: Polymer Chemistry, 34, p. 1623-1627 (1996)
28. Vandeweerdt, P., Berghmans, H., and Tervoort, Y., *Temperature-concentration behaviour of solutions of polydisperse, atactic poly(methyl methacrylate) and its influence on the*

formation of amorphous, microporous membranes, Macromolecules, 24, p. 3547-3552 (1991)
29. Graham, P.D., Pervan, A.J., and McHugh, A.J., *The dynamics of thermal-induced phase separation in PMMA solutions*, Macromolecules, 30, p. 1651-1655 (1997)
30. Caneba, G.T., and Soong, D.S., *Polymer membrane formation through the thermal-inversion process. 1. Experimental study of membrane structure formation*, Macromolecules, 18, p. 2538-2545 (1985)
31. Tsai, F.J., and Torkelson, J.M., *Roles of phase separation mechanism and coarsening in the formation of poly(methyl methacrylate) asymmetric membranes*, Macromolecules, 23, p. 775-784 (1989)
32. Tsai, F.J., and Torkelson, J.M., *Microporous poly(methyl methacrylate) membranes: effect of a low-viscosity solvent on the formation mechanism*, Macromolecules, 23, p. 4983-4989 (1990)
33. Song, S.-W., and Torkelson, J.M., *Coarsening effects on microstructure formation in isopycnic polymer solutions and membranes produced via thermally induced phase separation*, Macromolecules, 27, p. 6389-6397 (1994)
34. Hikmet, R.M., Callister, S., and Keller, A., *Thermoreversible gelation of atactic polystyrene: phase transformation and morphology*, Polymer, 29, p. 1378-1388 (1988)
35. Aubert, J.H., *Structural coarsening of demixed polymer solutions*, Macromolecules, 23, p. 1446-1452 (1990)
36. Song, S.-W., and Torkelson, J.M., *Microstructure formation and coarsening of polystyrene membranes via thermally induced phase separation (TIPS)*, Polymer preprints, 34, p. 496-497 (1993)
37. Song, S.-W., and Torkelson, J.M., *Coarsening effects on the formation of microporous membranes produced via thermally induced phase separation of polystyrene-cyclohexanol solutions*, Journal of Membrane Science, 98, p. 209-222 (1995)
38. Arnauts, J., Berghmans, H., and Koningsveld, R., *Structure formation in solutions of atactic polystyrene in trans-decalin*, Makromolekulare Chemie, 194, p. 77-85 (1993)
39. Matsuyama, H., Berghmans, S., and Lloyd, D.R., *Formation of hydrophilic microporous membranes via thermally induced phase separation*, Journal of Membrane Science, 142, p. 213-224 (1998)
40. Matsuyama, H., Berghmans, S., and Lloyd, D.R., *Formation of anisotropic membranes via thermally induced phase separation*, Polymer, 40, p. 2289-2301 (1999)
41. Atkinson, P.M., and Lloyd, D.R., *Anistropic flat sheet membrane formation via TIPS: atmospheric convection and polymer molecular weight effects*, Journal of Membrane Science, 175, p. 225-228 (2000)
42. Atkinson, P.M., and Lloyd, D.R., *Anisotropic flat sheet membrane formation via TIPS: thermal effect*, Journal of Membrane Science, 171, p. 1-18 (2000)
43. Koningsveld, R., and Staverman, A.J., *Liquid-liquid phase separation in multicomponent polymer solutions. III. Cloud point curves*, Journal of Polymer Science: Part A-2, 6, p. 349-366 (1968)
44. Koningsveld, R., Stockmayer, W.H., and Nies, E., *Polymer phase diagrams*. 1. ed., Oxford: Oxford University Press (2001)
45. Khoury, F., and Passaglia, E., *The morphology of crystalline synthetic polymers*, in *Treatise on solid state chemistry*, Editor: Hannay, N.B., New York: Plenum Press: p. 335-496 (1976)
46. Kelley, F.N., and Bueche, F., *Viscosity and glass transition temperature relations for polymer-diluent systems*, Journal of Polymer Science, 50, p. 549-556 (1961)
47. Wunderlich, B., *Thermal Analysis*. , London: Academix Press, Inc. (1990)
48. Mathot, V.B.F., *Calorimetry and thermal analysis of polymers*. 1. ed, Munich: Hanser Publishers (1994)
49. Reading, M., Hahn, B.K., and Crowe, B.S., *Method and apparatus for modulated differential analysis*,US-patent 5224775 (1993)

Chapter 2

Quenching of concentrated polymer-diluent systems

Abstract

Concentrated polymer solutions showing an Upper Critical Solution Temperature behavior are studied with respect to liquid-liquid demixing after a temperature quench. Models proposed in literature are compared and critically evaluated. These models describe the kinetics of liquid-liquid demixing accurately only in a limited region of quench depths. Growth of liquid-liquid demixed domains shows a growth rate of the cell diameter following a power law with an exponent of 1/3 only in a limited region. Quench depths close to the binodal and close to the glass transition temperature show much lower growth rate exponents. The time scales of theoretical descriptions on the formation of demixed domains differ orders of magnitudes with experimental growth rate data. A model is proposed to relate the knowledge of isothermal experiments to non-isothermal experiments and it appears that besides the influence of the quench depth more physical phenomena play a role, like the hydrodynamic flow stage and viscoelasticity.

2.1 Introduction

A porous membrane can be prepared by liquid-liquid demixing of a polymer solution followed by a structure fixation step. Polymer solutions used for the formation of membranes frequently have polymer concentrations higher than the critical concentration and show Upper Critical Solution Temperature behavior. Liquid-liquid demixing is assumed to occur by binodal or spinodal demixing followed by growth of the demixed domains. The fixation step can take place by crystallization or vitrification of the polymer-rich phase, or gelation of the solution [1]. Ostwald ripening, coalescence and hydrodynamic flow [2] are used to describe the growth of the demixed domains in analogy to low molecular weight solutions. This physical picture for polymer solutions is discussed critically by Tanaka [3]. He mentioned the different influence of viscoelasticity in low molecular weight solutions and polymer solutions. In a polymer solution, there is a large difference between the characteristic decay time of a concentration fluctuation and the characteristic viscoelastic time representing the disentanglement time of a polymer chain. This viscoelastic effect plays no role for low molecular weight solutions.

Binodal (also known as nucleation and growth mechanism) and spinodal demixing may result in four types of structure [4]: an open cell structure, a closed cell structure, a lacy structure, and a nodular structure. The origin of these types of structures is listed in Table 1. ϕ represents the volume fraction of polymer in the solution and ϕ_c is the critical concentration (see Chapter 1, Fig. 1).

Table 1. *Resulting morphologies as function of liquid-liquid demixing according to Zeman et al. [4].*

Spinodal		**Binodal**		
		($\phi<\phi_c$)	**($\phi>\phi_c$)**	
Lacy	Closed cell	Nodular	Closed cell	Open Cell

It can be concluded from Table 1 that a one-to-one relationship between morphologies and the demixing mechanism is not straightforward; both spinodal and binodal demixing can give, for example, closed cell morphologies. In addition, the growth of the demixed domains is important for the final morphology as well. An open cell structure with many interconnections resembles a bicontinuous lacy

structure obtained from spinodal demixing. Furthermore, the fixation step has also an influence on the final morphology. Vitrification of the polymer-rich phase will not influence the morphology of the liquid-liquid demixed solution, but crystallization of the polymer-rich phase can cause a dramatic morphology change. Many factors influence the final morphology of a demixed polymer solution. Therefore it is extremely difficult to relate a visually observed morphology to the nature of the demixing process.

In this chapter the demixing process of concentrated polymer solutions will be described based on theoretical and experimental work related to isothermal quenches. During such an experiment, a polymer solution is rapidly quenched to a certain temperature below the cloud point and the evolution of the demixed domains is recorded in time. This difference between the cloud point temperature and quench temperature is defined as the quench depth (see Fig. 1). (The construction of this phase diagram will be described in Chapter 3.)

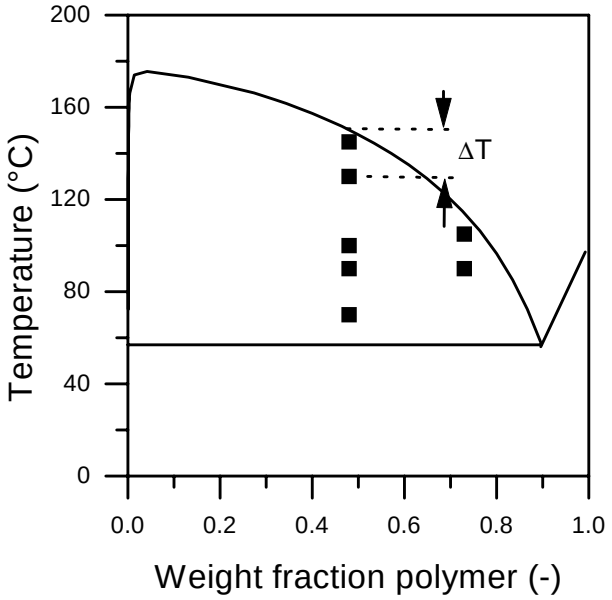

Figure 1. *Phase diagram for the polymer-diluent system atactic polystyrene in 1-dodecanol. Black squares indicate quench temperatures for the experiments carried out in the experimental section (§2.3) representing different quench depths.*

To establish the state of knowledge and to compare the various experimental and theoretical studies with respect to liquid-liquid demixing, their essential aspects are summarized in §2.2. Besides the overview of models describing liquid-liquid

demixing for an isothermal quench and the experiments quantifying growth dynamics (§2.4), the relation of these results to non-isothermal cooling processes will also be elaborated (§2.5). This non-isothermal condition needs to be considered, since in cooling processes a cooling rate is always involved because of limited heat transfer. In experimental and theoretical studies however, this is often neglected.

2.2 Models describing liquid-liquid demixing and growth

The growth of demixed domains can be described by a power law expression [2]:

$$d_{cell} = Kt^{\alpha} \qquad (1)$$

where d_{cell} is the domain diameter, t the time, and K and α the growth rate constants. In the following paragraphs, different models will be evaluated and if necessary quantified. All the models and experiments described in §2.2 have been developed and carried out for an isothermal quench.

2.2.1 Song *et al.* (coalescence and hydrodynamic flow stage)

Song *et al.* [5] carried out isothermal experiments with atactic polystyrene (aPS) in different diluents at time scales larger than 10 s to prove the growth rates proposed by Siggia [2]. They followed the growth of the demixed domains by taking Scanning Electron Microscopy pictures at different demixing times. They proposed three growth regimes. After the initial demixing step via spinodal or binodal demixing, growth proceeds by coarsening and coalescence. In the coarsening regime, domains of the dispersed phase grow at the expense of small domains to decrease the interfacial area. During coalescence various domains may fuse. Both coarsening and coalescence are diffusion controlled and the growth can be described with an α of 1/3. After this first growth regime, hydrodynamic flow starts with an α of 1. This hydrodynamic flow is caused by the difference in surface tension between the demixed phases. The authors mention that the transition between diffusive controlled growth and the hydrodynamic flow regime scales with the inverse square root of the interfacial tension between the two phases. Furthermore they showed that typical cell sizes, in which this transition between coalescence and the hydrodynamic flow stage

takes place, are in the order of magnitude of 10 μm for their polymer-diluent systems (aPS in various diluents). Hydrodynamic flow has no influence on the shape of the cells and can only be observed by recording the growth rate. Song indeed experimentally showed that the α is 1/3 (coarsening and coalescence) and increases to 1 in the hydrodynamic flow stage for a 10 weight.% aPS in diethylmalonate at a quench depth of 7.5 K. The third regime is the 'gravity-dominated stage', in which growth does not follow a power law anymore, and macroscopic layering of the polymer-rich and polymer-lean phase is achieved. This last regime is not observed in the experiments of Song *et al* within a time scale of 10^4 min.

2.2.2 Caneba *et al.* (spinodal demixing)

Caneba *et al*. [6] used the Cahn-Hilliard theory [7] to describe the demixing process of a solution consisting of a polymer segment fraction of 10%. This theory has been developed to describe spinodal demixing of metals and has later been generalized to describe spinodal demixing in polymer solutions. The Cahn-Hilliard theory describes the spontaneous growth of concentration fluctuations during spinodal demixing initially present in the homogeneous solution. These concentration fluctuations are the origin of the demixed domains. In the calculation of Caneba *et al.*, the dominant wavelength, which equals the domain size, does not change (the domain size is constant at a value of ~0.1 μm). Only the concentration difference between the polymer-rich and polymer-lean phase increases between times of $2 \cdot 10^{-6}$ and $2.56 \cdot 10^{-6}$ s, hence the α equals 0 (see Fig. 14 in [6]). The quench depth used in this calculation was 20 K.

2.2.3 Barton *et al.* (spinodal demixing and growth).

Barton *et al.* [8] interpolated simulations with the non-linear Cahn-Hilliard equation (see §2.2.2) at a small time scale (~10^{-5} s) with light-scattering experiments at a time scale of seconds. Data of a 35 wt.% PMMA in cyclohexane solution at a quench depth of 11 K were interpolated with a power law of the exponent of 1/3. It was observed that the growth rate depends on the quench depth; with deep quenches (close to the glass transition temperature) the decreased mobility of the polymer solution restricts the growth rate. Furthermore, it was observed that the bicontinuous structure breaks apart into a droplet structure, representing the percolation to cluster

transition. This again visualizes the difficulty to establish the formation mechanism (spinodal or binodal) from a final morphology.

2.2.4 Muratov (growth after spinodal demixing)

Muratov [9] proposed a theoretical model in which he distinguished three stages of growth and derived scaling rules for the growth in each stage:

1- Spinodal demixed regions grow in a transient network of stretched polymer chains interconnecting the different polymer-rich clusters. The growth rate is $d_{cell} \sim t^{1/6}$ for a three-dimensional network.

2- In the second stage the large clusters grow on the expense of the small clusters. The growth rate is $d_{cell} \sim 1/\ln(t)$.

3- When the polymer-rich clusters are at far enough distance such that they are not interconnected anymore by polymer chains, the polymer-rich domains grow by coarsening, described by an α of 1/3 (as summarized in §2.2.1).

The transition between stage 1 and 2 is at length scales in the order of the radius of gyration (r_g) of the polymer chain in a good solvent, which is about 10 nm [4]. The reason is that an initially single chain becomes part of several droplets at the same time. When the distance between the polymer-rich clusters is about the r_g, the interconnections between the polymer-rich clusters will form a network. The transition between stage 2 and 3 is at a length scale of a fully stretched polymer chain, because clusters can not be interconnected by a polymer chain anymore. Assuming that the size of one styrene monomer is 0.7 nm and that the chain consists of 100 monomers, a stretched chain length of 0.07 μm will be obtained.

Muratov did not quantify his theoretical findings. Furthermore his model was not compared to experimental data. For plotting his model in Fig. 2, the data of spinodal demixing of Barton *et al.* (see §2.2.3) are used as the starting point. To calculate the distance between the clusters, cubic polymer-lean and polymer-rich domains are assumed. The number of polymer-rich clusters can be determined and by using the relation of the cluster size growth (also derived by Muratov), the distance between the clusters can be calculated. When this distance reaches the radius of gyration, stage two starts and can be calculated by using the data of stage one at the transition point. For the r_g a value of 10 nm has been chosen. The same calculation procedure is valid for the intersection between stage two and three. Here

it is assumed that the distance between the polymer-rich clusters is the same as the cluster size itself. For a polymer chain, a length of 100 nm is chosen.

It is necessary to mention that Muratovs model assumes demixing of a concentrated polymer solution by the growth of polymer-rich clusters which is normally only expected with liquid-liquid demixing in diluted solutions with polymer concentrations lower than the critical concentration.

2.2.5 Zeman *et al.* (nucleation and growth)

Zeman *et al.* [4] described binodal demixing (nucleation and growth) on the basis of work of Boom [10]. The formation of nuclei is very fast in comparison with the growth of the nuclei. This is observed with light scattering experiments [4]. The growth of the domains proceeds according to:

$$r_{cell} = \left(r_{\min} + 2Dt\Delta\phi\right)^{0.5} \qquad (2)$$

where D is the mutual diffusion coefficient and $\Delta\phi$ an indication of the supersaturation. Boom [10] showed the dependency between the supercooling and supersaturation of a polymer-diluent system for a small extent of supercooling. For the polymer-diluent system aPS in1-dodecanol at 30 vol-%, $\Delta\phi$ in Eq. 2 can be substituted by $\Delta T/35$ (from Flory-Huggins calculations with an empirical interaction-parameter of $-2.28+1258/T$ (see Chapter 4)). Typical values for the mutual diffusion coefficient in the liquid state are 10^{-11}~10^{-12} $m^2 \cdot s^{-1}$ [4]. With a value of 10^{-11} $m^2 \cdot s^{-1}$, a supercooling of 1 K, and the assumption that nuclei are formed instantaneously ($r_{\min} = 0$ at $t = 0$), the nucleation and growth theory can be quantified (see Fig. 2).

To obtain an indication about the time scale of the formation of nuclei, the minimum stable nucleus size can be calculated [4]:

$$r_{\min} = \frac{2\gamma}{\Delta G_v} \qquad (3)$$

where γ is the interfacial tension and ΔG_v the free enthalpy of demixing. Values of $r_{\min}$ between 0 and 0.2 μm are estimated from Eq. 3. This minimum stable nucleus size is also plotted in Fig. 2. (The minimum nucleus size is plotted in Fig. 2 at a

length scale of 10 nm, which is the order of magnitude of the radius of gyration of a polymer in a homogeneous polymer-diluent system.)

In this model the growth rate exponent of a three dimensional domain by diffusion gives an α of ½ instead of an α of 1/3, the latter being for coarsening and coalescence in §2.2.1.

2.2.6 Liu *et al.* (molecular dynamics simulation)

Liu *et al.* [11] studied liquid-liquid demixing by molecular dynamics simulations. To apply their dimensionless Molecular Dynamics calculations to a real polymer (e.g. polystyrene), absolute values for the Lennard-Jones parameters have to be used as input parameters. Liu *et al.* concluded that the surface tension is the main driving force behind the coarsening and growth of circular domains. They found values of α close to 0.33, which is in agreement with the α belonging to the coarsening mechanism. The calculations were carried out for 30 vol.% polymer solutions with polymer chains consisting of 100 monomers. The dimensionless quench temperature was 0.5 and the dimensionless θ-temperature was 3. The dimensionless temperature (T_d) is defined as:

$$T_d = -\frac{k_b T}{\varepsilon}. \qquad (4)$$

Lennard-Jones parameters for benzene [12] are used as input to quantify the MD simulations.

2.2.7 Termonia (Monte Carlo simulations)

Termonia [13] carried out 3 dimensional Monte Carlo simulations with 10 vol.% polyethylene in a diluent. The dimensionless quench depth (defined in Eq. 4) was 2. From his data he distinguished two regions: one at very small times (10^{-5} s) where a linear relation between domain diameter and time was observed and one region with a power law behavior with a power of ¼.

2.2.8 Summary of models describing liquid-liquid demixing

In the previous paragraphs different models were described and quantified. Table 2 summarizes the basic characteristics of the different models.

Table 2. *Summary of the models and experimental work used in Fig.2.*

Theory	**§**	**Ref.**	**Technique**
Song (coalescence and hydrodynamic flow stage)	2.2.1	[2, 5]	Scanning Electron Microscopy
Caneba (spinodal demixing)	2.2.2	[6]	Numerical solution of Cahn-Hilliard theory
Barton (spinodal demixing and growth)	2.2.3	[8]	Interpolation between numerical solution Cahn-Hilliard theory and light scattering data
Muratov (growth after spinodal demixing)	2.2.4	[9]	Scaling rules
Zeman (nucleation and growth)	2.2.5	[4, 10]	Calculation with the help of crystallization theories
Liu	2.2.6	[11]	Molecular Dynamics simulation
Termonia	2.2.7	[13]	Monte Carlo simulation

Table 3. *Conditions of experiments obtained from literature. The polymer is atactic polystyrene, the diluent is mentioned in the table.*

Diluent		**wt.% pol.**	**M_w ($g \cdot mol^{-1}$)**	**M_w/M_n**	**Ref.**	**Symbol**
Diisodecyl-phthalate	DIDP	5.7	$1.1 \cdot 10^5$	1.06	[14]	
Diisodecyl-phthalate	DIDP	16.6	$1.1 \cdot 10^5$	1.06	[14]	
Diethyl-malonate	DEM	5	$1.9 \cdot 10^6$	1.3	[5]	
Diethyl-malonate	DEM	10	$1.9 \cdot 10^6$	1.3	[5]	
Diethyl-malonate	DEM	10	$2.9 \cdot 10^5$	1.06	[5]	
Cyclohexanol	CHNOL	15	$2.9 \cdot 10^5$	1.06	[15]	
Cyclohexane	CH	7.5	$1.9 \cdot 10^6$	1.3	[5]	

Fig. 2 shows the relation between *t* and *d* and the growth exponent (α) for these various models and experiments. The figure aims to give an impression on the time and length scales involved in the process of liquid-liquid demixing as proposed by various authors.

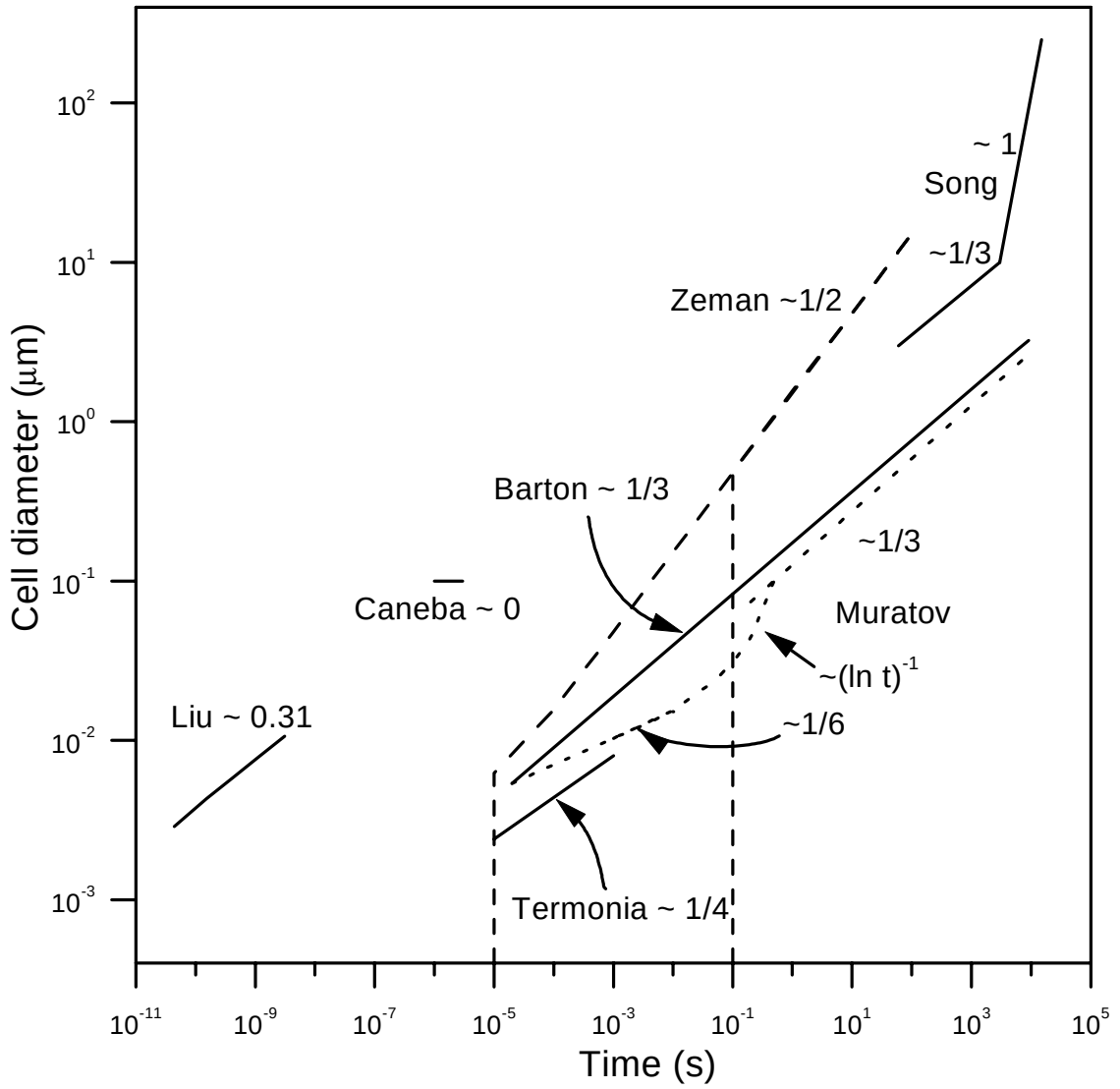

Figure 2. *Length and time scales of different models describing liquid-liquid demixing and growth.*

2.2.9 Influence of quench depth on growth rate exponent

Experimental data of solutions of atactic polystyrene in different diluents (see Table 3 and Fig. 3) shows that an exponential growth of 1/3 is only present in a limited

range of quench depths. At low polymer concentrations and small quench depths, smaller exponents have been observed.

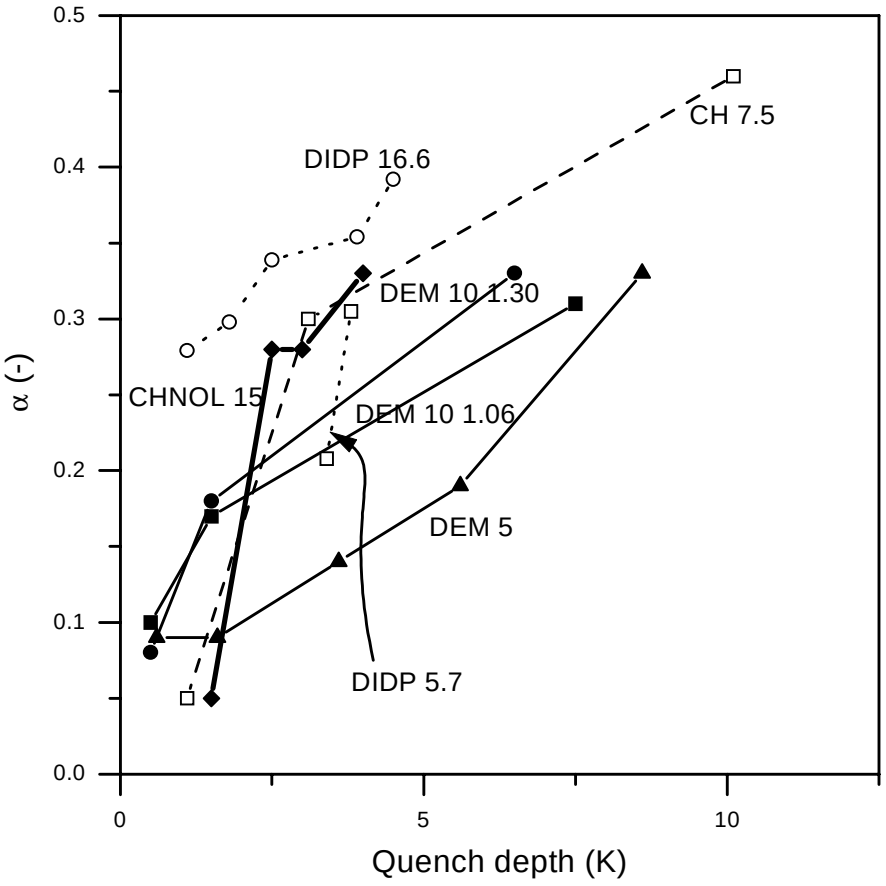

Figure 3. *Reported growth rate exponents (α) as function of quench depth. Table 3 explains the symbols.*

The increase in the growth rate exponent with increasing quench depth has been observed with light scattering for a polymer blend of perdeuterated and protonated 1,4-polybutadiene [16]. An empirical relation was proposed to describe this trend:

$$\alpha^2 \sim \frac{1}{T_{quench}}. \qquad (5)$$

Song *et al.* [5, 15] verified this relation for the polymer-diluent system polystyrene in diethylmalonate and they explained this observation with the help of a study of Brown *et al.* [17]. Brown *et al.* numerically integrated the Cahn-Hilliard theory for

an off-critical quench and they observed for deep quenches a growth rate exponent of 1/3 which was independent of temperature. However, at shallow quenches, the growth rate decreased upon reaching the spinodal curve. According to Song *et al.* this effect 'is apparently associated with thermally induced fluctuations in local concentration which are important for polymer blends, but irrelevant for small molecules systems'. This explanation raises some doubts because the study of Brown *et al.* was carried out for a polymer blend with a critical concentration of 0.5 and the quench temperatures were all just below the spinodal. The study of Song *et al.* however, deals with a polymer solution in which the polystyrene has a molecular weight of at least $M_n \sim 10^5$ g·mol^{-1}. Assuming mono-dispersity of the solution, this results in a critical point of at max 3 vol.% [18]. It is unlikely that an influence of the spinodal is observed in the experiments of Song *et al.* with a solution of 15 wt.% aPS in cyclohexanol at a quench depth of 0.5 K. This quench depth is in the meta-stabile region between the binodal and spinodal and can not be influenced by spinodal demixing. Furthermore, the observations of Brown *et al.* are observed by numerically solving the Cahn-Hilliard theory, and it is not expected that this theory describes phenomena at length scales of microns and time scales of seconds in polymer solutions (see Fig. 2).

A possible explanation of the increasing growth rate with increasing quench depth can be the relatively small difference in coexisting concentrations of both the polymer-rich and polymer-lean phase at small quench depths. The small difference in concentration is an indication of a small interfacial tension between both phases. Upon cooling deeper into the demixing gap the concentration difference between the coexisting phases will increase and the driving force to grow will increase as well.

In summary, the experimentally observed quench depth dependency of the growth rate exponent remains an open question and will be accepted as an empirical fact in the remainder of this chapter.

For long time periods, the α changes to 1 and this transition depends on the quench depth as well (Fig. 4). At small quench depths it takes a long time before the hydrodynamic flow stage (see §2.2.1) starts. This is due to a certain cell size required for demixed domains in which the hydrodynamic flow mechanism is valid. As already mentioned, the growth rate is smaller at small quench depths, hence it requires more time to reach a critical cell size at which hydrodynamic flow can occur.

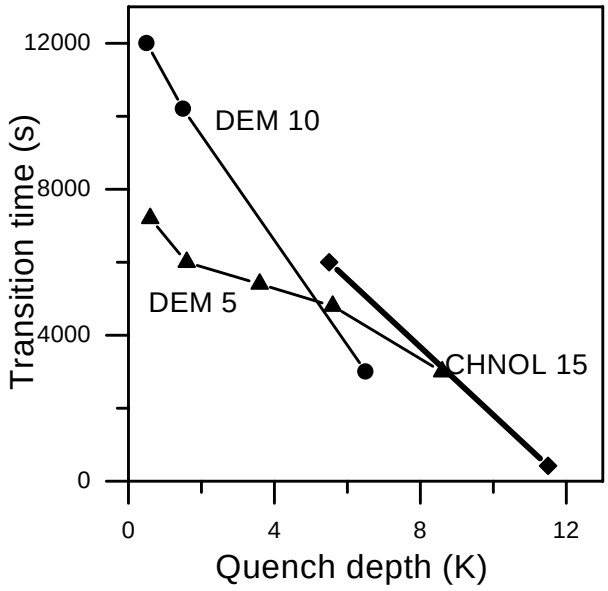

Figure 4. *Transition time between coalescence and the hydrodynamic flow stage. Table 3 explains the symbols.*

2.2.10 Experimental limitations in studying demixing and growth

Scattering techniques have been frequently used to study liquid-liquid demixing. In this paragraph limitations of different scattering techniques will be mentioned.

With light scattering, typical sizes of the observed structures are in the range of 0.14 - 6.7 μm, for neutron scattering this is 3.5 - 14 nm and with X-ray scattering typical sizes of 0.018 - 1.9 nm can be observed [4]. These sizes are only a rough indication and by using, for example, small angle scattering techniques, much larger length scales can be observed.

Optical based techniques have been used to determine growth at large length scales, so the corresponding demixing times are also in the order of magnitude of seconds. In literature many authors claimed to observe spinodal demixing with light scattering, e.g. [19], but considering Fig. 2, it is very optimistic to relate light scattering signals to phenomena at such a small time and length.

The behavior of polymer chains in good solvents and spinodal demixing of a polymer blend (starting at an initial time of 0.05 s) have been studied with neutron scattering. X-ray scattering has been used to determine initial sizes (correlation lengths) of polymer solutions, necessary as input parameter in the Cahn-Hilliard theory [4]. It is clear that experimental techniques can not completely cover the time and length scales of the liquid-liquid demixing process. Experiments can be carried

out in the homogeneous solution to determine the radius of gyration. Experiments can also be carried out at large time and length scales to follow the growth of demixed domains. But no scattering technique can cover the complete time domain and length domain of liquid-liquid demixing.

2.2.11 Conclusive remarks

From theoretical models proposed in literature (see Fig. 2), it can be concluded that the formation of demixed structures starts at time scales of approximately 10^{-5} s. Experimentally, growth of demixed domains can only be observed at time scales larger than seconds. There is a difference in time scale of about 5 orders of magnitude between the start of liquid-liquid demixing and the experimentally observed structures. It is thought that after the formation of the liquid-liquid demixed structure, either by binodal or spinodal demixing, growth of the demixed domains is diffusion limited and grows with an growth rate exponent (α) of 1/3. From reported isothermal quench experiments, it can be concluded that growth of the demixed domains only follows the power of 1/3 in a limited region of quench depths. After reaching a certain cell size of the demixed domains, the hydrodynamic flow regime is reached with a growth rate exponent of 1.

2.3 Experimental

Non-isothermal and isothermal cooling experiments were carried out for the polymer-diluent system aPS - 1-dodecanol. The phase diagram of this polymer-diluent system is determined in Chapter 3. Small amounts of demixed and vitrified aPS - 1-dodecanol solution (the preparation method is described in Chapter 3) were inserted in an aluminum DSC sample pan and heated in a DSC-instrument of Perkin-Elmer (DSC7) to 200°C. In the isothermal experiments, the samples were quenched to the desired temperature and kept at that temperature during a certain period of time. The quench temperatures used for these experiments are denoted by black squares in Fig. 1. Afterwards the samples were cooled down to 0°C, which was far below the glass transition temperature and hence the polymer-rich phase vitrified. The cooling rate between the initial, isothermal and end temperature was 120 $K \cdot min^{-1}$. In the non-isothermal cooling experiments, the samples were cooled down

with a constant cooling rate to 0°C. In addition, samples were quenched directly in a liquid nitrogen bath. The cooling rate of a sample quenched in liquid nitrogen as well as the temperature gradient in a sample stemming from the cooling dynamics is calculated in Appendix 2.

To analyze the structure, the sample pans were opened at room temperature and the polymer-diluent system was broken in liquid nitrogen and extracted with ethanol to remove the 1-dodecanol. After drying it for one night in a vacuum oven, Scanning Electron Microscopy pictures were made using a JEOL JSM-T220A after sputtering for 3 min at I = 13 mA, p = 0.1 bar in a Balzers SCD 040 unit.

The average cell diameter was determined directly from the SEM pictures with a ruler. The average cell diameter and the standard deviation of the cell size were calculated.

2.4 Results isothermal quench

Most experimental and theoretical work reported in literature has been carried out for an isothermal quench to a constant temperature. In practical situations, however, a cooling rate is involved because of heat transfer restrictions in the sample. In this paragraph the results of the isothermal experiments will be presented to obtain information about the growth rate as function of quench depth. With the help of the reported experimental results (§2.2.9) and the experimental result described in this paragraph, the qualitative development of the growth rate exponent (α) will be discussed and related to non-isothermal experiments. This model will be verified with experimental data in §2.5.

2.4.1 Experimental results

It was shown that the temperature dependency of α down to quench depths of about 10 K has been quantified experimentally and reported extensively in literature (see §2.2.9). However, the magnitude of α close to the glass transition temperature has rarely been studied. In order to get a better insight in the growth rate over the whole quench depth interval, isothermal quench experiments were carried out. The concentrations and quench depths used for the experiments are plotted in Fig. 1. Cell size distributions derived from SEM pictures are given in Fig. 5 and 6.

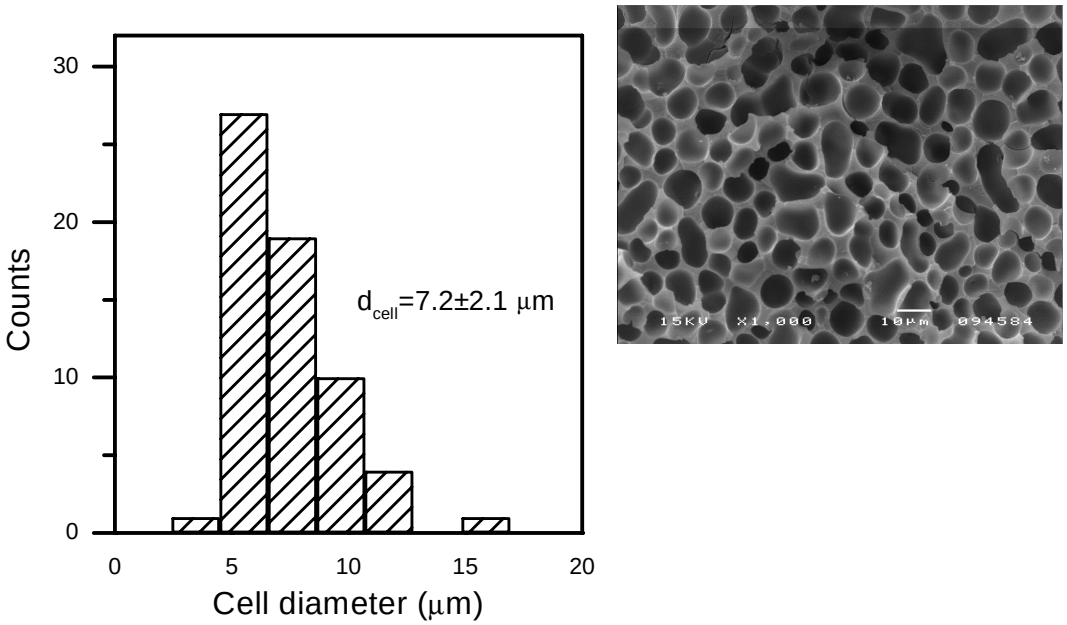

Figure 5. *SEM picture and cell size distribution of 48 wt.% polymer at t = 100 min and a quench depth of 63 K.*

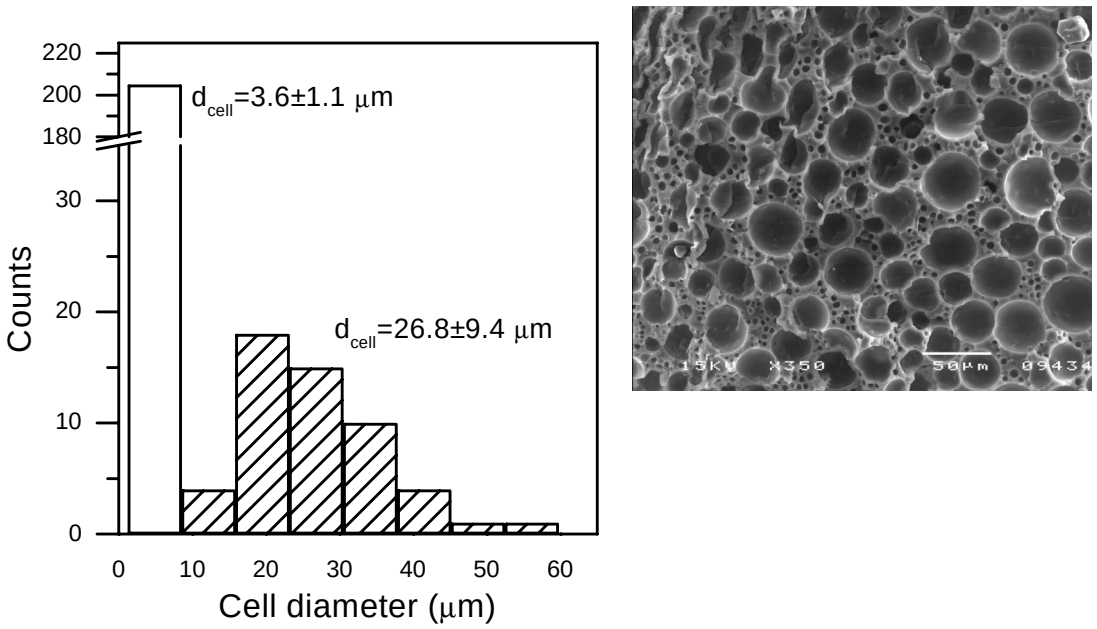

Figure 6. *SEM picture and cell size distribution of 48 wt.% polymer at t = 500 min and a quench depth of 23 K.*

From the SEM picture at the right side of Fig.5, cell diameters of at least 60 cells are measured and plotted as histogram at the left side of Fig. 5. The average and the standard deviation are also listed in the histogram. This standard deviation is a measure for the cell size distribution. In this chapter however, only the average cell diameter will be used.

From Fig. 6, two average cell sizes can be observed. This phenomenon was also reported in [15]. The reason is that in fact two quench steps have been carried out during the isothermal experiment. The first step is from the homogeneous solution to the quench temperature, and the second step is from the quench temperature to 0°C. In principle, cells with two different sizes should be present in all the isothermal quench experiments. However, because of the small growth rate, this can only be observed in the experiments with the largest growth rates at an intermediate quench depth of 23 K.

Fig. 7 shows the average cell diameter as a function of the quench depth for a polymer solution containing 48 wt.% of polymer. The $T_{L\text{-}L}$ is 153°C and the T_g is 61°C, hence the total liquid-liquid demixing gap is 92 K. Only at a quench depth of 23 K, an increase in cell size can be observed in comparison with the other quench depths. However, considering the standard deviation, one cannot conclude an influence of the quench depth on the cell diameter for a growth period to t = 10 min. To investigate the influence of the latter, the time for domain growth was varied over a range from 1 to 500 min in Fig. 8.

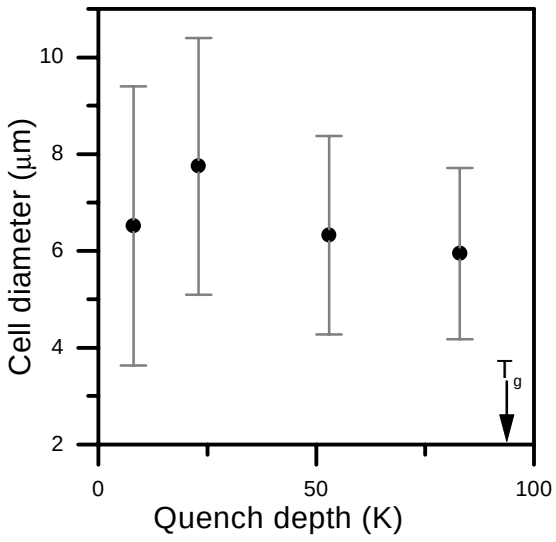

Figure 7. *Average cell diameter at t = 10 min. Concentration polymer is 48 wt.%. Error bars represent the standard deviation.*

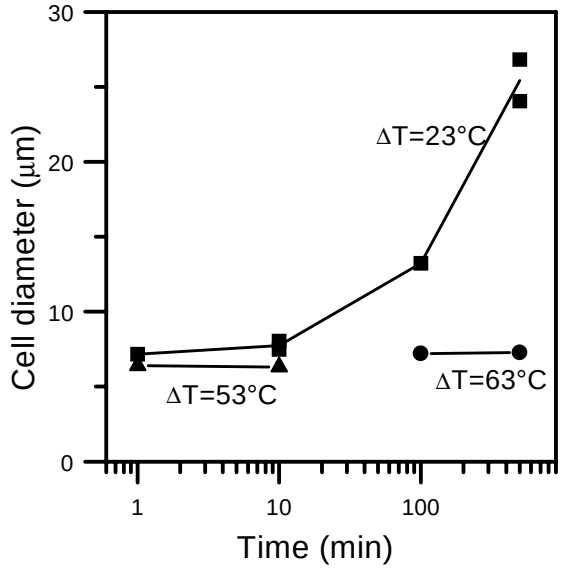

Figure 8. *Cell diameter as function of time for different quench depths. Concentration polymer is 48 wt.%. Lines have been drawn to guide the eye.*

The α of the 48 wt.% polymer solution at a quench depth of 23 K is 0.20. At the other quench depths the growth rate is much lower or even no growth is detected. From Fig. 8 it can be concluded that at large quench depths hardly any growth takes place.

Isothermal growth experiments were carried out for a highly concentrated polymer solution containing 73 wt.% of polymer ($T_{L\text{-}L}$ = 111°C) at quench depths of 6 and 21 K for t = 1 and 10 min as well. No growth is observed in these experiments. A typical structure obtained by quenching a 73 wt.% solution is plotted in Fig. 9.

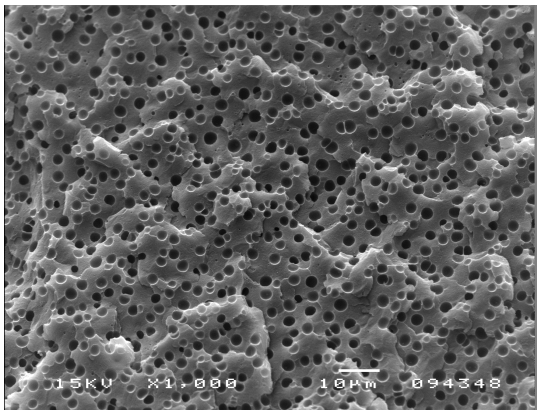

Figure 9. *Structure of quenched polymer solution containing 73 wt.% of polymer. Quench depth is 6 K, t = 10 min.*

Single cells are observed in the polymer-rich matrix, therefore coalescence of demixed domains can hardly occur in this structure. This observation is in agreement with the influence of the quench depth; a large quench depth results in a restricted polymer chain and diluent mobility and so does a high polymer concentration.

2.4.2 Quench depth dependency on growth rate

A qualitative model of the growth rate exponent as function of the quench depth, based on the reported experimental data from §2.2.9 and the experiments (§2.4.1) carried out in this study, will be proposed in this paragraph. It is of course a very empirical approach. Nevertheless, the purpose of this model is to show the more complex growth mechanism in comparison with the normally proposed growth rate of α = 1/3. The other reason to propose such a model is to check whether it is possible to exchange isothermal data with non-isothermal data as will be shown in §2.5. A schematic representation of the growth exponent can be drawn like Fig. 10.

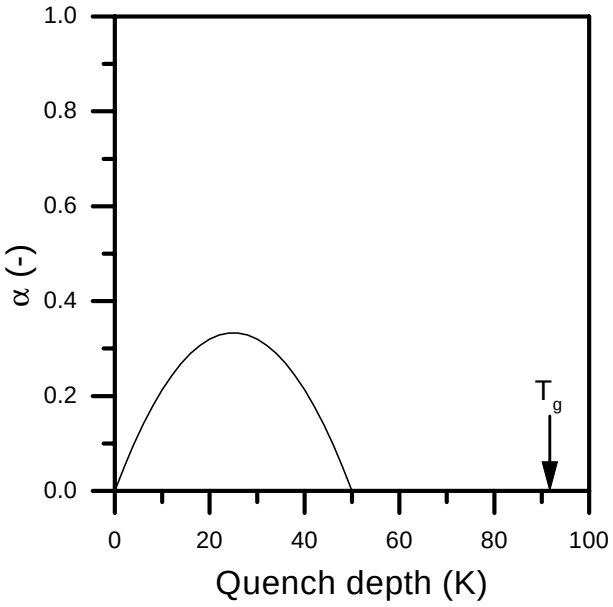

Figure 10. *Model for growth rate exponent (α).*

The following trends observed from experimental data are introduced in this model:

- α increases with increasing quench depth (at small quench depths).
- α decreases at larger quench depths.
- α equals zero at temperatures close to the glass transition temperature.

In this model only physical processes depending on the quench depth are included, other effects like the hydrodynamic flow regime are not included. The shape of the curve depends on many physical parameters of the polymer solution like polymer concentration, viscosity and the interaction between polymer and diluent. Therefore the location of the maximum in Fig. 10 is arbitrary drawn. The start of the hydrodynamic flow regime does not depend on the quench depth but on the size of the demixed domains and therefore on the time for sufficient diluted polymer-diluent systems and quench depths sufficiently far away from T_g. This hydrodynamic flow regime can be introduced if the cell size exceeds a certain value, which depends on physical properties of the solution.

2.5 Non-isothermal quench

The influence of the cooling rate on the domain size has hardly been studied. Matsuyama *et al.* [20] observed a linear relationship between the logarithm of the pore diameter and the logarithm of the cooling rate for the crystalline polymer system polypropylene–diphenylether in a small cooling rate domain (between 1 and 100 $K \cdot min^{-1}$). To use experimental data and theories obtained from isothermal experiment to describe non-isothermal quenches, a mathematical model will be derived below to link isothermal and non-isothermal quenches. Furthermore with comparing isothermal and non-isothermal results, physical processes depending on the quench depth and other processes can be distinguished. This distinction is difficult to observe in isothermal experiments, because all the processes are incorporated in one growth rate exponent.

2.5.1 Derivation of relation between non-isothermal cooling and isothermal cooling

It can be observed from Eq. 1 that the cell size scales with the time. When it is assumed that the growth rate exponent only depends on the quench depth the following scaling relation is valid:

$$d_{cell} \sim t^{\alpha(\Delta T)}. \qquad (6)$$

The relation between time, temperature, and the quench depth is:

$$t = \frac{\Delta T}{CR}. \qquad (7)$$

Substituting Eq. 7 in Eq. 6 gives:

$$d_{cell} \sim \Delta T^{\alpha(\Delta T)} CR^{-\alpha(\Delta T)}. \qquad (8)$$

In a non-isothermal quench experiment the complete demixing gap is passed for any cooling rate. Hence, the value of the term $\Delta T^{\alpha(\Delta T)}$ does not depend on the cooling rate and Eq. 8 can be written as:

$$d_{cell} \sim CR^{-\alpha(\Delta T)}. \qquad (9)$$

The quench depth dependency of α is the same for all the cooling rates, consequently, a linear relation has to be obtained when plotting the logarithm of the cell size versus the logarithm of the cooling rate, independent on the mathematical form of the model.

2.5.2 Results

In this paragraph the results of non-isothermal quenching experiments will be discussed using the concepts of isothermal quenching. Fig. 11 shows the cell diameter against the cooling rate for three different polymer concentrations.

A linear relationship with a slope of –0.54 is observed between the logarithm of the cell diameter and the logarithm of the cooling rate for the experiment with 27 wt.% of aPS in 1-dodecanol in accordance to the experimental observations of Matsuyama *et al.* [20]. At higher concentrations there is a large deviation from linearity. The cooling rate of the data point obtained from cooling in liquid nitrogen is calculated (= $3 \cdot 10^3$ K·min^{-1}) and has a large error (see Appendix 2). However, even for extreme values of this cooling rate, no linear trend will be observed on a double logarithmic scale for the 48 wt.% and 73 wt.% polymer solutions. The result of the 48 wt.% polymer solution can be separated in two regimes: one regime is from 2 to 100 K·min^{-1} and the second regime is between 100 K·min^{-1} and $3 \cdot 10^3$ K·min^{-1}.

The slope of a linear fit between the data points between 2 and 100 K·min^{-1} has a value of –0.16.

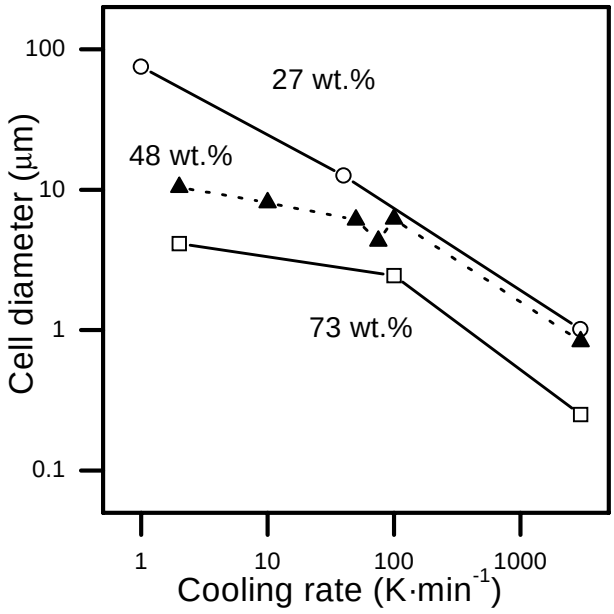

Figure 11. *Cell diameter versus cooling rate of aPS in 1-dodecanol solution at different concentrations. Lines are drawn to guide the eye*

The linear behavior expected when assuming a quench depth dependent growth rate according to Eq. 9 is not observed in my experiments. Therefore, physical processes take place which do not depend on the quench depth. The start of the hydrodynamic flow regime may be considered as such an effect. When the demixed domains have a certain size, the growth rate exponent increases to a value of 1. However, this contribution should give an increase in growth rate with decreasing cooling rate; the opposite as observed in my experiments. The observed α for the cooling experiment 48 wt.% polymer solution (α = 0.16) indicates that the growth of the demixed domains is slower than expected according to the coarsening and coalescence mechanism with an α of 1/3 (see §2.2.1). Tanaka [3] discussed the presence of a viscoelastic effect during liquid-liquid demixing because of entanglements of the polymers. The growth of domains will be counteracted by the relaxation of polymer chains. This viscoelastic effect is more pronounced at long demixing times because the polymer has more time to relax into a more favorable conformation. Passing the demixing gap of 92 K in my system with a cooling rate of $3 \cdot 10^3$ K·min^{-1} gives a demixing time of 1.8 s, whereas liquid-liquid demixing can take place and hence

polymer relaxation for 46 min when the solution is cooled at 2 $K \cdot min^{-1}$. This is the explanation from the deviation from linearity for the experiments between 48 and 73 wt.%. The fact that at the experiment of 27 wt.% shows a rather linear relation is observed between cell size and cooling rate can be explained by the occurrence of the two proposed effects: the hydrodynamic flow effect and viscoelastic effect. The slope of α = 0.54 is larger than α = 1/3 belonging to coarsening and coalescence. This indicates that the hydrodynamic flow regime indeed plays a role.

2.6 Conclusions

From models in literature describing the growth rate of cells formed during liquid-liquid demixing for concentrated polymer solutions at a constant quench depth, it can be concluded that the start of liquid-liquid demixing takes place at time scales of about 10^{-5} s, followed by growth of demixed domains by coarsening and coalescence. It is difficult and speculative to draw conclusions about the demixing mechanism (either spinodal or binodal demixing) on the basis of experiments carried out at times scales of seconds. Experimental data show a dependency of the growth rate exponent on the quench depth. At quench depths close to the binodal and close to the glass transition temperature, the growth rate exponent is smaller than the theoretical value of 1/3 observed for coarsening and coalescence. The hydrodynamic flow regime showing a growth rate exponent of 1 has been observed in reported literature data at long demixing times at small quench depths and starts after shorter demixing times when the quench depth is larger.

Non-isothermal experiments show no linear relation between cell size and cooling rate. This means that the growth rate does not only depend on the quench depth. Two other processes are important as well during a non-isothermal experiment: the hydrodynamic flow regime and a viscoelastic effect caused by entanglements of the polymer chains. Due to their counteracting character, they are difficult to quantify exactly. They cause the growth rate exponent to deviate to smaller values for the viscoelastic effect and to deviate to larger values for the hydrodynamic flow stage.

2.7 Acknowledgements

B.A. de Geeter (University of Twente) is acknowledged for stimulating discussions.

2.8 List of Symbols

ε	Lennard-Jones energy	J
γ	Interfacial tension	$N \cdot m^{-1}$
α	Growth rate exponent	-
$\Delta\phi$	Indication of the supersaturation	-
ΔG_v	Free enthalpy of demixing	J
ΔT	Quench depth	K
CR	Cooling rate	$K \cdot s^{-1}$
D	Mutual diffusion coefficient	$m^2 \cdot s^{-1}$
d_{cell}	Domain diameter	m
K	Growth rate prefactor	$m \cdot s^{-\alpha}$
k_B	Boltzmann constant	$J \cdot K^{-1}$
r_g	Radius of gyration	m
r_{min}	Minimal nucleus size	m
t	Time	s
T_d	Dimensionless quench temperature	-
T_g	Glass transition temperature	K
$T_{L\text{-}L}$	Liquid-liquid demixing	K
T_{quench}	Quench temperature	K

2.9 References

1. Mulder, M., *Basic principles of membrane technology*, Dordrecht: Kluwer Acedemic Publishers (1996)
2. Siggia, E.D., *Late stages of spinodal decomposition in binary mixtures*, Physical Review A, 20, p. 595-605 (1979)

3. Tanaka, H., *Critical dynamics and phase-separation kinetics in dynamically asymmetric binary fluids: New dynamic universally class for polymer mixtures or dynamic crossover?*, Journal of Chemical Physics, 100, p. 5323-5337 (1994)
4. Zeman, L.J., and Zydney, A.L., *Microfiltration and Ultrafiltration*, New York: Marcel Dekker, Inc. (1996)
5. Song, S.-W., and Torkelson, J.M., *Coarsening effects on microstructure formation in isopycnic polymer solutions and membranes produced via thermally induced phase separation*, Macromolecules, 27, p. 6389-6397 (1994)
6. Caneba, G.T., and Soong, D.S., *Polymer membrane formation through the thermal-inversion process. 2. Mathemathecal modeling of membrane structure formation*, Macromolecules, 18, p. 2545-2555 (1985)
7. Cahn, J.W., and Hilliard, J.E., *Free energy of a nonuniform system. I. Interfacial free energy*, The Journal of Chemical Physics, 28, p. 258-267 (1958)
8. Barton, B.F., Graham, P.D., and McHugh, A.J., *Dynamics of spinodal decomposition in polymer solutions near a glass transition*, Macromolecules, 31, p. 1672-1679 (1998)
9. Muratov, C.B., *Unusual coarsening during phase separation in polymer systems*, Physical Review Letters, 81, p. 3699-3702 (1998)
10. Boom, R., *Membrane formation by immersion precipitation: the role of a polymeric additive* ,PhD thesis University of Twente, Enschede (1992)
11. Liu, H., Bhattacharya, A., and Chakrabarti, A., *Network domain structure in phase-separating polymer solutions*, Journal of Chemical Physics, 111, p. 11183-11191 (1999)
12. Atkins, P.W., *Physical Chemistry* 4 ed, Oxford: Oxford University Press (1990)
13. Termonia, Y., *Molecular Modeling of structure development upon quenching of a polymer solution*, Macromolecules, 30, p. 5367-5371 (1997)
14. Nojima, S., Shiroshita, K., and Nose, T., *Phase separation process in polymer systems. II. Microscopic studies on a polystyrene and diisodecyl phthalate mixture*, Polymer Journal, 14, p. 289-294 (1982)
15. Song, S.-W., and Torkelson, J.M., *Coarsening effects on the formation of microporous membranes produced via thermally induced phase separation of polystyrene-cyclohexanol solutions*, Journal of Membrane Science, 98, p. 209-222 (1995)
16. Bates, F.S., and Wiltzius, P., *Spinodal decomposition of a symmetric critical mixture of deuterated and protonated polymer*, Journal of Chemical Physics, 91, p. 3258-3274 (1989)
17. Brown, G., and Chakrabarti, A., *Phase separation dynamics in off-critical polymer blends*, Journal of Chemical Physics, 98, p. 2451-2458 (1993)
18. Hiemenz, P.C., *Polymer Chemistry, The basic concepts*, New York: Marcel Dekker Inc. (1984)
19. Nunes, S.P., and Inoue, T., *Evidence for spinodal decomposition and nucleation and growth mechanisms during membrane formation*, Journal of Membrane Science, 111, p. 93-103 (1996)
20. Matsuyama, H., Berghmans, S., Batarseh, M.T., and Lloyd, D.R., *Effects of thermal history on anisotropic and asymmetric membranes formed by thermally induced phase separation*, Journal of Membrane Science, 142, p. 27-42 (1998)

Appendix 2

Heat transfer in a DSC-pan

In Chapter 2, isothermal and non-isothermal experiments were carried out in order to study the growth of demixed domains. Through a finite-element method, a partial differential heat transfer equation will be solved below to quantify heat transfer limitations in my experiments. Furthermore, an estimation of the 'infinite' cooling rate can be made with these calculations.

Temperature profiles of a polymer solution in a DSC pan are calculated for two situations:

1. Cooling of the bottom side of the DSC-pan and free convection and radiation at the other sides.
2. Instantaneously immersing of the DSC-pan in liquid nitrogen.

Therefore, the temperature profile is calculated over the two dimensional figure in Fig. A1. The thickness of the aluminum sample pan is 0.12 mm. By assuming a mass of the polymer solution in the pan of 10 mg, the height of the polymer solution is about 0.8 mm. The remaining of the sample pan is filled with air. Femlab software [1] was used to calculate the heat transfer equation via a finite element method. To calculate the temperature profile, Eq. A1 is solved for the DSC-pan, the polymer solution, and the air phase:

$$\rho cp\frac{\partial T}{\partial t}-\nabla\cdot\left(k\nabla T\right)=0 \qquad \text{(A1)}$$

with ρ is the density, cp the specific heat capacity, T the temperature, t the time and k the heat conduction coefficient. The input values are listed in Table A1.

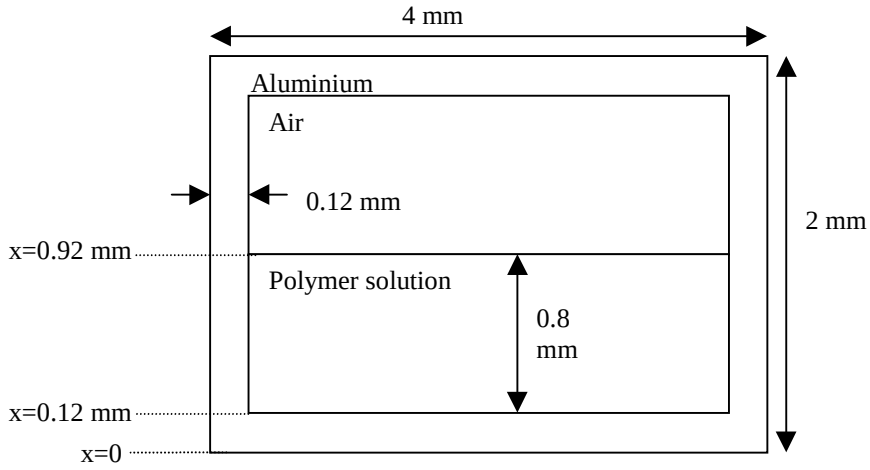

Figure A1. *Sizes DSC-pan.*

Table A1. *Input parameters for the heat transfer equation. The values belong to ambient temperatures (0 - 25 °C) and they are assumed to be constant.*

	ρ **(kg·m^{-3})**	**cp** **(kJ·kg^{-1}·K^{-1})**	**k** **(kW·m^{-1}·K^{-1})**	**Ref.**
Aluminum	2700	0.88	0.230	[2, 3]
Air	1.3	1	$2.4 \cdot 10^{-5}$	[2, 3]
Polymer solution	1050	1 - 3	$1.05\ 10^{-4}$-$1.5 \cdot 10^{-4}$	[3-5]

Situation 1: Constant cooling rate

The boundary condition for situation 1 at the bottom side of the sample pan is a linear cooling rate:

$$T = T_0 - CR \cdot t \qquad \text{(A2)}$$

with T_0 is the initial temperature, and CR the cooling rate.

Free convection and radiation from the aluminum pan to air occur at the other three sides of the sample pan

$$\rho cp \frac{\partial T}{\partial t} - \nabla \cdot (k \nabla T) = h(T_\infty - T) + e(T_\infty^4 - T^4) \qquad \text{(A3)}$$

where *h* (the heat transfer coefficient) is 5 $W \cdot m^{-2} \cdot K^{-1}$ and *e* (emission) is $5.103 \cdot 10^{-8}$ $W \cdot m^{-2} \cdot K^{-4}$ [3]. The temperature profile in the sample is plotted in Fig.A2 for situation 1. In Fig. A2, the situation in the x direction (see Fig. A1) is drawn in the center of the sample pan for two different cooling rates, 10 and 75 $K \cdot min^{-1}$. The situation is drawn in which the temperature of the oven is 323 K, just below the glass transition temperature of the polymer solution.

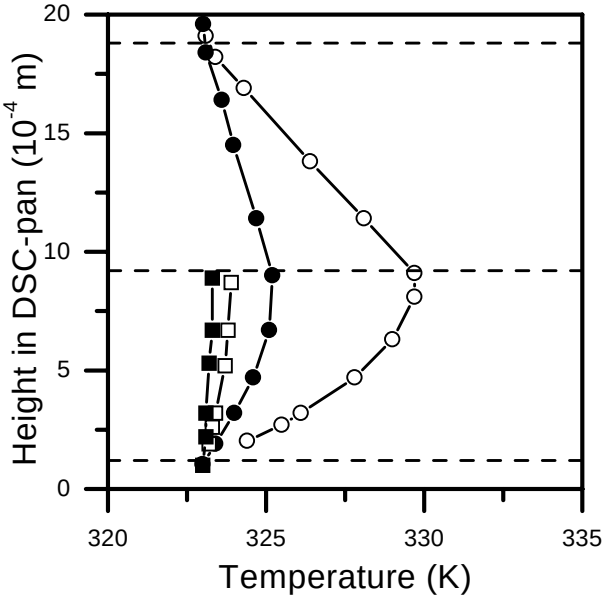

Figure A2. *Temperature gradient of polymer solution in a DSC-pan. Circles: cooling rate is 75 $K \cdot min^{-1}$. Squares: cooling rate is 10 $K \cdot min^{-1}$. Open symbols: cp_{ps} = 3 $kJ \cdot kg^{-1} \cdot K^{-1}$. Closed symbols: cp_{ps} = 1 $kJ \cdot kg^{-1} \cdot K^{-1}$. The dashed lines at x = 1.2 and x = $18.8 \cdot 10^{-4}$ m represent the aluminum interface. The dashed line at $9.2 \cdot 10^{-4}$ m represents the polymer solution – air interface (defined in Figure A1). The input value for the k_{PS} is 0.15 $W \cdot m^{-1} \cdot K^{-1}$.*

From this calculation it can be concluded that a small temperature gradient exists within the DSC sample, even at cooling rates of 10 $K \cdot min^{-1}$.

Situation 2: Quench in liquid nitrogen

The boundary conditions for the second situation are an instantaneous temperature of the four sides of the aluminum pan of 77 K. Fig. A3 shows that the heat capacity of the polymer solution has to be known very accurate to avoid large errors.

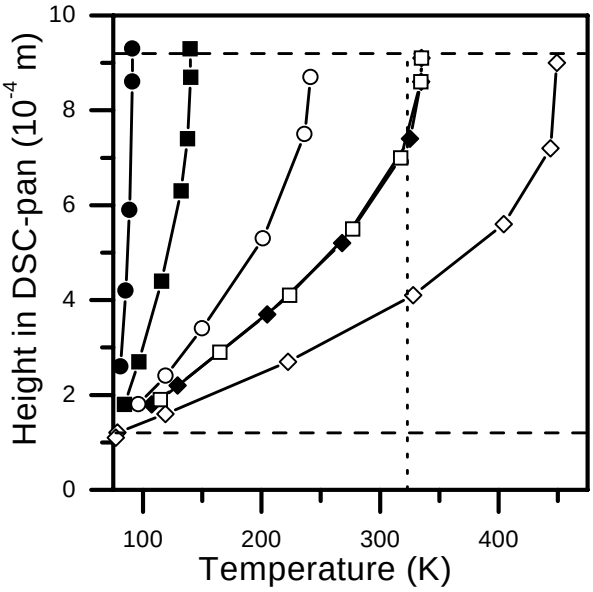

Figure A3. *Temperature profile in DSC sample after quenching in liquid nitrogen. At x = 1.2, interface aluminum – polymer solution. At x = 9.2, interface polymer solution – air. Diamonds: t = 1 s, Squares: t = 3 s, Circles: t = 5 s. Open symbols: cp_{PS} = 3 kJ·kg^{-1}·s^{-1}, closed symbols: cp_{PS} = 1 kJ·kg^{-1}·s^{-1}. Dotted line: T = 323 K. k_{PS} = 0.15 W·m^{-1}·K^{-1}.*

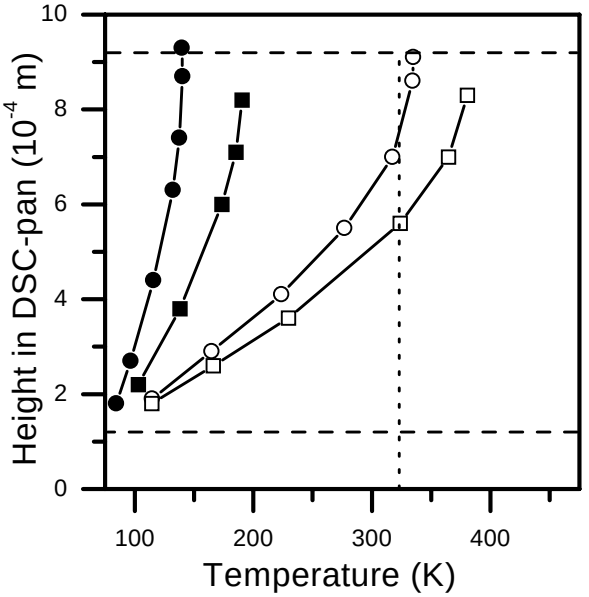

Figure A4. *Temperature profile in polymer solution after a quench in liquid nitrogen at t = 3 s. Squares: k_{PS} = 0.105 W·m^{-1}·K^{-1}. Circles: k_{PS} = 0.15 W·m^{-1}·K^{-1}. Closed symbols: cp_{PS} = 1 kJ·kg^{-1}·K^{-1}. Open symbols: cp_{ps} = 3 kJ·kg^{-1}·K^{-1}.*

After 3 seconds the temperature of the polymer solution is below the glass transition temperature over the whole x-direction. The same calculation with a value of k_{PS} = 0.105 $W \cdot m^{-1} \cdot K^{-1}$ gives the result in Fig. A4. By choosing the minimal and maximal time of the sample to pass the glass transition temperature (T = 323 K), the cooling rate can be estimated. The experimental handling to replace the sample from the oven to the liquid nitrogen is 0.5 s and the time necessary to pass the glass transition temperature is 3 s. Hence, the total time to cool down to solution below the glass transition temperature is 3.5±1 s, this corresponds to a cooling rate over the temperature interval 473-323 K between $2 \cdot 10^3$ and $3.6 \cdot 10^3$ $K \cdot min^{-1}$. In Chapter 2, an infinite cooling rate of $3 \cdot 10^3$ $K \cdot min^{-1}$ will be used.

A2.1 List of symbols

ρ	Density	$kg \cdot m^{-3}$
cp	Specific heat capacity	$kJ \cdot kg^{-1} \cdot s^{-1}$
cp_{PS}	Specific heat capacity polymer solution	$kJ \cdot kg^{-1} \cdot s^{-1}$
CR	Cooling rate	$K \cdot min^{-1}$
e	Emission	$W \cdot m^{-2} \cdot K^{-4}$
h	Heat transfer coefficient	$W \cdot m^{-2} \cdot K^{-1}$
k	Heat conduction coefficient	$W \cdot m^{-1} \cdot K^{-1}$
k_{PS}	Heat conduction coefficient polymer solution	$W \cdot m^{-1} \cdot K^{-1}$
T	Temperature	K
t	Time	s
T_0	Initial temperature	K

A2.2 References

1. Comsol, *www.femlab.com* (2001)
2. Verkerk, G., Broens, J.B., Kranendonk, W., van der Puijl, F.J., Sikkema, J.L., and Stam, C.W., *Binas*. 2. ed, Groningen: Wolters-Noordhoff (1986)
3. Coulson, J.M., and Richardson, J.F., *Chemical engineering*. 5. ed. Vol. 1, Oxford: Butterworth-Heinemann Ltd (1996)
4. Daubert, T.E., Danner, R.P., Sibul, H.M., and Stebbins, C.C., *Physical and thermodynamic properties of pure chemicals. Data compilation*. , Pennsylvania: Taylor&Francis (1989)
5. Brandrup, J., and Immergut, E.H., *Polymer Handbook*. 3th. ed, New York: John Wiley & sons (1989)

Chapter 3

Phase behavior of polymer-diluent systems characterized by temperature modulated differential scanning calorimetry*

Abstract

The thermodynamic phase behavior of a polymer – diluent system (atactic polystyrene – 1-dodecanol) forms the fundamental basis of the description of thermally-induced demixing processes. In this chapter, I demonstrate that temperature modulated differential scanning calorimetry (TMDSC) can accurately detect the liquid-liquid demixing transition. This transition can be clearly observed in the modulus of the complex heat capacity signal and in the phase angle. The phase angle shift is very small during liquid-liquid demixing so liquid-liquid demixing of a polymer-diluent system takes place at time scales instantaneous in comparison with the modulation period of TMDSC. In addition, the glass transition temperature of the polymer-rich phase and the crystallization temperature of the diluent can be determined as well within the same TMDSC experiment.

* Accepted for publication in Thermochimica Acta

3.1 Introduction

Liquid-liquid demixing of polymer solutions is extensively studied since the last half of the twentiest century (for references see [1, 2]). Phase diagrams of many polymer-diluent systems have been determined visually or with other optical techniques like optical microscopy and light scattering [1, 3-8]. These techniques are also used to follow the time dependency of the demixing process to study the kinetics of demixing [8-14]. By using light based techniques it is necessary to use a transparent system and the refractive index difference between the polymer and diluent should be large enough to obtain reliable results. Also other experimental techniques have been occasionally used to compose phase diagrams or to follow the demixing process like viscometry [15], NMR [16], X-ray scattering [17] and DSC [18-21].

In this chapter, differential scanning calorimetry (DSC) is used for investigating the phase behavior of a polymer solution. By using an alternative technique, measuring heat instead of light, I expect to obtain new insights in the liquid-liquid demixing process. DSC is a well-known experimental technique to study solid-liquid demixing (crystallization) [7, 22-24] and vitrification [3, 19, 21] of liquid-liquid demixed polymer solutions. Berghmans and co-workers [18-21] used DSC as well for the determination of the liquid-liquid demixing temperature. They carried out DSC experiments for the systems atactic polystyrene / decalin and atactic polymethylmethacrylate / 1-butanol and cyclohexanol respectively. Upon cooling (cooling rate 5 $K \cdot min^{-1}$), an exothermic heat flow shift was observed and the onset of it was taken as the liquid-liquid demixing temperature. This signal agreed very well with optical observations. With one DSC run they could determine both the liquid-liquid demixing temperature and the glass transition temperature of the polymer-rich phase. But in general, DSC is hardly used for the determination of liquid-liquid demixing because the heat effect is very small and disappears easily in the base line drift.

Recently, a rather new technique has been developed: temperature modulated differential scanning calorimetry (TMDSC) [25, 26] which shows a higher sensitivity and is very useful in studying phase transitions in polymeric systems. In spite of some discussion about the interpretation of the measured signals [27-34], TMDSC is a very

useful device to measure small heat signals and to separate overlapping thermal events.

In this chapter, I will demonstrate that TMDSC allows the accurate determination of the phase diagram of atactic polystyrene (aPS) - 1-dodecanol, a system showing an Upper Critical Solution Temperature behavior. For miscible polymer blends showing Lower Critical Solution Temperature behavior, TMDSC has been used in Ref. [35]. The TMDSC results are compared with optical microscopy. Liquid-liquid demixing temperatures of aPS - cyclohexanol and aPS – diisodecyl-phthalate are determined as well and compared with literature data. Also the glass transition temperature of the polymer-rich phase and the crystallization temperature of the diluent is measured. For later modeling of the observed heat effects (see Chapter 4) the dependency of the experimental conditions of the TMDSC instrument on the observed signals will be presented. This contribution aims to establish a sound experimental basis for TMDSC in characterizing demixing polymer-diluent systems.

3.1.1 Temperature Modulated DSC

An extensive description can be found in Ref. [25, 29], a short description of TMDSC will be given below by using these references. With Temperature Modulated DSC, a second function (for example a sine wave) is superimposed onto the conventional linear or isothermal temperature ramps.

The temperature ramp can then be described as:

$$T = T_0 + bt + A\sin\omega t \qquad (1)$$

where T_0 is the initial temperature, b the underlying scanning rate, A the temperature amplitude, ω the angular frequency, and t the time. The resulting heat flow consists of two contributions: the first part is caused by rapid process and is proportional to the scanning rate, while the second part is caused by kinetically hindered or irreversible processes and hence independent of the scanning rate:

$$\frac{dQ}{dt} = cp\frac{dT}{dt} + f(t,T)\,. \qquad (2)$$

dQ/dt is the heat flow, cp the specific reversing heat capacity, and $f(t,T)$ a contribution to kinetic events. The resulting heat flow can be separated in a cyclic signal and an underlying signal (which is equivalent with the conventional DSC). The modulus of the complex heat capacity ($|cp^*|$) is calculated with only the amplitude of both the temperature and the heat flow modulation. This modulus of the complex heat capacity can be separated in a part in phase with the modulated temperature (reversing heat capacity) and a part out of phase (non-reversing heat capacity) with the help of the phase angle. The kinetic part in Eq. 2 can cause a contribution to the phase angle, but this response can be made insignificantly small by ensuring that there are many cycles within a transition. Consequently only physical events with a time scale comparable with the modulation period (10-100 s) have been observed in the phase angle [33]. Very fast events, like vibrations and rotations of atoms take place instantaneously in comparison with a modulation. Slow events, like the mobility of vitrified polymers with time scales much larger than a modulation period does not influence the phase angle either.

3.2 Experimental

3.2.1 Materials

Two types of atactic polystyrene (aPS) were used: Commercial aPS (Styron* 686E) was kindly supplied by Dow Benelux NV (M_w and M_w/M_n: $2.3 \cdot 10^5$ g.mol^{-1} and 2.1 respectively, determined with GPC) and aPS synthesized in our own laboratory (M_w = $6 \cdot 10^4$, M_w/M_n = 1.05) via an anionic polymerization reaction with *n*-butyllitium as initiator [36]. The commercial aPS was used for the experiments unless otherwise mentioned. The diluents used, 1-dodecanol (purity > 98%, Merck-Schuchardt), diisodecylphthalate (purity > 99%, Merck-Schuchardt) and cyclohexanol (purity > 99%, Merck-Schuchardt) were used without further purification.

3.2.2 Sample preparation

A homogeneous solution of aPS and 1-dodecanol was prepared in a three-neck bottle under nitrogen at 200°C. 1-Dodecanol vapor was allowed to evaporate during stirring with a mechanical stirrer. Small amounts of various polymer concentrations were

poured in Petri-dishes and cooled in air. The compositions of the samples were determined by thermogravimetric analysis. About 20 mg of the sample was inserted on a platinum sample pan of a TGA 2950 Thermogravic Analyzer of TA Instruments and heated up to 200°C with a heating rate of 10 $K \cdot min^{-1}$. Afterwards the temperature was kept constant at 200°C for as maximum of 2 h to evaporate all the 1-dodecanol. From the ultimate weight loss the polymer concentration was determined.

3.2.3 Temperature Modulated Differential Scanning Calorimetry (TMDSC)

The TMDSC used is a DSC 2920 of TA Instruments. Calibration with indium and high density polyethylene (HDPE) (for calibration of the heat capacity) was carried out. About 5 mg of the sample was put in the aluminum closed sample pan. The TMDSC was heated to 200°C and kept isothermally for 30 min to ensure homogeneity. The cooling rate was set to 2 $K \cdot min^{-1}$ to 0°C and after an isothermal step of 5 min the sample was heated again with 2 $K \cdot min^{-1}$. The amplitude of the superimposed sine wave was 1 K with a period of 60 s (recommended values in the TA Instruments user manual). The glass transition temperature T_g and the liquid-liquid demixing temperature $T_{L\text{-}L}$ as well as the heat capacity shift at $T_{L\text{-}L}$ was determined with the TA Universal Analysis software.

3.2.4 Optical Microscopy (OM)

The polymer sample was placed on an object glass within an aluminum ring (thickness 0.1 mm, inner diameter 5 mm) and covered by a second glass. To prevent diluent loss caused by evaporation, laboratory grease was used to stick the aluminum spacer to the object glasses [7]. The sample was placed in a hot stage (Linkam THMS 600) which was controlled by the Linkam TMS92 hot stage controller. The sample was heated and cooled with a rate of 2 $K \cdot min^{-1}$ and demixing was observed visually with an Olympus BH2 microscope (magnification 200x).

3.3 Results and discussion

3.3.1 Liquid-liquid demixing and glass transition temperature

In Fig. 1 the result of one TMDSC cooling run is plotted showing the modulus of the complex heat capacity as a function of temperature.

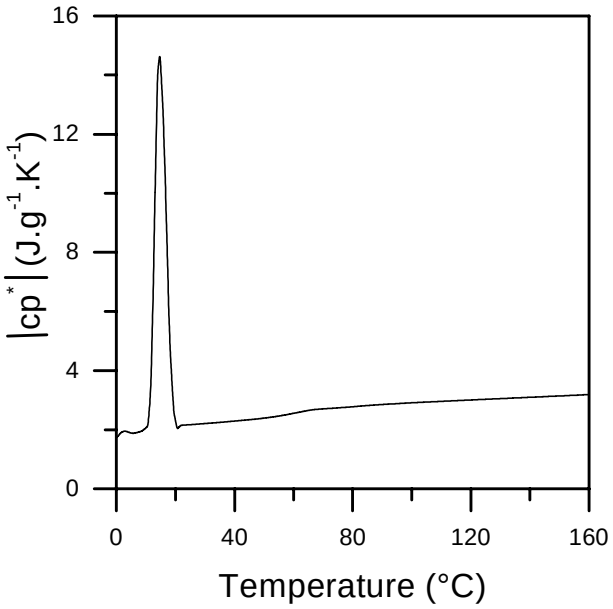

Figure 1. *Modulus of the complex heat capacity as function of temperature for cooling of aPS in 1-dodecanol (weight fraction polymer is 0.38).*

The only clearly observed transition in Fig. 1 is the crystallization of 1-dodecanol (large peak). The heat effects of vitrification and liquid-liquid demixing can hardly be seen on this scale of modulus of the complex heat capacity.

Cooling and subsequent heating curves of aPS - 1-dodecanol without the crystallization peak of the diluent are plotted in Fig. 2 for two polymer concentrations (weight fractions of 0.38 and 0.69). Two transitions can be observed: the glass transition and a small baseline shift at higher temperatures, which is assumed to be the liquid-liquid demixing temperature. In the following, the onset of this signal upon cooling is defined as the liquid-liquid demixing temperature ($T_{L\text{-}L}$) comparable with the observations of Arnauts *et al.* and Vandeweerdt *et al.* with the conventional DSC [18-21]. The glass transition temperature (T_g) is chosen as the onset upon cooling because below this temperature influences can be expected of vitrification on the liquid-liquid demixing behavior.

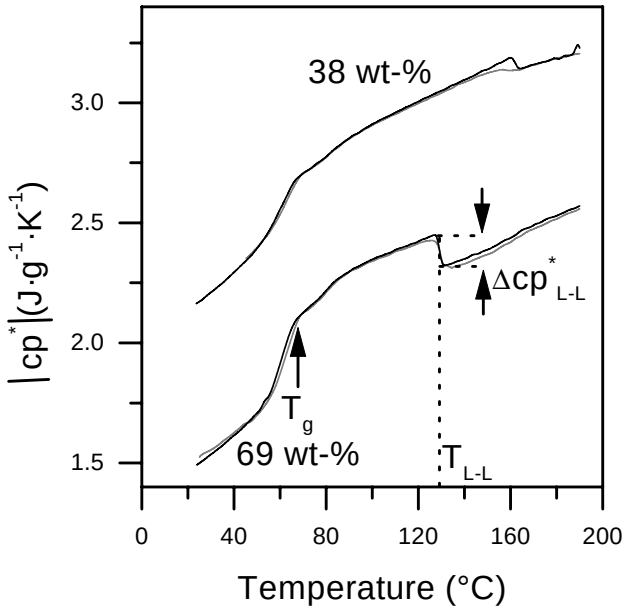

Figure 2. *Cooling and subsequent heating curves (weight fractions of polymer: 0.38 and 0.69). Gray lines: heating curves, black lines: cooling curves.*

In the cooling curves the L-L phase transitions at $T_{L\text{-}L}$ are represented by a steep heat capacity shift. The heating curves have the same slopes as the cooling curves only at the liquid-liquid demixing temperatures the transition is not as distinct. A generally observed phenomenon in polymer phase-separation is that crystallization peaks are more sharply than melting peaks. With crystallization having a certain degree of supercooling, heat is released instantaneously, while melting shows a more gradual transition with DSC experiments. Liquid-liquid demixing at high polymer concentration is also thought to be influenced by nucleation and growth, hence, supercooling may be present in this transition. However there is no significant difference observed between the end of the heat capacity shift upon heating and the onset upon cooling, so the physical reason of this observed difference is not completely clear yet. In the following, the details of the cooling curves will be further used and discussed only.

Performing such TMDSC cooling experiments over a large concentration range allows the construction of the phase diagram of the polymer-diluent system. To support the assumption of the base line shift to stem from the L-L demixing, the TMDSC results are compared with optical microscopy (OM) data indicating visually the phenomenon of L-L demixing.

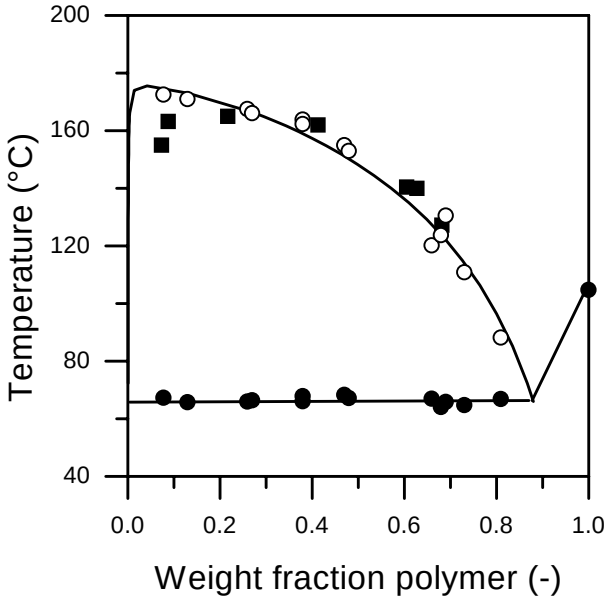

Figure 3. *Phase diagram aPS – 1-dodecanol. Open circles: TMDSC data L-L demixing. Closed squares: OM data L-L demixing (cloud points). Closed circles: TMDSC data glass transition. Lines are drawn to guide the eye.*

In Fig. 3, the $T_{L\text{-}L}$ and T_g determined with TMDSC and OM are plotted. The open circles represent the TMDSC liquid-liquid demixing data whereas the filled black squares are the Optical Microscopy data. The closed circles are the glass-transition temperature data points. Assuming that the observed demixing temperatures represent the binodal and coexistence curve (only valid for a mono-disperse polymer), this phase diagram can be read as follows: By passing the binodal upon cooling, the homogeneous solution will demix in two phases determined by the coexistence curve. With cooling a solution consisting of for example 40 wt.% polymer, a polymer-lean phase consisting of almost pure diluent will be dispersed in a polymer-rich phase determined by the coexistence curve. After further cooling below temperatures of T = 58°C, the polymer-rich phase will vitrify (at the intersection between the coexistence curve and the glass transition curve). Cooling of a polymer solution with a weight fraction above 90 % will directly result in vitrification of the solution. Further physical explanation of such a phase diagram can be found in many textbooks and papers, such as [37].

At low polymer concentrations (polymer concentrations smaller than 20 wt-%) liquid-liquid demixing observed with OM is located at a somewhat lower temperature

than the TMDSC signal. This is probably caused by the small concentration difference of the two co-existing phases at low concentrations, therefore the refractive index difference of the polymer-rich and polymer-lean phase is very small and difficult to observe visually. The cloud point is thus observed after a certain time later than the actual liquid-liquid demixing resulting in a too low temperature measured. At higher concentrations this problem disappears because the concentration difference between the polymer-rich and polymer-lean phase is larger and L-L demixing is easier to observe visually.

The experimental error of both techniques will also have an influence, in particular the evaporation of diluent. TMDSC experiments with a mass loss larger than 0.2 mg after experimentation were omitted. With the optical microscopy experiments the average error in the temperature was 4 K, averaged over 6 experiments. But in spite of the small deviation between the TMDSC and OM data, it can be concluded that the observed heat capacity shift is indeed caused by liquid-liquid demixing. The observed $T_{L\text{-}L}$'s with TMDSC can be regarded as the cloud point curve of the polymer solution at a high polymer concentration (larger than about 20 wt.%).

3.3.2 Liquid-liquid demixing for aPS-cyclohexanol and aPS-diisodecylphthalate

TMDSC results of atactic polystyrene in cyclohexanol and diisodecylphthalate respectively are plotted in Fig. 4. The concentration of polystyrene is 30 wt.%. These cloud points observed with TMDSC compare well with reported values of these systems: Song *et al.* [38] observed liquid-liquid demixing for a 20 wt.% aPS (M_w = $2.9 \cdot 10^5$ g mol^{-1}) in cyclohexanol solution at $T_{L\text{-}L}$ = 80.5°C (my work with the TMDSC: $T_{L\text{-}L}$ = 81.4°C). Nojima *et al.* [9] determined the cloud point of aPS (M_w = $1.1 \cdot 10^5$ g mol^{-1}, M_w/M_n < 1.06) with diisodecylphthalate at $T_{L\text{-}L}$ = 47°C for 30 vol.% (my work with the TMDSC: $T_{L\text{-}L}$ = 49.7°C). The glass transition of aPS - diisodecylphthalate is not observed from the DSC curve because this transition is at a lower temperature than the temperature interval of the experiment. From this comparison between experimental and reported data it can also be concluded that the measured heat capacity shift has to be caused by liquid-liquid demixing.

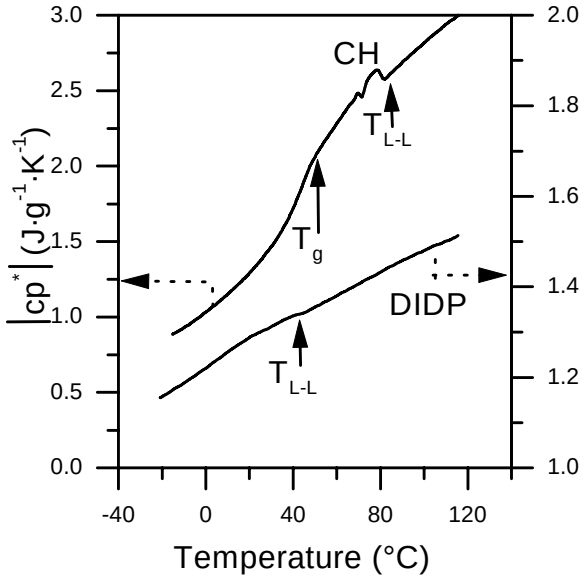

Figure 4. *Modulus of the complex heat capacity of aPS in diisodecylphthalate (DIDP) and cyclohexanol (CH). Weight fraction of polymer is 0.30 for both curves.*

The difference in values in the heat capacity shift (Δcp^* at $T_{L\text{-}L,}$ defined in Fig. 2) between the different diluents is caused by the interaction between polymer and diluent. This can be quantified by calculating the enthalpy of mixing with the help of the Flory-Huggins theory [21]. More details about the quantification of this heat capacity shift will be given in Chapter 4.

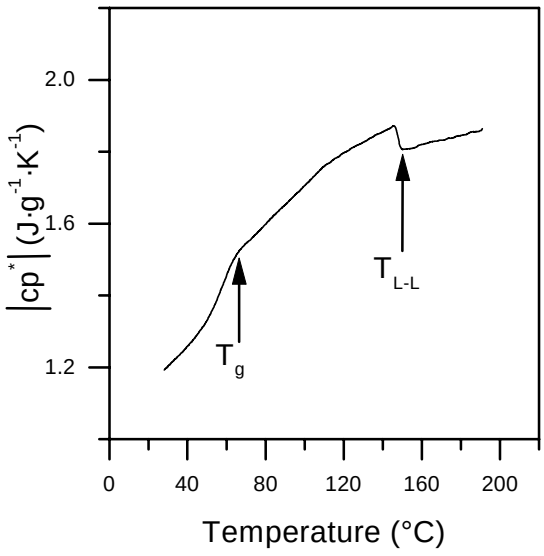

Figure 5. *Modulus of the complex heat capacity versus temperature of aPS (M_w = $6{\cdot}10^4$ g mol^{-1}, M_w/M_n is 1.05) in 1-dodecanol. Weight fraction of polymer is 0.40.*

3.3.3 TMDSC results of atactic polystyrene (M_w/M_n 1.05) with 1-dodecanol

Fig. 5 shows the experimental result of a cooling run for aPS having a low M_w/M_n (M_w is $6{\cdot}10^4$, M_w/M_n is 1.05) in 1-dodecanol (mass fraction aPS is 0.40). The $T_{L\text{-}L}$ shows a lower value than the value plotted in Fig. 3 for a poly-disperse aPS - 1-dodecanol system (151°C and 157°C respectively). This experimental finding is in accordance with theory [1], since the molecular weight of the sample with a low M_w/M_n (M_w is $6{\cdot}10^4$ g mol^{-1}) is smaller than the poly-disperse sample (M_w is $2.3{\cdot}10^5$ g mol^{-1}).

3.3.4 Influence of experimental conditions on modulus of the complex heat capacity

To minimize the error in the calculation of the modulus of the complex heat capacity with the TMDSC software, it is recommended that at least 4 complete superimposed cycles fit within a phase transition (according to Manual TA instruments). This requirement is satisfied for the glass transition because this transition covers a temperature range of at least 10 K. However, in case of liquid-liquid demixing the heat capacity shift only covers a temperature interval of 2 K, so only one modulated cycle fits within this transition. By lowering the underlying cooling rate, the number of cycles within the transition can be increased; the resulting DSC curves are shown in Fig. 6.

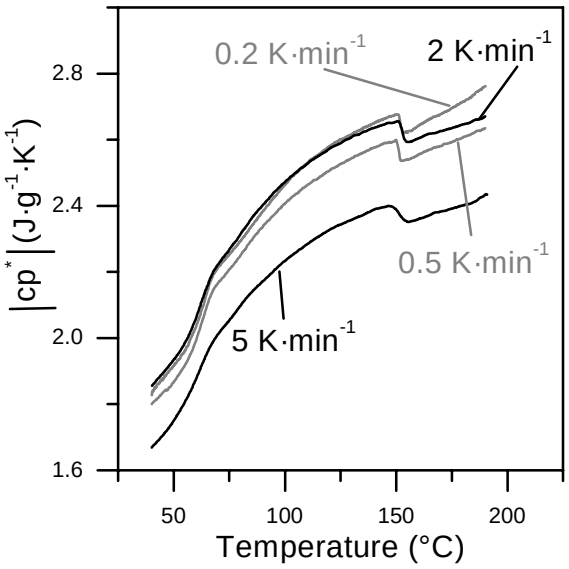

Figure 6. *Influence of cooling rate on modulus of the complex heat capacity. Weight fraction of polymer is 0.48.*

From Fig. 6 it can be concluded that cooling rates of 2 $K \cdot min^{-1}$ and lower has no significant influence on the measured modulus of the complex heat capacity.

The results given in this chapter are all measured with a modulation period of 60 s. It would be of much interest to study the influence of the modulation period on the modulus of the complex heat capacity. Such information may reveal details on the time scale of liquid-liquid demixing. The results of the TMDSC experiments with different modulation periods are plotted in Fig. 7.

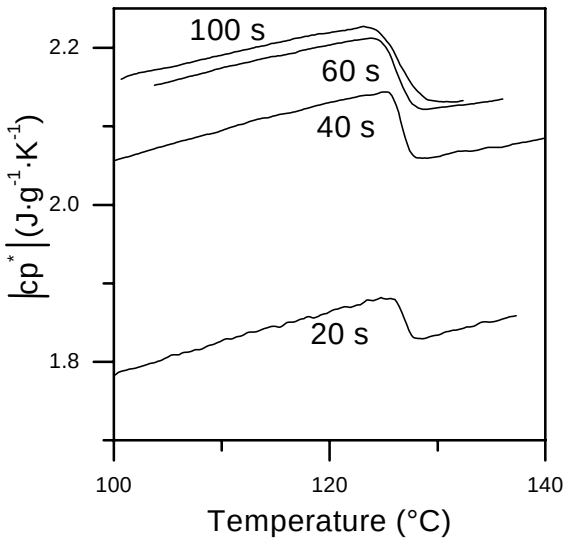

Figure 7. *Influence of modulation period on modulus of complex heat capacity. Weight fraction of polymer is 0.68.*

As can be observed from Fig. 7, the experiments with the lower modulation periods (20 and 40 s) have much lower modulus of the complex heat capacity values compared to the higher modulation periods (60 and 100 s), even in the homogeneous solution region. The values of the heat capacity for the experiments with a modulation period of 60 and 100 s give comparable results; so from these results I may conclude that at lower modulation periods the system cannot follow the modulation. The observed difference is not caused by physical phenomena in the sample, because in the homogeneous solution it is not expected that thermal events of these periods take place. This has to be caused by the time lag of the TMDSC instrument (caused by heat transfer in the furnace and the sample). Therefore, high modulation periods (>60 s) are necessary to exclude the instrumental time lag. Plotting the phase angle versus the temperature (Fig. 8), one can observe that the phase angle shifts to lower values

for increasing modulation period. As already mentioned there is a time lag in the TMDSC instrument, and in general the phase shift caused by the instrument is very large in comparison with the phase shift caused by physical events of the polymer-diluent system.

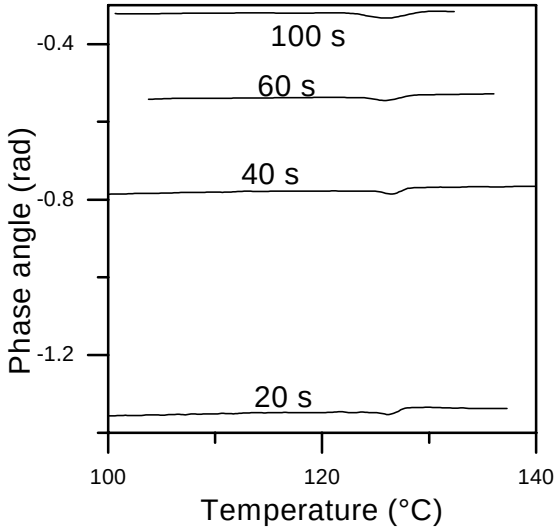

Figure 8. *Influence modulation period on phase angle. Weight fraction of polymer is 0.68.*

A method to exclude the influence of the phase angle shift caused by the TMDSC instrument from the total phase angle is to define regions in the DSC curve where no influence of physical events is expected, so where the phase angle has to be zero. By assuming that the polymer-diluent sample shows no contribution on the phase angle in the region where the polymer is vitrified [29], the contribution of the phase shift caused by the TMDSC instrument can be excluded. For all polymer concentrations the phase angle change caused by the polymer-diluent system are only about 0.08 rad over the temperature interval from 30 to 200 °C and it shows besides a peak at T_g, a small peak at $T_{L\text{-}L}$ of about 0.005 rad. So the influence of the out of phase contribution is very small at $T_{L\text{-}L}$ and the modulus of the complex heat capacity can indeed be regarded as the reversing heat capacity. The shift in the heat capacity has to be caused by phenomena of a time scale instantaneous in comparison with the modulation period; liquid-liquid demixing takes place at time scales instantaneous in comparison with the modulation period of TMDSC.

3.4 Conclusions

With Temperature Modulated DSC liquid-liquid demixing of polymer-diluent systems can be determined as well the glass transition of the polymer-rich phase and crystallization of diluent in one run. Both the modulus of the complex heat capacity and the phase angle show a signal at the demixing temperature. Liquid-liquid demixing observed with TMDSC agrees well with visually observed cloud points. The underlying cooling rate must be 2 $K \cdot min^{-1}$ or lower and the modulation period must be above 60 s to be sure that the experimental setup has no influence on the results. The phase angle shift is very small during liquid-liquid demixing so liquid-liquid demixing of a polymer-diluent system takes place at time scales instantaneous in comparison with the modulation period of TMDSC.

3.5 Acknowledgements

I thank Ruurd Lammers, Johan Bos and Elwin Schomaker of Akzo Nobel Central Research in Arnhem for their support to use the TMDSC apparatus and discussions. Daniel Brooke (Akzo Nobel) is acknowledged for carrying out part of the experiments. Mark Hempenius (University of Twente) is acknowledged for synthesizing the near mono-disperse polystyrene sample and Clemens Padberg (University of Twente) for the GPC experiments to determine the molecular weight distribution.

3.6 List of symbols

ω	Angular frequency	$rad \cdot s^{-1}$
$\lvert cp^* \rvert$	Modulus of the complex heat capacity	$J \cdot g^{-}1 \cdot K^{-1}$
A	Temperature amplitude	K
b	Underlying scanning rate	$K \cdot s^{-1}$
cp	Specific reversing heat capacity	$J \cdot g^{-1} \cdot K^{-1}$
dQ/dt	Heat flow	$J \cdot s^{-1} \cdot g^{-1}$
f(t,T) .	Contribution to kinetic events	$J \cdot s^{-1} \cdot g^{-1}$
t	Time	s
T_0	Initial temperature	K

T_g	Glass transition temperature	K
T_{L-L}	Liquid-liquid demixing temperature	K

3.7 References

1. Koningsveld, R., and Staverman, A.J., *Liquid-liquid phase separation in multicomponent polymer solutions. III. Cloud point curves*, Journal of Polymer Science: Part A-2, 6, p. 349-366 (1968)
2. Koningsveld, R., Stockmayer, W.H., and Nies, E., *Polymer phase diagrams*., Oxford: Oxford University Press (2001)
3. Hikmet, R.M., Callister, S., and Keller, A., *Thermoreversible gelation of atactic polystyrene: phase transformation and morphology*, Polymer, 29, p. 1378-1388 (1988)
4. Tsai, F.J., and Torkelson, J.M., *Roles of phase separation mechanism and coarsening in the formation of poly(methyl methacrylate) asymmetric membranes*, Macromolecules, 23, p. 775-784 (1989)
5. Jackson, C.L., and Shaw, M.T., *The phase behavior and gelation of a rodlike polymer in solution and implications for microcellular foam morphology*, Polymer, 31, p. 1070-1084 (1990)
6. Lloyd, D.R., Kim, S.S., and Kinzer, K.E., *Microporous membrane formation via thermally-induced phase separation. II. Liquid-liquid phase separation*, Journal of Membrane Science, 64, p. 1-11 (1991)
7. Kim, S.S., and Lloyd, D.R., *Thermodynamics of polymer/diluent systems for thermally induced phase separation: 3. Liquid-liquid phase separation systems.*, Polymer, 33, p. 1047-1057 (1992)
8. Cha, B.J., Char, K., Kim, J.-J., Kim, S.S., and Kim, C.K., *The effects of diluent molecular weight on the structure of thermally-induced phase separation membrane*, Journal of Membrane Science, 108, p. 219-229 (1995)
9. Nojima, S., Shiroshita, K., and Nose, T., *Phase separation process in polymer systems. II. Microscopic studies on a polystyrene and diisodecyl phthalate mixture*, Polymer Journal, 14, p. 289-294 (1982)
10. Lal, J., and Bansil, R., *Light-scattering study of kinetics of spinodal decomposition in a polymer solution*, Macromolecules, 24, p. 290-297 (1991)
11. Laxminarayan, A., McGuire, K.S., Kim, S.S., and Lloyd, D.R., *Effect of initial composition, phase separation temperature and polymer crystallization on the formation of microcellular structures via thermally induced phase separation*, Polymer, 35, p. 3060-3068 (1994)
12. McGuire, K.S., Laxminarayan, A., and Lloyd, D.R., *Kinetics of droplet growth in liquid-liquid phase separation of polymer-diluent systems: experimental results*, Polymer, 36, p. 4951-4960 (1995)
13. Graham, P.D., Pervan, A.J., and McHugh, A.J., *The dynamics of thermal-induced phase separation in PMMA solutions*, Macromolecules, 30, p. 1651-1655 (1997)
14. Szydlowski, J., and Van Hook, W.A., *Studies of liquid-liquid demixing of polystyrene solutions using dynamic light scattering. Nucleation and droplet growth from dilute solution*, Macromolecules, 31, p. 3255-3265 (1998)
15. Wolf, B.A., and Sezen, M.C., *Viscometric determination of thermodynamic demixing data for polymer solutions*, Macromolecules, 10, p. 1010-1014 (1977)
16. Caneba, G.T., and Soong, D.S., *Polymer membrane formation through the thermal-inversion process. 1. Experimental study of membrane structure formation*, Macromolecules, 18, p. 2538-2545 (1985)

17. Xie, Y., Ludwig, K.F.J., Basnil, R., Gallagher, P.D., Konák, C., and Morales, G., *Time-resolved small-angle X-ray scattering studies of spinodal decomposition kinetics in a semidilute polystyrene-dioctylphthalate solution*, Macromolecules, 29, p. 6150-6157 (1996)
18. Arnauts, J., and Berghmans, H., *Amorphous thermoreversible gels of atactic polystyrene*, Polymer Communications, 28, p. 66-68 (1987)
19. Vandeweerdt, P., Berghmans, H., and Tervoort, Y., *Temperature-concentration behaviour of solutions of polydisperse, atactic poly(methyl methacrylate) and its influence on the formation of amorphous, microporous membranes*, Macromolecules, 24, p. 3547-3552 (1991)
20. Arnauts, J., Berghmans, H., and Koningsveld, R., *Structure formation in solutions of atactic polystyrene in trans-decalin*, Makromolekulare Chemie, 194, p. 77-85 (1993)
21. Arnauts, J., De Cooman, R., Vandeweerdt, P., Koningsveld, R., and Berghmans, H., *Calorimetric analysis of liquid-liquid phase separation*, Thermochimica Acta, 238, p. 1-16 (1994)
22. Aubert, J.H., *Isotactic polystyrene diagrams and physical gelation*, Macromolecules, 21, p. 3468-3473 (1988)
23. Kinzer, K.E., and Lloyd, D.R., *Thermally induced phase separation mechanisms for microporous membrane formation*, Polymer Materials Science Engineering, 61, p. 794-798 (1989)
24. Aerts, L., Kunz, M., Berghmans, H., and Koningsveld, R., *Relation between phase behaviour and morphology in polyethylen/diphenyl ether systems*, Macromolekulare Chemie, 194, p. 2697-2712 (1993)
25. Reading, M., *Modulated differential scanning calorimetry-A new way forward in materials characterization*, Trends in Polymer Science, 1, p. 248-253 (1993)
26. Reading, M., Hahn, B.K., and Crowe, B.S., *Method and apparatus for modulated differential analysis*,US-patent 5224775 (1993)
27. Schawe, J., *A comparison of different evaluation methods in modulated temperature DSC*, Thermochimica Acta, 260, p. 1-16 (1995)
28. Ozawa, T., and Kanari, K., *Linearity and non-linearity in DSC: A critique on modulated DSC*, Thermochimica Acta, 253, p. 183-188 (1995)
29. Jones, K.J., Kinshott, I., Reading, M., Lacey, A.A., Nikolopoulos, C., and Pollock, H.M., *The origin and interpretation of the signals of MTDSC*, Thermochimica Acta, 304/305, p. 187-199 (1997)
30. Höhne, G.W.H., *Remarks on the interpretation of the imaginary part C" of the complex heat capacity*, Thermochimica Acta, 304/305, p. 121-123 (1997)
31. Schawe, J.E.K., *Principles for the interpretaton of temperature-modulated DSC experiments. Part 2: A thermodynamic approach*, Thermochimica Acta, 304/305 (1997)
32. Wunderlich, B., Boller, A., Okazaki, I., and Ishikiriyama, K., *Heat-capacity determination by temperature-modulated DSC and its separation from transition effects*, Thermochimica Acta, 304/305, p. 125-136 (1997)
33. Scherrenberg, R., Mathot, V., and Van Hemelrijck, A., *The practical applicability of TMDSC to polymeric systems*, Thermochimica Acta, 330, p. 3-19 (1999)
34. Scherrenberg, R., Mathot, V., and Steeman, P., *The applicability of TMDSC to polymeric systems*, Journal of Thermal Analysis, 54, p. 477-499 (1998)
35. Dreezen, G., Groeninckx, G., Swier, S., and van Mele, B., *Phase separation in miscible polymer blends as detected by modulated temperature differential scanning calorimetry*, Polymer, 42, p. 1449-1459 (2001)
36. Worsfold, D.J., and Bywater, S., *Anionic polymerization of styrene*, Can. J. Chem, 38 (1960)
37. Mathot, V.B.F., *Calorimetry and thermal analysis of polymers*. 1. ed, Munich: Hanser Publishers (1994)
38. Song, S.-W., and Torkelson, J.M., *Coarsening effects on the formation of microporous membranes produced via thermally induced phase separation of polystyrene-cyclohexanol solutions*, Journal of Membrane Science, 98, p. 209-222 (1995)

Chapter 4

Quantification and interpretation of temperature modulated differential scanning calorimetry data on liquid-liquid demixing and vitrification

Abstract

With temperature modulated differential scanning calorimetry (TMDSC) one can study the liquid-liquid demixing behavior of a polymer-diluent solution with an amorphous polymer with an Upper Critical Solution Temperature behavior. This chapter describes in detail the thermodynamics of the measured heat capacity shift and the liquid-liquid demixing temperature using the Flory-Huggins theory. Experimental heat capacity shifts due to liquid-liquid demixing agree well with the thermodynamic prediction. It will be shown that this approach allows me to extract information on the demixing process by comparing the experimental and the predicted heat capacity shift upon cooling within the liquid-liquid demixing gap. The observation of arrested heat development indicates that the demixing polymer-diluent system freezes in well above the glass transition temperature of the system.

4.1 Introduction

In Chapter 3, it was demonstrated that Temperature Modulated Differential Scanning Calorimetry (TMDSC) has the potential to determine liquid-liquid demixing and the glass transition temperature of a polymer-diluent system with an amorphous polymer and an Upper Critical Solution Temperature. The temperature onset of the heat capacity shift upon cooling agreed well with visually observed cloud points. Using conventional DSC measurements, Van de Witte [1] and Arnauts *et al.* [2] tried to quantify the observed exothermic heat effect with the help of the enthalpy of mixing using the Flory-Huggins theory. However, experimental data did not give conclusive results. With the introduction of TMDSC [3, 4], a more accurate tool is available to measure transitions with small heat effects like liquid-liquid demixing. In this chapter the observed heat capacity shift will be interpreted with the help of the Flory-Huggins theory. In particular this chapter is focussed on:

- Algorithm to evaluate and use the experimental data.
- Physical interpretation of observed phenomena concluding a structure arrestment at temperatures significantly above the glass transition temperature of the polymer-diluent system.
- Assumptions and their validity for the Flory-Huggins model.

4.2 Theory

4.2.1 Heat capacity calculation with Flory-Huggins theory

The Flory-Huggins (F-H) theory [5] can be used to describe demixing of a polymer solution. It is not the most sophisticated theory to describe liquid-liquid demixing and it has been modified frequently (e.g. [6]). Nonetheless, this chapter is based on the F-H theory because of its simplicity and its sufficiently descriptive strength through its empirical interaction parameter. The binodal points of a mono-disperse binary system can be calculated by simultaneously solving of the chemical potential equations (μ) for the diluent (d) and the polymer (p) in the two coexisting phases 1 and 2 which appear upon demixing:

$$\mu_{d,1}=\mu_{d,2} \qquad (1)$$
$$\mu_{p,1}=\mu_{p,2} \quad .$$

According to the F-H theory the chemical potential of the diluent is given by [7]:

$$\frac{\mu_d}{RT}=\ln\phi_d+\left(1-\frac{N_d}{N_p}\right)(1-\phi_d)+\chi N_d(1-\phi_d)^2 \qquad (2)$$

where N_d and N_p are the number of lattice sites occupied by diluent and polymer respectively, ϕ_d and ϕ_p the volume fractions of diluent and polymer, and χ the empirical interaction parameter. The influence of concentration in the interaction parameter is assumed to be negligible (Assumption 1), hence it only depends on the temperature according to [2, 7]:

$$\chi=a+\frac{b}{T} \qquad (3)$$

with *a* and *b* being empirical parameters specific for the considered system.
All the assumptions made in this chapter will be discussed in Appendix 4A.

By solving Eq. 1 to 3 for the coexisting polymer concentrations ϕ_1 and ϕ_2 and by using $\phi_d+\phi_p = 1$, $N = N_p/N_d$, the following relation for the binodal temperature can be derived:

$$T_{bin}=-\frac{b(\phi_2^2-\phi_1^2)}{\ln\frac{1-\phi_2}{1-\phi_1}+\left(1-\frac{1}{N}\right)(\phi_2-\phi_1)+a\left(\phi_2^2-\phi_1^2\right)} \qquad (4)$$

with ϕ_1 and ϕ_2 representing the polymer volume fractions in the polymer-lean and polymer-rich phase. For concentrated polymer solutions, the polymer concentration in the polymer-lean phase is very close to zero and by assuming $\phi_1 = 0$ (Assumption 2), Eq. 4 becomes:

$$T_{bin} = -\frac{b\phi_2^2}{\ln(1-\phi_2) + \left(1-\frac{1}{N}\right)\phi_2 + a\phi_2^2}. \quad (5)$$

The enthalpy of mixing can be calculated according to Ebert *et al.* [8] and Arnauts *et al.* [2]. Upon cooling from a starting polymer concentration (ϕ_0) with a mixing enthalpy of ΔH_0 to a certain temperature, the system will demix in two phases with concentrations ϕ_1 and ϕ_2 with the corresponding mixing enthalpies ΔH_1 and ΔH_2. For every temperature, the mixing enthalpy difference between the starting concentration and the demixed concentrations can be calculated with the Flory-Huggins theory and the lever rule:

$$\frac{\Delta H_{F-H}}{RT} = \frac{\chi}{\phi_2 - \phi_1}\left[(\phi_2 - \phi_0)\phi_1(1-\phi_1) + (\phi_0 - \phi_1)\phi_2(1-\phi_2) - (\phi_2 - \phi_1)\phi_0(1-\phi_0)\right]. \quad (6)$$

The heat capacity equals the temperature derivative of the enthalpy of mixing:

$$\Delta cp_{F-H} = \frac{1}{M}\left(\frac{d\Delta H_{F-H}}{dT}\right) = \frac{R}{M} b\left[\frac{d\phi_1}{dT}(\phi_2 - \phi_0) + \frac{d\phi_2}{dT}(\phi_1 - \phi_0)\right] +$$
$$\frac{R}{M} a\left[T\frac{d\phi_1}{dT}(\phi_2 - \phi_0) + T\frac{d\phi_2}{dT}(\phi_1 - \phi_0) + (\phi_2\phi_1 - \phi_0\phi_2 - \phi_1\phi_0 + \phi_0\phi_0)\right] \quad (7)$$

with M being the molecular mass of one lattice site. According to Eq. 7, the heat capacity shift caused by L-L demixing depends on the slopes of the concentrated and diluted branch of the binodal. The following additional assumptions are made:

- The binodal at the diluted branch is much steeper than at the concentrated branch, the following holds for the inverse slope of the binodal: $d\phi_1/dT << d\phi_2/dT$ (Assumption 3).
- An infinite polymer size ($1/N = 0$) (Assumption 4).
- M lies between the molecular weight of the styrene monomer (104 g·mol^{-1}) and of the pure diluent (186 g·mol^{-1}) (Assumption 5).

Eq. 7 will be discussed for two situations: in situation 1 the magnitude of the heat capacity shift at the binodal temperature will be calculated (Δcp_{bin}) for different

polymer concentrations, and in situation 2 the temperature dependency of the heat capacity shift will be followed ($\Delta cp_{F\text{-}H}$).

4.2.1.1 Heat capacity shift at the binodal (Δcp_{bin})

Since only concentrated solutions are considered ($\phi > \phi_{critical}$), the polymer concentration at the moment of the start of liquid-liquid demixing is at the concentrated branch of the binodal: $\phi_0 = \phi_2$. Applying all assumptions mentioned above, the heat capacity at T_{bin} (Δcp_{bin}) can be written as:

$$\Delta cp_{bin} = -\frac{RT_{bin}(a + bT_{bin}^{-1})}{M}\frac{d\phi_2}{dT}\phi_2 = -\frac{RT_{bin}\chi}{M}\frac{d\phi_2}{dT}\phi_2 . \qquad (8)$$

The derivative of ϕ_2 with respect to T ($d\phi_2 / dT$) can be obtained by differentiation of Eq. 5.

$$\frac{d\phi_2}{dT_{bin}} = \left(\frac{dT_{bin}}{d\phi_2}\right)^{-1} = -\frac{(\phi_2 - 1)\left[\ln(1-\phi_2) + \phi_2 + a\phi_2^2\right]^2}{b\phi_2\left[2\ln(1-\phi_2)\phi_2 - 2\ln(1-\phi_2) - 2\phi_2 + \phi_2^2\right]} . \qquad (9)$$

Substitution of Eq. 5 and 9 in Eq. 8 gives:

$$\Delta cp_{bin} = \frac{R}{M}\frac{\left[\ln(1-\phi_2) + \phi_2\right](\phi_2 - 1)\left[\ln(1-\phi_2) + \phi_2 + a\phi_2^2\right]}{2\ln(1-\phi_2)\phi_2 - 2\ln(1-\phi_2) - 2\phi_2 + \phi_2^2} . \qquad (10)$$

According to Eq. 10, the shift in heat capacity depends only on the empirical parameter a in the temperature-dependent Flory-Huggins parameter χ.

4.2.1.2 Temperature dependency of heat capacity shift ($\Delta cp_{F\text{-}H}$)

Besides the expression of the heat capacity shift at the binodal temperature described in the previous paragraph, also an expression can be derived for the temperature dependency of the heat capacity shift. With this expression the heat capacity shift can be predicted for a certain polymer concentration when it is cooled within the demixing gap. The difference with the calculation procedure in §4.2.1.1 is that ϕ_0 is

not equal to ϕ_2. To follow $\Delta cp_{F\text{-}H}$, Eq. 7 is solved by using assumptions 1 to 5. Eq. 9 is used to calculate $d\phi_2 / dT$.

4.2.2 Vitrification according to the Kelley-Bueche model

For polymer concentrations showing only a T_g depression but no liquid-liquid demixing, the measured glass transition temperature of the polymer-diluent system can be compared with the theoretical prediction according to the Kelley-Bueche model [9]:

$$T_g = \frac{R\phi_d T_{g,d} + \phi_p T_{g,p}}{R\phi_d + \phi_p} \tag{11}$$

where T_g is the glass transition temperature of the polymer-diluent mixture and $T_{g,d}$ and $T_{g,p}$ the glass transition temperature of the single diluent and polymer respectively. Originally, the value of R is defined as the ratio of the differences in thermal expansion coefficient between liquid and glass of both components leading to a value of R = 2.1 [9, 10]. Frequently, R is used as a fitting parameter; however, in this work the value of 2.1 has been used. The glass transition temperature of the pure diluent can be estimated with the relation of Fedors [11]:

$$\gamma = \frac{T_{m,d} + T_{b,d}}{T_{g,d} + T_{b,d}} \tag{12}$$

where γ is an empirical parameter (= 1.15) and $T_{m,d}$ and $T_{b,d}$ the melting and boiling point of the diluent respectively. Using these values, the glass transition temperature can be predicted of the polymer-diluent phase outside the L-L demixing gap with the help of Eq. 11 and its intersection with the polymer-rich branch of the binodal (Eq. 5). The temperature and the polymer concentration of this intersection defines the so-called Berghmans point [12] at which all compositions within the L-L demixing gap are expected to vitrify.

4.3 Experimental

4.3.1 Materials

Two types of atactic polystyrene (aPS) were used: a high poly-dispersity (M_w/M_n), (Styron* 686E, kindly supplied by Dow Benelux NV, M_w/M_n = 2.1, M_w = $2.3 \cdot 10^5$ g·mol^{-1}) and a low M_w/M_n, (M_w/M_n = 1.05, M_w = $6 \cdot 10^4$ g·mol^{-1}). The diluent, 1-dodecanol (purity >98%, Merck-Schuchardt) was used without further purification.

4.3.2 Temperature Modulated Differential Scanning Calorimetry (TMDSC)

The TMDSC experiments were carried out on a DSC 2920 of TA Instruments. The sample size of the polymer-diluent solution was about 5 mg. The cooling rate was set to 2 K·min^{-1} to 0°C and after an isothermal step of 5 minutes the sample was heated again with 2 K·min^{-1}. The amplitude of the superimposed sine wave was 1 K with a period of 60 s. The glass transition temperature T_g and the liquid-liquid demixing temperature $T_{L\text{-}L}$ as well as the heat capacity shift at $T_{L\text{-}L}$ have been determined with the TA Universal Analysis software. Further details about the chemicals used, the sample preparation, and the experimental setup have been given in Chapter 3 (§3.2.1).

4.4 Experimental signal analysis

4.4.1 Models to describe the binary phase diagram

The change in the onset temperature of liquid-liquid demixing ($T_{L\text{-}L}$) for different concentrations of polymer (ϕ_0) can be fitted to the Flory-Huggins model with the empirical interaction parameter (see Fig. 1). Values for the empirical interaction parameters are: a = -2.28 and b = 1258 for $N = \infty$.

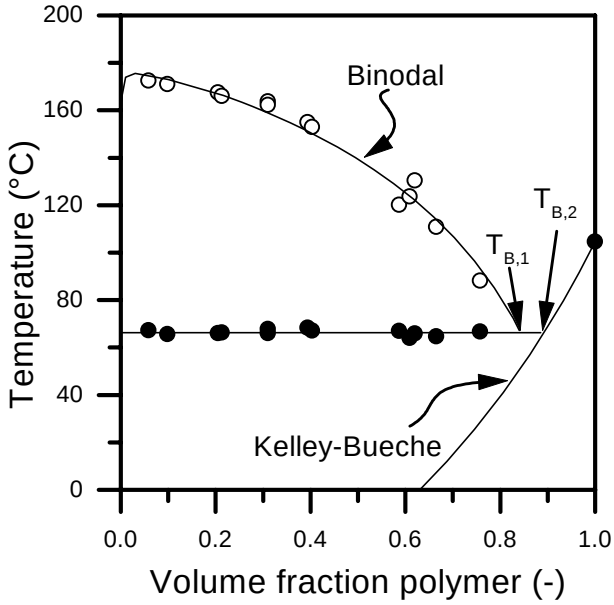

Figure 1. *Phase diagram of aPS in 1-dodecanol. Open circles: TMDSC data L-L demixing. Closed circles: TMDSC data glass transition temperature. Line through $T_{L\text{-}L}$ data points: Binodal according to Flory-Huggins fit. $T_{B,1}$ is the Berghmans point obtained from the intersection between the binodal and the experimental glass transition temperatures. $T_{B,2}$ is the Berghmans point obtained from the intersection between the Kelley-Bueche theory and the experimental glass transition temperatures.*

Here it is assumed that the binodal temperature of the Flory-Huggins model (T_{bin} as derived for a mono-disperse polymer) equals the experimental observed liquid-liquid demixing temperature ($T_{L\text{-}L}$ measured for a poly-disperse polymer). The validity of this assumption (Assumption 6) will be discussed in detail later in Appendix 4A. The weight fractions are converted to volume fractions by assuming linear interpolation between the pure densities at a constant temperature (Assumption 7).

The Kelly-Bueche equation is used to describe the glass transition temperature outside the L-L demixing gap. The input parameters of the Kelley-Bueche model (Eq. 11) are listed in Table 1. Fig. 1 shows the fit of Eq. 5 through the experimental data for the temperatures at which L-L demixing occurs. Fig. 1 also shows the glass transition temperatures of the polymer-diluent mixture within the L-L demixing gap.

Table 1. *Input parameters for the Kelley-Bueche model.*

Variable	Value	Ref.
$T_{g,p}$ (K)	375.8	this work
$T_{b,d}$ (K)	537.0	[13]
$T_{m,d}$ (K)	297.0	[13]
γ (-)	1.15	[10]
R (-)	2.1	[9, 10]
ρ_p (kg·m^{-3})	1050 (see Assumption 7)	supplier
ρ_d (kg·m^{-3})	770 (see Assumption 7)	[13]

Intersection of the binodal and the experimental data of T_g fix the position of the Berghmans point ($T_{B,1}$). This should be the same as the Berghmans point obtained from the intersection of the experimental data of T_g and the Kelley-Bueche model ($T_{B,2}$). Fig. 1 only shows a small difference between $T_{B,1}$ and $T_{B,2}$.

4.4.2 Magnitude of the complex heat capacity signal caused by L-L demixing

Eq. 7 predicts the shift in the heat capacity due to L-L demixing. To compare the magnitude of this shift predicted from the Flory-Huggins model with my experimental data, it is necessary to develop an algorithm for processing the experimental data of the heat capacity as a function of temperature. Fig. 2 shows the existence of a small shift at 80°C, besides T_{L-L} and T_g. For now, this transition will be defined as T_s. (Later in this chapter, it will be shown that the physical origin of T_s is an early freezing in of the polymer-rich phase well above the glass transition temperature.) It is assumed that the heat capacity shift between T_s and T_{L-L} is completely caused by the enthalpy of demixing (Assumption 8). T_s allows me to perform an interpolation procedure between the region of the homogeneous solution ($T>T_{L-L}$) and the two phase system comprising the polymer-rich phase and the polymer-lean phase ($T_g<T<T_s$).The values obtained from the experimental measured specific complex heat capacity $|cp^*|$ are indicated with an asterix to make a clear distinction between experimental and theoretical heat capacities. To divide the measured specific complex heat capacity ($|cp^*|$) into the interpolated heat capacity (cp^*_i) and a contribution caused by the enthalpy demixing (Δcp^*) according to Eq. 13:

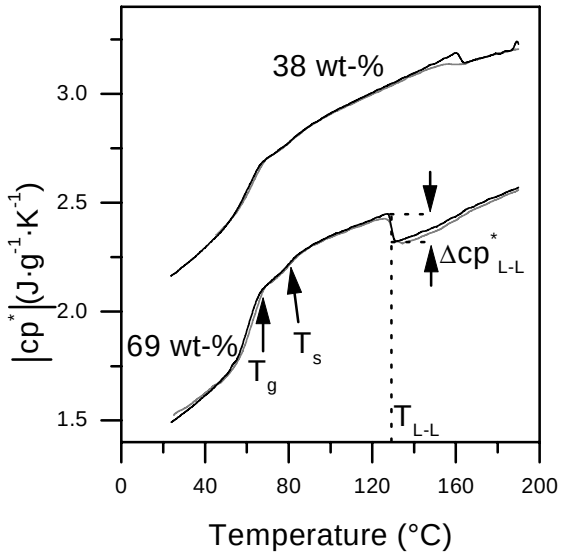

Figure 2. *Cooling and subsequent heating curves (mass fraction of polymer: 0.38 and 0.69) (gray lines: heating curves, black lines: cooling curves). Both the T_{L-L} and T_g are defined as the onset upon cooling.*

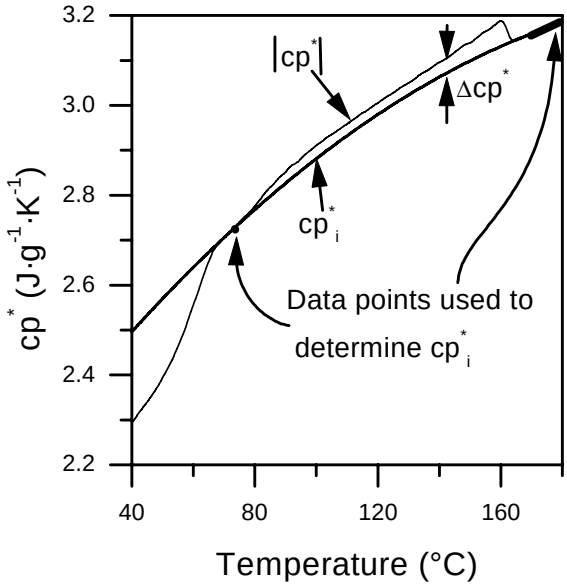

Figure 3. *Interpolated heat capacity curve (cp^*_i) and specific complex heat capacity $|cp^*|$ for a volume fraction of polymer of 0.31. The thick lines represent the region of data points used to determine cp^*_i. The region of a homogeneous solution at high temperatures continues to T = 190°C.*

$$\left|cp^*\right| = cp_i^* + \Delta cp^* \qquad (13)$$

the following procedure is applied. Data points for $T > T_{L\text{-}L}+10$ are used together with the data points belonging to a temperature between T_g and T_s ($T \sim 70$°C) to determine cp^*_i. The data points in this region are not influenced by liquid-liquid demixing nor vitrification processes. These regions of data points are connected by a second order polynomial (see Fig. 3). The motivation for choosing this mathematical form will be given in Appendix 4B. Appendix 4B will also treat the comparison of the cp^*_i and the predicted theoretical value of the heat capacity (cp_{th}). Δcp^* is now obtained by subtracting cp^*_i from $\left|cp^*\right|$ (according to Eq. 13).

4.5 Results

4.5.1 Heat capacity shift at $T_{L\text{-}L}$ ($\Delta cp^*_{L\text{-}L}$)

Fig. 4 shows the experimentally observed heat capacity at $T_{L\text{-}L}$, defined as $\Delta cp^*_{L\text{-}L}$, as a function of the volume fraction of polymer together with the shift in heat capacity at the binodal temperature predicted by the F-H theory (Δcp_{bin}) by Eq. 10.

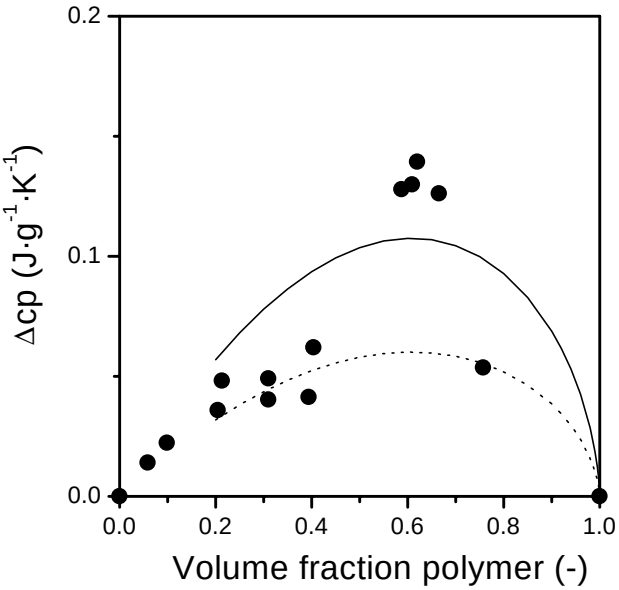

Figure 4. *Experimental and calculated heat capacity at the liquid-liquid demixing temperature. Points: $\Delta cp^*_{L\text{-}L}$. Lines: Δcp_{bin}. Solid line: M = 104 g·mol^{-1}. Dotted line: M = 186 g·mol^{-1}. Input parameters to calculate Δcp_{bin}: a = -2.28, b = 1258.*

Δcp_{bin} is drawn from a volume fraction of ϕ_0 = 0.2 only, because Eq. 10 has been derived for concentrated solutions. From the discussion on Assumption 2 and 3 in Appendix 4A it appears that at a volume fraction of ϕ_0 = 20 vol.%, Eq. 10 only shows a small error.

It should be realised that for the calculation of Δcp_{bin}, the interaction parameter determined from the binodal fit is used. This implies that the model predictions in Fig. 4 are calculated using independent input parameters. The order of magnitude and the trend predicted by Δcp_{bin} is correct in comparison with the experimental data. By using the molecular weight of 1-dodecanol to calculate the heat capacity, Δcp_{bin} even predicts the correct magnitude up to a volume fraction of ϕ_0 = 0.4. At higher concentrations the model underestimates the heat capacity shift. The deviation between the interpolated and the theoretical heat capacity is the largest in this concentration region as well (see Table B3 in Appendix 4B) and these data points are considered to be less reliable. A physical explanation for the large deviation between the interpolated and the theoretical heat capacity is not at hand today.

The good agreement between Δcp_{bin} and the experimental data, implies that the experimental values of both $T_{L\text{-}L}$ and $\Delta cp^*_{L\text{-}L}$ can be used to determine the empirical constants *a* and *b* in the F-H interaction parameter. In Chapter 6, a procedure will be discussed to determine the complete binodal curve with the help of one single TMDSC experiment.

4.5.2 Temperature dependency of the heat capacity shift ($\Delta cp_{F\text{-}H}$)

The temperature dependency of $\Delta cp_{F\text{-}H}$ can be compared with the Δcp^* (as determined in Fig. 3 and described in §4.4.2) and is plotted in Fig. 5. Fig. 5 shows the good agreement between Δcp^* and $\Delta cp_{F\text{-}H}$ at $T_{L\text{-}L}$, which in fact was shown already by the comparison between $\Delta cp^*_{L\text{-}L}$ and Δcp_{bin} (see §4.5.1, Fig. 4). At lower temperatures there is an increasing deviation between $\Delta cp_{F\text{-}H}$ and Δcp^*. The shape of Δcp^* strongly depends on the numerical algorithm to extract Δcp^*, hence it is too preliminary to draw conclusions about the shape of the curve. Curves for different polymer concentration show a comparable shape as the solid curve in Fig. 5. However, as I showed that the shift in the heat capacity is caused by L-L demixing, the disappearance of the heat capacity shift means that demixing stops at a

temperature above the onset of the glass transition temperature; in fact the heat contribution of liquid-liquid demixing stops at T_s.

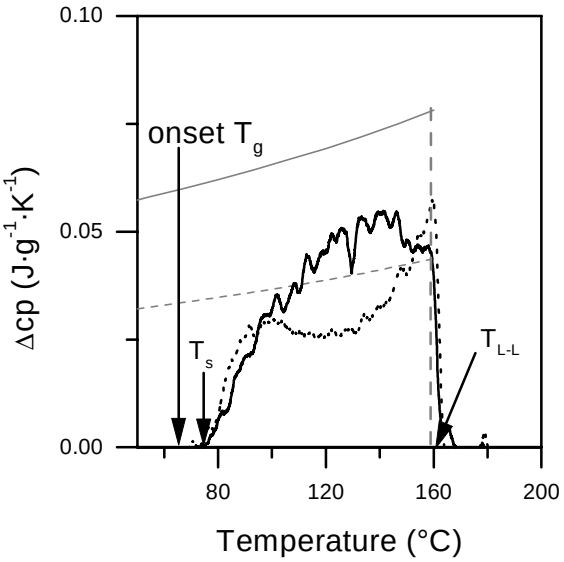

Figure 5. *Heat capacity shift as function of temperature for a volume fraction of polymer of 0.31. Curved lines: Duple experiments Δcp^*. Straight lines: heat capacity shift according to Flory-Huggins theory ($\Delta cp_{F\text{-}H}$). Input parameters: a = -2.28, b = 1258. Solid gray line: M = 104 g·mol^{-1}, dotted gray line: M = 186 g·mol^{-1}.*

4.6 Discussion

It is important to take into account that the experimental data are valid for a modulation period of 60 s. Physical phenomena occurring at time scales below this modulation period are observed, while slow physical events on time scales larger than 60 s cannot effect this signal. Furthermore, a clear distinction should be made between two processes occuring during cooling through the liquid-liquid demixing gap:

- The equilibrium concentrations of both the polymer-lean and polymer-rich phase change upon cooling indicated by the binodal (thermodynamics)
- The demixed domains grow by coarsening and coalescence caused by minimizing of the interfacial area [14] (kinetics).

In Appendix 4A the validity of Assumption 8 is demonstrated: the role of the interface formation during liquid-liquid demixing only plays a minor role on the time

scale of a TMDSC experiment. With growth of the demixed domains, the interfacial area decreases, hence growth will not be observed in the complex heat capacity signal of a TMDSC experiment. Also from the cooling rate dependency of the heat capacity shift (see Assumption 9), it can be observed that growth of the demixed phases does not influence the complex heat capacity signal; different cooling rates (from 0.2 to 5 $K \cdot min^{-1}$) give comparable complex heat capacity curves.

The experiments are interpreted in such a way that the final concentrations of both the polymer-lean and polymer-rich phase are reached even above the glass transition. The final concentration of the polymer-rich phase is lower than the equilibrium concentration as given by the binodal. This means that the polymer-rich phase is supersaturated with diluent. Berghmans *et al.* [15] hypothesized that liquid-liquid demixing proceeds even below the glass transition temperature because passing the glass transition temperatures only decreases the mobility within a polymer-diluent system, a driving force is still present to change concentration in the polymer-rich and lean phase. From my experiments it is hypothesized that the concentration in the polymer-rich and polymer-lean phases do not change anymore below T_s, at least within a time scale of 60 s. A further change in composition of the polymer-rich and polymer-lean phase has to take place at much larger time scales. The presence of the supersaturated polymer-rich phase will be proven with the help of the crystallization and melting behavior of the diluent as will be described in Chapter 5.

4.7 Conclusions

The heat capacity shift resulting from liquid-liquid demixing at the liquid-liquid demixing temperature is in good agreement with theoretical predictions of the Flory-Huggins theory. Upon cooling deeper into the demixing gap, the deviation between the measured heat capacity shift and the theoretical heat capacity shift increases and at a temperature significantly higher than the onset temperature of the glass transition temperature the measured heat capacity shift completely disappears. The interpretation of this observation is that the polymer-rich phase of the demixed polymer solution can not reach the binodal concentrations. Moreover, at a temperature significantly higher than the glass transition temperature liquid-liquid

demixing even stops. Upon cooling deep in the liquid-liquid demixing gap, the change in concentration between the polymer-rich and lean phase can not follow the modulation period (60 s) because of the decrease in mass transfer between the polymer-lean and polymer-rich phase. The growth of the demixed domains has no influence on the measured complex heat capacity signal.

4.8 Acknowledgements

Dr. N.F.A. van de Vegt (Twente University) is acknowledged for the discussions. I want to thank Akzo Nobel in Arnhem (The Netherlands) for giving the possibility to carry out the TMDSC experiments.

4.9 List of symbols

χ	Interaction parameter	-
γ	Empirical parameter Kelley-Bueche model	-
Δcp^*	Experimental heat capacity shift	$J \cdot g^{-1} \cdot K^{-1}$
$\Delta cp^*_{L\text{-}L}$	Experimental heat capacity shift at $T_{L\text{-}L}$	$J \cdot g^{-1} \cdot K^{-1}$
Δcp_{bin}	Theoretical heat capacity shift at T_{bin}	$J \cdot g^{-1} \cdot K^{-1}$
$\Delta cp_{F\text{-}H}$	Heat capacity according to Flory-Huggins theory	$J \cdot g^{-1} \cdot K^{-1}$
$\Delta H_{F\text{-}H}$	Enthalpy of demixing according to Flory-Huggins theory	$J \cdot mol^{-1}$
ΔH_j	Enthalpy of demixing at binodal of phase j	$J \cdot mol^{-1}$
ϕ_i	Volume fraction component i	-
$\mu_{i,j}$	Chemical potential component i, j	$J \cdot mol^{-1}$
ϕ_j	Volume fraction polymer at binodal	-
a	Empirical parameter	-
b	Empirical parameter	K
$\lvert cp^* \rvert$	Specific complex heat capacity	$J \cdot g^{-1} \cdot K^{-1}$
cp^*_i	Interpolated heat capacity	$J \cdot g^{-1} \cdot K^{-1}$
f	Ratio volume interface and total volume	-
M	Molecular weight of one lattice site	$g \cdot mol^{-1}$

M_i	Molecular weight component i	$g \cdot mol^{-1}$
N	Ratio N_p/N_d	-
N_i	Number of lattice sites occupied by component i	-
r	Cell radius	m
R	Gas constant	$J \cdot mol^{-1} \cdot K^{-1}$
R	Constant Kelley-Bueche model	-
T	Temperature	K
$T_{B,1}$, $T_{B,2}$	Berghmans temperature	K
$T_{b,d}$	Boiling point diluent	K
T_{bin}	Binodal temperature	K
T_g	Glass temperature solution	K
$T_{g,i}$	Glass transition temperature component i	K
$T_{L\text{-}L}$	Liquid-liquid phase separation temperature	K
$T_{m,d}$	Melting point diluent	K
T_s	Stop temperature of demixing	K
w_i	Weight fraction component i	-

Remarks to the table: when necessary °C has been used instead of K.

The superscript (*) denotes an experimentally measured heat capacity

Subscripts

i	p	Polymer
	d	Diluent
j	0	Starting solution
	1	Diluted branch binodal
	2	Concentrated branch binodal

4.10 References

1. Witte, P.v.d., *Polyactide membranes, correlation between phase transitions and morphology* ,PhD thesis University of Twente, Enschede (1994)
2. Arnauts, J., De Cooman, R., Vandeweerdt, P., Koningsveld, R., and Berghmans, H., *Calorimetric analysis of liquid-liquid phase separation*, Thermochimica Acta, 238, p. 1-16 (1994)
3. Reading, M., Hahn, B.K., and Crowe, B.S., *Method and apparatus for modulated differential analysis*,US patent 5224775 (1993)
4. Reading, M., *Modulated differential scanning calorimetry-A new way forward in materials characterization*, Trends in Polymer Science, 1, p. 248-253 (1993)
5. Flory, P.J., *Principles of polymer chemistry*, Ithaca: Cornell University Press (1953)

6. Lacombe, R.H., and C., S.I., *Statistical thermodynamcs of fluid mixtures*, Journal of Physical Chemistry, 80, p. 2568-2580 (1976)
7. Brandrup, J., and H., I.E., *Polymer Handbook* 3th ed, New York: John Wiley & sons (1974)
8. Ebert, M., Garbella, R.W., and Wendorff, J.H., *Studies on the heat of demixing of poly(ethylene acrylate)-poly(vinylidene fluoride) blends*, Makromol. Chem. Rapid Commun., 7, p. 65-70 (1986)
9. Kelley, F.N., and Bueche, F., *Viscosity and glass transition temperature relations for polymer-diluent systems*, Journal of Polymer Science, 50, p. 549-556 (1961)
10. Burghardt, W.R., Yilmaz, L., and McHugh, A.J., *Glass transition, crystallization and thermoreversible gelation in ternary PPO solutions; relationship to asymmetric membrane formation*, Polymer, 28, p. 2085-2092 (1987)
11. Fedors, R.F., *A universal reduced glass transition temperature for liquids*, Journal of Polymer Science: Polymer Letters Edition, 17, p. 719-722 (1979)
12. Arnauts, J., and Berghmans, H., *Amorphous thermoreversible gels of atactic polystyrene*, Polymer Communications, 28, p. 66-68 (1987)
13. Daubert, T.E., Danner, R.P., Sibul, H.M., and Stebbins, C.C., *Physical and thermodynamic properties of pure chemical. Data compilation*, Pennsylvania: Taylor&Francis (1989)
14. Siggia, E.D., *Late stages of spinodal decomposition in binary mixtures*, Physical Review A, 20, p. 595-605 (1979)
15. Berghmans, H., De Cooman, R., De Rudder, J., and Koningsveld, R., *Structure formation in polymer solutions*, Polymer, 39, p. 4621-4629 (1998)

Appendix 4A

Verification of the assumptions proposed in Chapter 4

Besides the normal limitations of the Flory-Huggins theory (for example incompressible lattice), additional assumptions were used in Chapter 4. Each of the assumptions will be discussed in more detail.

Assumption 1: Concentration independent interaction parameter

From isothermal studies it appears that the Flory-Huggins interaction parameter strongly depends on the polymer concentration [1]. In Chapter 4, I neglect this concentration dependency since the interaction parameter is only determined to support my hypothesis on the origin of the heat capacity shift and the extent of demixing deduced from it. It would be of course possible to add extra empirical parameters to describe the concentration dependency of the interaction parameter [1, 2]. However, this would not change the conclusions of this research.

Assumption 2: Concentration of polymer at diluted branch of binodal is 0

Fig. A1 shows the difference of the Flory-Huggins calculation of the binodal with and without the assumption of negligible polymer concentration in the polymer-lean phase. Below 20 vol.% of polymer, the error in temperature exceeds 1 K. For higher polymer concentrations the error is even smaller than the experimental error of the TMDSC experiments. The major part of the experiments was carried out at polymer concentrations larger than 20 vol.% and the assumption has therefore hardly any effect on the predictions.

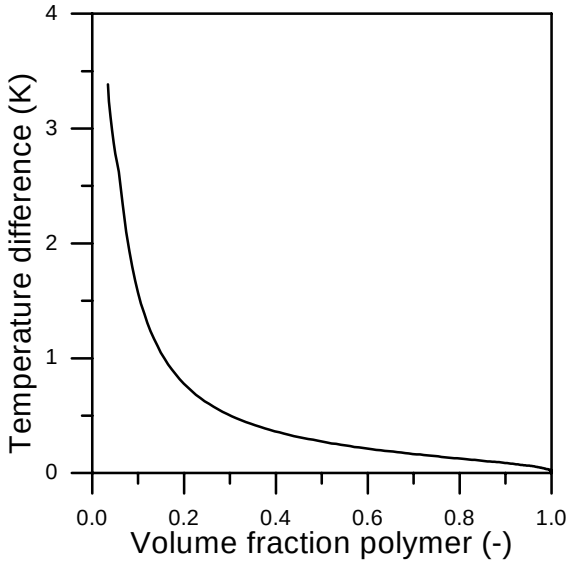

Figure A1. *Difference in binodal temperature calculated according to the Flory-Huggins theory with and without the assumption $\phi_1 = 0$. Input parameter $\chi = -2.28 + 1258 \cdot T^{-1}$.*

Assumption 3: Derivative of the diluted branch of the binodal is much larger than the derivative of the concentrated branch

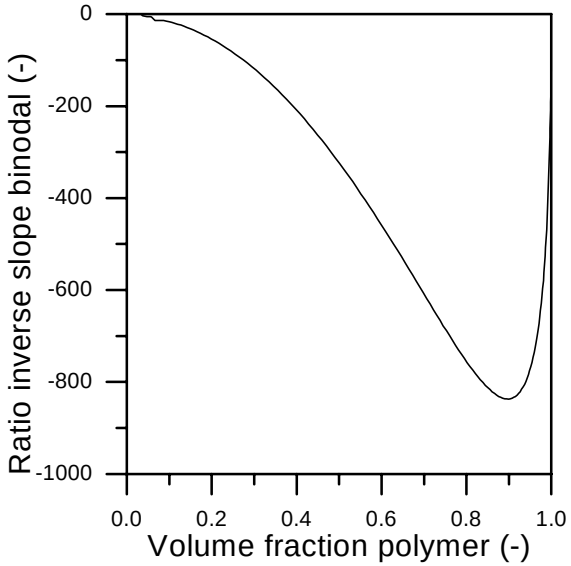

Figure A2. *Ratio of the inverse slope of the diluted and concentrated branch of the binodal. Input parameter: $\chi = -2.28 + 1258 \cdot T^{-1}$.*

Fig. A2 shows the ratio of the inverse of the derivative of ϕ_2 and ϕ_1 with respect to the temperature ($d\phi_2 / dT$ and $d\phi_1 / dT$ is plotted using the same parameters as for Fig.A1). It can be observed that the ratio exceeds 50 already at about 20 vol.%.

Assumption 4: Infinite molecular weight of the polymer

Table A1 shows the influence of the degree of polymerization on the interaction parameter. The values of N are based on a lattice consisting of monomer sites ($N = M_p/M_m = 1.1\ 10^5/104 \approx 1000$), diluent sites ($N = M_p/M_d = 1.1\ 10^5/186 \approx 600$) or the situation of an infinite ratio between the molecular weights of the polymer and the lattice site ($N = \infty$).

Table A1. *Results Flory-Huggins fit. Input parameter: N. Calculated parameters: a and b.*

χ = a+b/T	**N = 600**	**N = 1000**	**N = ∞**
a	-2.19	-2.23	-2.28
b	1229	1239	1258

The influence of N on the results of the fit is small. To reduce the amount of unknown parameters in the Flory-Huggins equation, the value for N is set to infinite.

Assumption 5: Molecular weight of the lattice site is between molecular weight of the diluent and of the monomer

Fig. 4 in Chapter 4 demonstrates that the magnitude of the predicted heat capacity shift is correct with the proposed molecular weights as input parameter for the calculation of the heat capacity shift. It would be of course also possible to choose a lattice site size between these extremes, however this would not change the conclusions of this paper.

Assumption 6: Poly-dispersity of the polystyrene sample

The Flory-Huggins theory used in this paper is strictly valid for a mono-disperse system only. For real polymers, the condition of mono-dispersity can never be achieved experimentally because any polymer shows a molecular mass distribution to some extent. The influence of poly-dispersity on the thermodynamic description of such a system can be performed by introducing the shadow curve [3] and by

calculating the Flory-Huggins theory for a multi-component system instead of a binary system. In this work the influence of poly-dispersity is studied by carrying out an experiment with a polystyrene sample of a poly-dispersity of 1.05. The measured heat capacity as a function of temperature is plotted in Fig. A3.

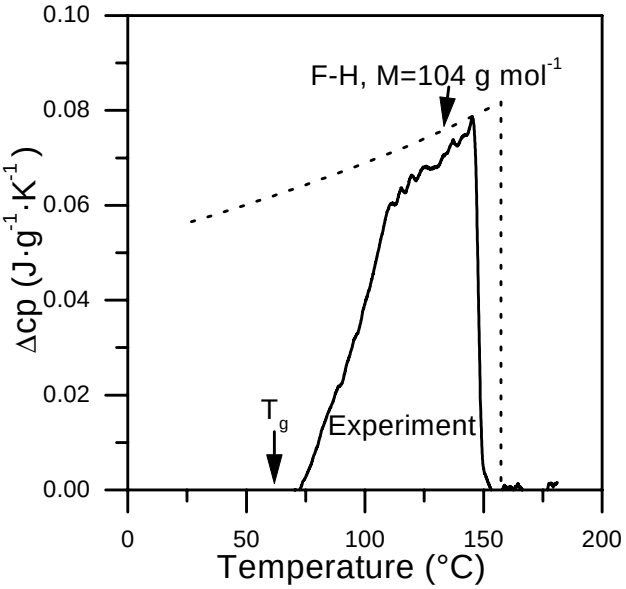

Figure A3. *Heat capacity development of aPS (poly-dispersity 1.05) in 1-dodecanol, weight fraction equals 0.4. The black continuous line represents the experimental data, using the procedure described in §4.4.2. The gray dotted line is obtained from the F-H theory (Chapter 4, Eq. 7), with the empirical interaction parameter obtained from the poly-disperse polystyrene sample.*

Due to the lack of extensive cloud point data for this polymer with a narrow poly-dispersity, the empirical Flory-Huggins parameters of the polymer with the broad molecular weight distribution were used as input to the model prediction to show the trend of the theoretical heat capacity shift. The magnitude of the experimental observed heat capacity shift close to $T_{L\text{-}L}$ cannot be compared with a theoretical prediction because the parameters for the poly-disperse polymer are used to describe the theoretical heat capacity shift. However, at later stages a growing deviation can be observed between experiment and the theoretical curve. Also for the narrow-disperse polymer, demixing stops far above the onset of the glass transition temperature. From this observation I conclude that poly-dispersity plays a minor role and for convenience the calculations carried out in Chapter 4 have been carried out assuming mono-dispersity.

Assumption 7: Linear interpolation pure component densities and constant temperature

This assumption consists of two parts, first I have to discuss whether a linear relation between the pure component density can be used and secondly the temperature dependency of the density will be discussed.

Eq. A1 describes the volume of a polymer solution [1].

$$v = w_d v_d + w_p v_p \qquad \text{(A1)}$$

where v is the specific volume of the solution, v_d and v_p the volume of diluent and polymer, w_d and w_p are the weight fractions of diluent and polymer respectively. In this equation, the value of v_d is chosen as the volume of the pure diluent and all the volume effects of mixing are incorporated in v_p. By comparing values of v_p for various solvents, an indication is obtained about specific interaction upon mixing. Literature data for the mixture 1-dodecanol and aPS were not reported, but all the values of v_p of solvents for aPS reported in the polymer handbook [1] vary between 0.899 and 0.948, corresponding to a polymer density of 1.05 to 1.11 g·cm^{-3}. On the basis of mixing properties for various solvents for aPS, the assumption of a linear density gives a sufficient description of the actual system.

The temperature dependency on the density of 1-dodecanol varies between [4] ρ_d = 810 kg·m^{-3} at T = 60°C and ρ_d = 720 kg·m^{-3} at T = 170°C. A density at a temperature of 115°C (= 770 kg·m^{-3}) is chosen as an average between 170°C (maximum observed $T_{L\text{-}L}$) and 60°C (T_g). The temperature dependency of polystyrene according to [1] is $d\rho_p/dT = -6.05\cdot10^{-4}$ g·cm^{-3}·K^{-1}. Hence the temperature of the polymer varies between 1030 kg·m^{-3} at T = 60°C and 960 kg·m^{-3} at T = 170°C. The temperature dependency of the density influences the relation between weight and volume fraction, but the physical picture given in Chapter 4 does not change.

Assumption 8: Influence of interface of demixed domains on enthalpy of (de)mixing

In this paragraph, the assumption will be discussed that the observed heat capacity shift is completely caused by the enthalpy of demixing and that the formation of new interfaces between the two phases only plays a minor role. During demixing of a

concentrated polymer solution, regions of almost pure diluent are embedded in a polymer rich matrix. An interface is formed between the polymer-rich and polymer-lean phase, which may contribute to the changes of the heat capacity shift. A model will be proposed to quantify the influence of an interface on the enthalpy of demixing: polymer-diluent contacts are broken and polymer-polymer and diluent-diluent contacts are created during demixing. In the interface layer between the polymer-rich phase and polymer-lean phase, the polymer-diluent contacts still exists. The polymer and diluent molecules in this region do not contribute to the enthalpy of demixing and the volume of the interface should not be taken into account:

$$\Delta H_{app} = (1 - f)\Delta H_{F-H} \tag{A2}$$

with f representing the ratio of the interface volume and the total volume:

$$f = \frac{V_{interface}}{V_{total}}. \tag{A3}$$

ΔH_{app} is the apparent demixing enthalpy, $\Delta H_{F\text{-}H}$ is the enthalpy of demixing based on the assumption of complete L-L demixing as predicted by the Flory-Huggins theory, $V_{interface}$ is the volume of the interfacial region and V_{total} is the total volume.
The volume of the interface can be described as:

$$V_{interface} = \delta A \tag{A4}$$

with δ is the interface thickness and A the area between the two phases.
Combination of Eq. A3 and A4 gives:

$$f = \frac{\delta A}{V_{total}}. \tag{A5}$$

Assuming a cellular demixed system with a certain cell density (ρ_{cell}) and cell radius (r), then f can be written as:

$$f = 4\pi r^2 \rho_{cell} \delta. \tag{A6}$$

The heat capacity is measured with TMDSC experiments, so the contribution of f to the heat capacity is represented by the total differential of ΔH_{app}:

$$\Delta cp_{app} \cdot M = \left(\frac{d\Delta H_{app}}{dT} \right) = (1-f)\left(\frac{d\Delta H_{F-H}}{dT} \right) + \Delta H_{F-H}\left(\frac{d(1-f)}{dT} \right). \quad \text{(A7)}$$

Furthermore it is assumed that the radius of a demixed domain and the cell density are related because the total volume of the cells can not exceed the total volume of the system. i.e.:

$$\tfrac{4}{3}\pi r^3 \rho_{cell} < 1. \quad \text{(A8)}$$

A combination of Eq. A6 and A8 gives the following constraint for f:

$$f < f_{\max} = \frac{3\delta}{r}. \quad \text{(A9)}$$

The value of f is by definition always between 0 and 1. Only when f deviates significantly from 0, the influence of the interface plays a role in the measured heat capacity shift. This becomes important only at the very initial stage of demixing where r and δ have about the same size. In the following paragraphs this equation will be evaluated with respect to $T_{L\text{-}L}$ and temperature.

Influence of interface at $T_{L\text{-}L}$

For the heat capacity shift at $T_{L\text{-}L}$, the value of $\Delta H_{F\text{-}H}$ is 0 (by assuming $\phi_0 = \phi_2$ and ϕ_1 is 0 in Eq. 6 in §4.2.1). Consequently, only the first term of the right hand side of Eq. A7 plays a role. Considering the interfacial layer to comprise a couple of diluent molecules in thickness (spherical diameter of 1-dodecanol is about 0.4 nm [4]), the thickness of the interface δ will be a few nanometers. The period of one modulation in a TMDSC experiment is 60 s. From experimental data, for example [5] and [6], it appears that typical cell sizes are between 0.1 and 1 μm at demixing times of seconds. Hence, the influence of the formed interface plays only a small role in the MDSC experiment at $T_{L\text{-}L}$.

Influence of interface on Δcp as function of temperature

The influence of the interface on the heat capacity is also negligible for cooling deeper into the liquid-liquid demixing gap. Eq. A7 can be written as:

$$\Delta cp_{app} = \frac{1}{M}\left(\frac{d\Delta H_{app}}{dT}\right) = \Delta cp_{F-H}(1-f) + \frac{\Delta H_{F-H}}{M}\left(\frac{d(1-f)}{dT}\right). \quad \text{(A10)}$$

The first term of the right-hand-side of Eq. A10 has already been studied and discussed in previous paragraph and it appeared that in the initial stage of liquid-liquid demixing the influence of the interface can have a small contribution to the heat capacity shift. To investigate the influence of a deep quench, the second term of the right-hand-side of Eq. A10 has to be studied. The cell density and cell radius will change during demixing, but this are time dependent effects caused by coarsening, consequently, ρ_{cell} and r are assumed to be independent of temperature. The thickness of the interfacial layer δ is independent of the temperature as well. Hence, there is no effect of the temperature on f. From this analysis the conclusion can be drawn that within the influence of interfaces can only play a small role at the beginning of liquid-liquid demixing.

Assumption 9: Influence of cooling rate on heat capacity shift

The influence of coalescence cannot be accessed through the measurement of the specific complex heat capacity signal because according to its definition, time dependent signals like coalescence are not measured. The dependency of the specific complex heat capacity from the temperature is also proven from the following results. Using data from Chapter 3 (Fig. 6) and treat them to the algorithm described in Chapter 4 (see §4.4.2), Δcp^* is obtained as a function of the cooling rate. The results are plotted in Fig. A4 and the conclusion can be drawn that there is no significant influence of the cooling rate on the Δcp^*.

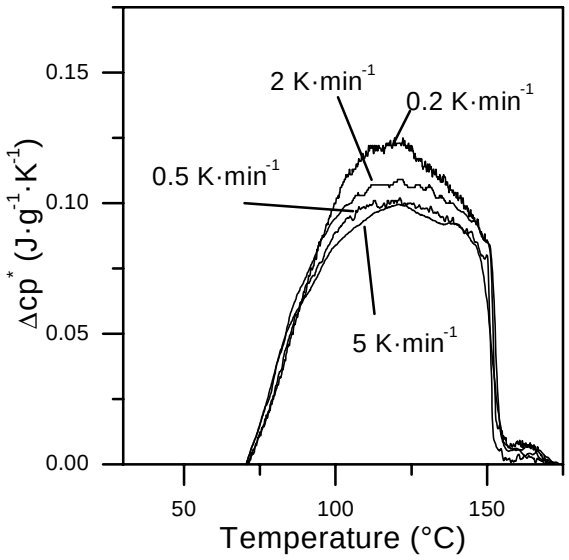

Figure A4. *Influence of cooling rate on experimental heat capacity shift (Δcp). Polymer weight fraction is 0.48.*

A4.1 List of Symbols

χ	Interaction parameter	-
δ	Thickness interface	m
ρ_{cell}	Cell density	m^{-3}
Δcp^*	Experimental heat capacity shift	$J{\cdot}g^{-1}{\cdot}K^{-1}$
$\Delta cp^*_{L\text{-}L}$	Experimental heat capacity shift at $T_{L\text{-}L}$	$J{\cdot}g^{-1}{\cdot}K^{-1}$
Δcp_{app}	Apparent heat capacity	$J{\cdot}g^{-1}.K^{-1}$
$\Delta cp_{F\text{-}H}$	Heat capacity according to Flory-Huggins theory	$J{\cdot}g^{-1}{\cdot}K^{-1}$
ΔH_{app}	Apparent enthalpy of demixing	$J{\cdot}mol^{-1}$
$\Delta H_{F\text{-}H}$	Enthalpy of demixing according to Flory-Huggins theory	$J{\cdot}mol^{-1}$
ϕ_i	Volume fraction component i	-
ρ_i	Density component i	$kg{\cdot}m^{-3}$
ϕ_j	Volume fraction polymer at binodal	-
A	Area interface	m^2
a	Empirical parameter	-
b	Empirical parameter	K
f	Ratio volume interface and total volume	-
f_{max}	Maximum ratio volume interface and total volume	-

M	Molecular mass of one lattice site	$g \cdot mol^{-1}$
M_i	Molecular mass component i	$g \cdot mol^{-1}$
N	Ratio N_p/N_d	-
N_i	Number of lattice sites occupied by component i	-
r	Cell radius	m
R	Gas constant	$J \cdot mol^{-1} \cdot K^{-1}$
T	Temperature	K
T_g	Glass temperature solution	K
T_{L-L}	Liquid-liquid phase separation temperature	K
v	Specific volume	$m^3 \cdot kg^{-1}$
v_i	specific volume component i	$m^3 \cdot kg^{-1}$
$V_{interface}$	Volume interface	m^3
V_{total}	Total volume	m^3
w_i	Weight fraction component i	-

Remarks to the table: when necessary °C has been used instead of K.
The superscript (*) denotes an experimentally measured heat capacity

Subscripts

i	p	Polymer
	d	Diluent
j	0	Starting solution
	1	Diluted branch binodal
	2	Concentrated branch binodal

A4.2 References

1. Brandrup, J., and Immergut, E.H., *Polymer Handbook*. 3th. ed, New York: John Wiley & sons (1989)
2. Arnauts, J., and Berghmans, H., *Amorphous thermoreversible gels of atactic polystyrene*, Polymer Communications, 28, p. 66-68 (1987)
3. Koningsveld, R., *On liquid-liquid phase relationships and fractionation in multicomponent polymer solutions* ,PhD thesis University of Leiden, Leiden (1967)
4. Daubert, T.E., Danner, R.P., Sibul, H.M., and Stebbins, C.C., *Physical and thermodynamic properties of pure chemicals. Data compilation*. , Pennsylvania: Taylor&Francis (1989)
5. Tsai, F.J., and Torkelson, J.M., *Roles of phase separation mechanism and coarsening in the formation of poly(methyl methacrylate) asymmetric membranes*, Macromolecules, 23, p. 775-784 (1989)
6. Graham, P.D., Pervan, A.J., and McHugh, A.J., *The dynamics of thermal-induced phase separation in PMMA solutions*, Macromolecules, 30, p. 1651-1655 (1997)

Appendix 4B

Physical significance of the interpolated heat capacity cp^*_i

In literature, experimentally obtained TMDSC data for polymers and polymer blends are often fitted to earlier published heat capacity values by shifting the TMDSC curve [1]. Typical regions used for the curve shifting are the glassy or rubbery state in which no transitions are observed nor expected. This procedure has not been applied in this study. The system considered here comprises two materials and in fact it is difficult to find experimental data for this mixture. The remaining question of the physical relevance of the interpolation by the polynomial will be answered by comparing the polynomial fit (cp^*_i) with a linear mixing rule-base model resulting in cp_{th}. The model to predict the theoretical heat capacity makes use of the heat capacity of the single components (cp_p [2] and cp_d [3]) and the weight fraction of polymer (w_p) according to:

$$cp_{th} = w_p.cp_p + (1 - w_p).cp_d \,. \qquad \text{(B1)}$$

This analytical form is a simple, linear mixing rule and is frequently used to determine the heat capacity of a semi-crystalline system composed of a pure crystalline contribution and a pure amorphous contribution assuming that no excess transitions take place [4]. It has been used as well to determine the heat capacity of polymer solutions [5]. Using the temperature-dependent values of the pure components heat capacity, Eq. B1 results in the theoretical heat capacity cp_{th} of the mixture as a second order polynomial ($p_{th}T^2+q_{th}T+r_{th}$). A calculation example for a solution consisting of 31 vol.% of polymer is shown in Table B1.

Now that I have established algorithms to estimate the interpolated heat capacity cp_i and to calculate a theoretical cp_{th} (it should be realized that the heat effects due to demixing are excluded), a comparison can be carried out.

Table B1: *Values theoretical heat capacity of polystyrene and 1-dodecanol.*

$\mathbf{cp_{th} = pT^2+qT+r}$	**aPS**	**1-dodecanol**	**Example for ϕ_0 = 0.31**
p_{th} ($J \cdot g^{-1} \cdot K^{-3}$)	-	$-2.79.10^{-5}$	$-1.74.10^{-5}$
q_{th} ($J \cdot g^{-1} \cdot K^{-2}$)	$2.55.10^{-3}$	$1.04.10^{-2}$	$7.42.10^{-3}$
r_{th} ($J \cdot g^{-1} \cdot K^{-1}$)	1.61	2.10	1.91

One possibility is to compare the absolute values of the heat capacities at a certain temperature; it is also possible to compare the polynomial coefficients. The latter is important for the following reason: the absolute values of the heat capacity at $T_{L\text{-}L}$ may well coincide by both the interpolated cp_i as well by the theoretical cp_{th}, but the curvature of both lines do not. To quantify both comparison methods I will introduce deviation measures. These deviation measures may be interpreted as the relative error of the interpolated heat capacity to the theoretical heat capacity, but since it is uncertain whether the theoretical curve describes real systems accurately, I prefer to use the term deviation measure instead of relative error. From experimental data, plotted in Fig. B1, the value of the deviation measures and the calculation procedure will be explained.

Deviation 1 (*D1*) is a straight forward comparison of the exact values of cp_i and the theoretical value cp_{th} at $T_{L\text{-}L}$, see Fig. B1:

$$D1 = \frac{cp_{th} - cp_i^*}{cp_i^*} \; at \; T_{L\text{-}L} \qquad \text{(B2)}$$

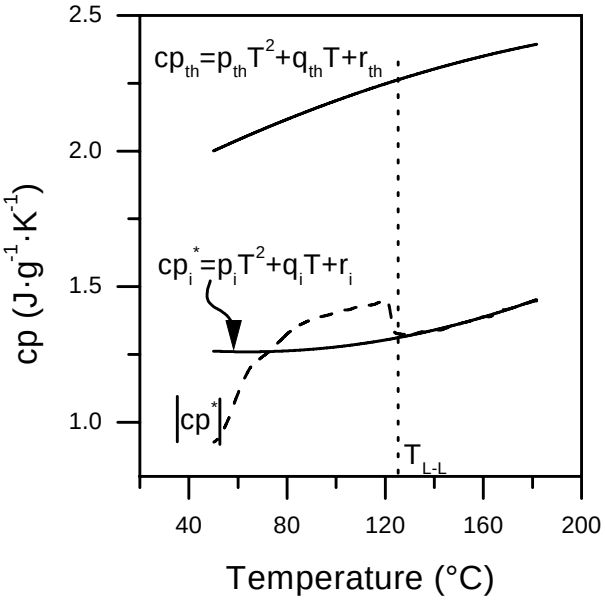

Figure B1. *Interpolated heat capacity (cp^*_i) determined from complex heat capacity ($|cp^*|$) compared with the theoretical heat capacity (cp_{th}). The vertical dotted line represents $T_{L\text{-}L}$, the temperature for which the deviation measures will be determined. Deviation 1 is the relative difference between the values for cp^*_i and cp_{th} at $T_{L\text{-}L}$. Deviation 2 is the relative difference between the values of the polynomial coefficients between cp_{th} and cp^*_i. The volume fraction of polymer is 0.61.*

Deviation 2 (*D2*) is calculated from the absolute difference in polynomial coefficients of both the interpolated curve and the theoretical curve: $\varepsilon(p) = |p_i - p_{th}|$, $\varepsilon(q) = |q_i - q_{th}|$ and $\varepsilon(r) = |r_i - r_{th}|$ (see Fig. B1). With these differences in polynomial coefficients the influence on the heat capacity difference at $T_{L\text{-}L}$ can be calculated according to:

$$\varepsilon(cp_{coeff}) = \varepsilon(p)T_{L\text{-}L}^2 + \varepsilon(q)T_{L\text{-}L} + \varepsilon(r). \qquad \text{(B3)}$$

Hence, *D2* is defined as:

$$D2 = \frac{\varepsilon(cp_{coeff})}{cp_i^*} \text{ at } T_{L\text{-}L}. \qquad \text{(B4)}$$

For polymer concentrations of 31 and 61 vol.%, the calculation procedure of both the deviation measures have been summarized in Table B2.

D2 is always positive by definition and *D1* can be either positive or negative. Also by definition *D1* can never exceed *D2*. It can be observed from Table B3 that at polymer concentrations up to 40 vol.%, cp^*_i and cp_{th} coincide well. At polymer concentrations of about 60 vol.% the deviation between cp^*_i and cp_{th} is quite large. Until now, it is unclear why this difference between theoretical and the experimental heat capacity is that large.

Table B2. *Calculation of deviation measures for two experiments at polymer volume fractions of 0.31 and 0.61.*

Polymer volume fraction			$\phi_0 = 0.31$ ($T_{L\text{-}L} = 164°C$)	$\phi_0 = 0.61$ ($T_{L\text{-}L} = 124°C$)
Deviation 1	cp at $T_{L\text{-}L}$	interpolated	3.14	1.31
		theoretical	2.66	2.26
	Deviation 1 (%)		-15	72
Deviation 2	p ($\cdot 10^{-5}$)	interpolated	-1.88	1.39
		theoretical	-1.73	-0.89
	q ($\cdot 10^{-3}$)	interpolated	9.05	-1.78
		theoretical	7.39	5.05
	r	interpolated	2.16	1.32
		theoretical	1.91	1.77
	Deviation 2 (%)		18	126

In Table B3, both the deviation measures are listed for all the experimental curves:

Table B3. *Deviation of experimental and theoretical results. Second column: D1 determined from Eq. B2. Third column: D2 determined from Eq. B4.*

Polymer volume fraction	D1 (%)	D2 (%)
0.06	47	81
0.10	-16	16
0.20	-17	17
0.21	-10	13
0.31	-15	18
0.31	-10	27
0.39	44	77
0.40	2	12
0.59	11	96
0.61	72	126
0.62	-2	40
0.67	71	122
0.76	8	13

B4.1 List of symbols

$\varepsilon(...)$	Error in ...	
ϕ_0	Volume fraction polymer	-
$\lvert cp^* \rvert$	Specific complex heat capacity	$J \cdot g^{-1} \cdot K^{-1}$
cp^*_i	Interpolated heat capacity	$J \cdot g^{-1} \cdot K^{-1}$
cp_d	Heat capacity diluent	$J \cdot g^{-1} \cdot K^{-1}$
cp_p	Heat capacity polymer	$J \cdot g^{-1} \cdot K^{-1}$
cp_{th}	Theoretical heat capacity	$J \cdot g^{-1} \cdot K^{-1}$
D1	Deviation 1 (Eq. B2)	-
D2	Deviation 2 (Eq. B4)	-
p_i	Coefficient cp^*_i polynom	$J \cdot g^{-1} \cdot K^{-3}$
p_{th}	Coefficient cp_{th} polynom	$J \cdot g^{-1} \cdot K^{-3}$
q_i	Coefficient cp^*_i polynom	$J \cdot g^{-1} \cdot K^{-2}$
q_{th}	Coefficient cp_{th} polynom	$J \cdot g^{-1} \cdot K^{-2}$

r_i	Coefficient cp^*_i polynom	$J \cdot g^{-1} \cdot K^{-1}$
r_{th}	Coefficient cp_{th} polynom	$J \cdot g^{-1} \cdot K^{-1}$
T	Temperature	K
T_{L-L}	Liquid-liquid demixing temperature	K
w_p	Weight fraction polymer	-

Remarks to the table: when necessary °C has been used instead of K.

B4.2 References

1. Jones, K.J., Kinshott, I., Reading, M., Lacey, A.A., Nikolopoulos, C., and Pollock, H.M., *The origin and interpretation of the signals of MTDSC*, Thermochimica Acta, 304/305, p. 187-199 (1997)
2. Wunderlich, B., *ATHAS Databank, http://web.utk.edu/~athas/databank/intro.html* (2000)
3. Daubert, T.E., Danner, R.P., Sibul, H.M., and Stebbins, C.C., *Physical and thermodynamic properties of pure chemicals. Data compilation*. , Pennsylvania: Taylor&Francis (1989)
4. Mathot, V.B.F., *Calorimetry and thermal analysis of polymers*. 1. ed, Munich: Hanser Publishers (1994)
5. Johansson, G., Joelsson, M., and Bastos, M., *Some physical measurements in the one-phase region of a water-dextran-poly(ethylene glycol) system*, Polymer, 33, p. 152-155 (1992)

Chapter 5

Diluent crystallization and melting in a liquid-liquid demixed and vitrified polymer solution

Abstract

Upon cooling the polymer-diluent system atactic polystyrene - 1-dodecanol, the diluent crystallizes after liquid-liquid demixing and vitrification. A crystallization temperature depression is observed experimentally. Such a temperature depression is frequently related to the size of a confinement in which the diluent crystallizes and this can be described with the Gibbs-Thomson equation. The possibility of a depressed crystallization temperature of 1-dodecanol in a confinement is rejected by comparing the crystallization and melting behavior of 1-dodecanol using inert ceramic porous materials. From scanning electron microscopy pictures of the demixed polymer-diluent system, a porous structure in the nanometer range is observed in the polymer-rich phase. This secondary diluent phase may originate from a supersaturated polymer-rich phase. Polymorphs of 1-dodecanol are formed upon cooling as well, which leads to a contribution to the DSC signals and X-ray patterns.

5.1 Introduction

In Chapter 3 and 4, liquid-liquid demixing and vitrification of a polymer – diluent system were studied using temperature modulated differential scanning calorimetry (TMDSC). The investigated polymer – diluent system showed liquid-liquid demixing upon cooling, followed by vitrification of the polymer-rich phase. Hence, a polymer-rich matrix was obtained with regions of the polymer-lean phase inside. From the demixing and vitrification behavior of atactic polystyrene (aPS) – 1-dodecanol, the phase diagram, plotted in Fig. 1, could be constructed.

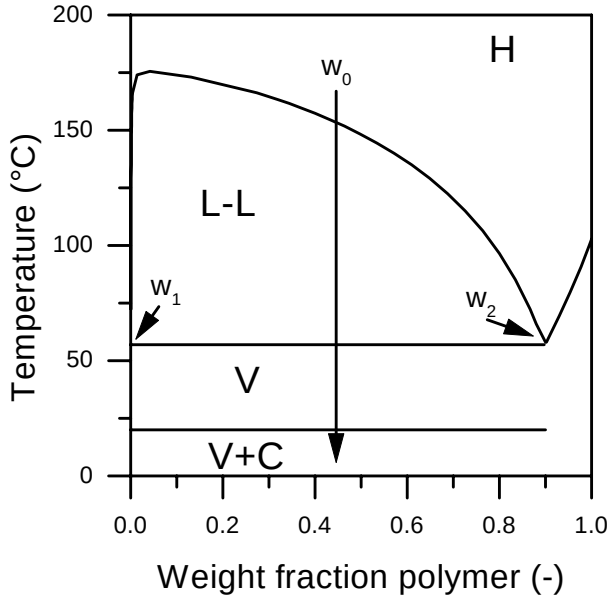

Figure 1. *Phase diagram of aPS in 1-dodecanol. Four different phases can be defined: The homogeneous solution (H), liquid-liquid demixing (L-L), vitrification of polymer-rich phase (V) and crystallization of the diluent (C). The weight fraction of the polymer in the polymer-lean phase (w_1), the polymer-rich phase (w_2) and the polymer concentration in the solution (w_0) are given as well. A typical cooling route is drawn with the long black arrow.*

In the TMDSC experiments described in Chapter 4, I found a contribution of the heat capacity shift upon cooling in the liquid-liquid demixing gap less than predicted from thermodynamic equilibrium. It was hypothesized that the polymer-rich phase remains supersaturated with diluent. This chapter aims to prove this hypothesis and

to further characterize the crystallization and melting behavior of the diluent in the polymer-lean phase and polymer-rich phase.

Tsai *et al.* [1] studied the melting behavior of sulfolane from a PMMA-sulfolane solution after a fast quench (160 $K \cdot min^{-1}$) with DSC experiments. They observed two melting peaks, which they explained to be caused by the melting of diluent in the polymer-rich phase and the polymer-lean phase. They also hypothesized that equilibrium concentrations were not reached in the time frame of their experiments. However, the authors mentioned this observation without any further analysis. To my knowledge no detailed work has been carried out to analyze the crystallization and melting behavior of the diluent of a liquid-liquid demixed solution.

This chapter has the following outline:

- §5.2 quantifies the DSC experiments on the crystallization and melting enthalpies as a function of the polymer concentration. The onset temperatures of a variety of melting and crystallization peaks are extracted. A depression in crystallization temperatures is found but the origin remains unclear at this point. There might be two reasons for this behavior: polymorphism of the diluent or a crystallization point depression due to crystallization in a confinement.
- A heat balance of the crystallizing system reveals that only the diluent stemming from liquid-liquid demixing crystallizes (§5.3). The diluent molecules dissolved in the polymer-rich phase do not crystallize.
- §5.4 describes the crystallization and melting behavior of 1-dodecanol in inert inorganic porous structures to further narrow down the physical origin of the melting and crystallization point depression.
- Motivated by the presence of confinement effects on the crystallization of 1-dodecanol in inorganic nanopores, a detailed electron microscopy study indeed revealed nanopores inside the cell walls (§5.5).
- The hypothesis of polymorphism is tested experimentally by temperature-dependent X-ray diffraction (§5.6).

5.2 Differential scanning calorimetry of crystallization and melting of 1-dodecanol in a liquid-liquid demixed and vitrified polymer solution

5.2.1 Experimental

Atactic polystyrene (aPS, Styron* 686E, kindly supplied by Dow Benelux NV, M_w and poly-dispersity: $2.3 \cdot 10^5$ g.mol^{-1} and 2.1 respectively, determined with GPC) and 1-dodecanol (purity >98%, Merck-Schuchardt) were used without further purification.

A homogeneous solution of aPS and 1-dodecanol was prepared in a three-neck bottle under nitrogen at 200°C. 1-Dodecanol vapor was allowed to evaporate. Small amounts of different polymer concentrations were poured in Petri-dishes and cooled down in air. The compositions of the samples were determined by subsequent thermogravic analysis. About 20 mg of the sample was inserted within a platinum sample pan of a TGA 2950 Thermogravic Analyzer of TA Instruments and heated up to 200°C with a heating rate of 10 K·min^{-1}. Afterwards the temperature was kept constant at 200°C for maximum 2 hours. Using the experimental relationship of weight as a function of time, the weight fraction of polymer and diluent could be quantified.

A DSC 2920 of TA Instruments was used to study the polymer-diluent system. About 5 mg of the sample was put in an aluminum closed sample pan. This was heated to 200°C and kept at this temperature for 5 minutes to ensure homogeneity. Samples were cooled down to 0°C and subsequently heated at a cooling rate of 2 K·min^{-1}. The temperature modulated differential scanning calorimetry (TMDSC) option was used, because the experimental results described in this chapter were obtained from the same experiments measuring the liquid-liquid demixing transition as described in Chapter 3 and 4. The modulation period was 60 s and the amplitude was 1 K. The information obtained from the TMDSC experiments, described in this chapter, can be compared to the heat flow measured with conventional DSC experiments. Details about the handling of the polymer-diluent sample and the use of TMDSC were given in Chapter 3.

The DSC results described in §5.2.1 to §5.2.3 were all determined on a MDSC2920 of TA Instruments in the TMDSC option. The experiments described at the end of this paragraph (§5.2.4) and in §5.4 were carried out on a conventional

DSC7 from Perkin Elmer. In spite of the difference in operation (modulated option versus conventional DSC) and the difference between a power compensation DSC (PE) and heat flux DSC (TA) [2], comparable DSC-curves are obtained and the same onset temperatures can be observed.

5.2.2 Definition of crystallization and melting peaks in a demixed polymer solution.

Fig. 2 shows the crystallization and melting curve of a solution of 48 wt.% aPs in 1-dodecanol. The locations of the onset temperatures were determined by linear extrapolation of the baseline and the maximum slope of the peak (see Fig. 2).

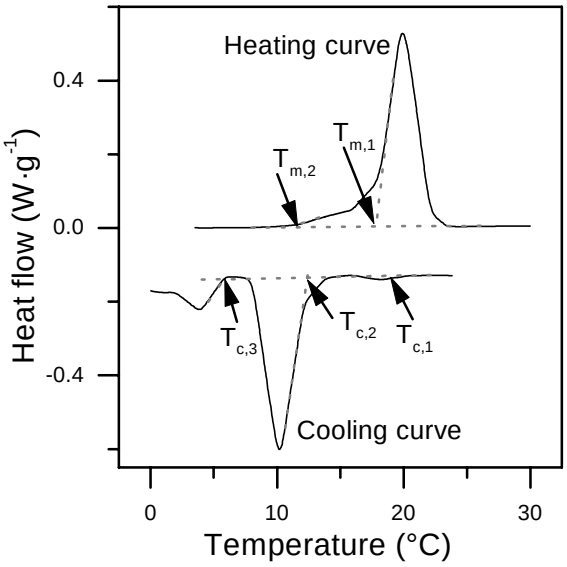

Figure 2. *Cooling and heating curves of a solution of 48 wt.% aPS in 1-dodecanol.*

One large melting peak is observed in the heating curve, the extrapolated onset of this peak is defined as $T_{m,1}$. A small heat flow signal is observed at a lower temperature. The onset of this peak is called $T_{m,2}$. Three crystallization peaks are observed in the cooling curve with the onset temperatures: $T_{c,1}$, $T_{c,2}$, and $T_{c,3}$, respectively.

5.2.3 Influence of the polymer concentration on the depression temperature

Cooling and heating curves of aPS – 1-dodecanol mixtures with varying aPS concentrations are plotted in Fig. 3a and 3b.

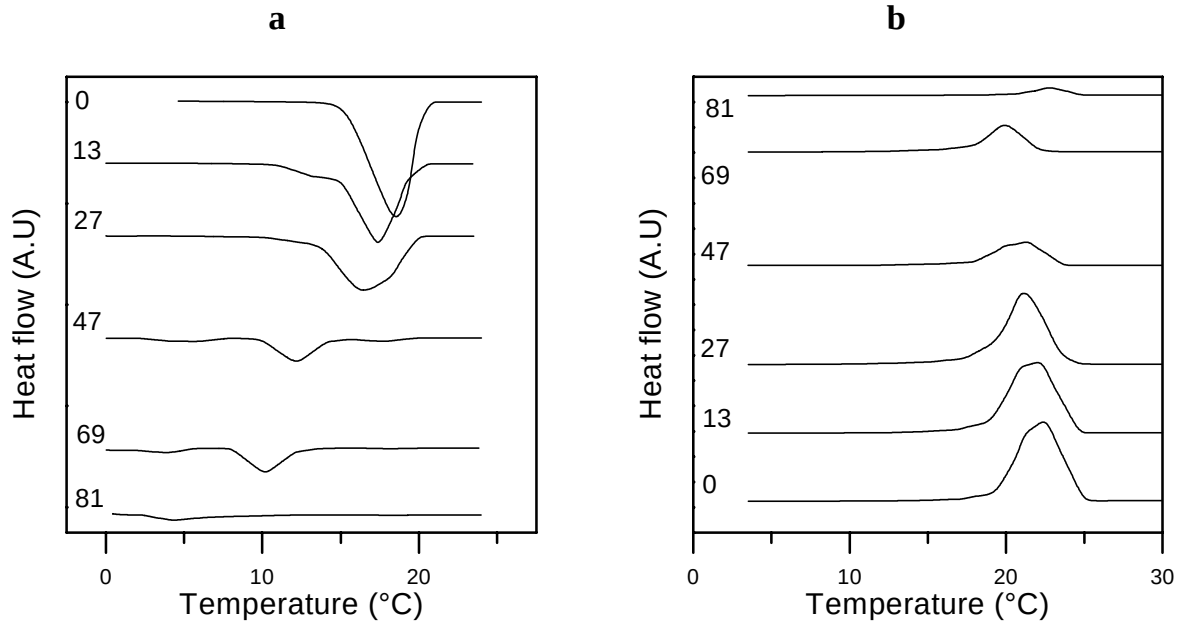

Figure 3. *Cooling curves (3a) and heating curves (3b) of 1-dodecanol for different polymer concentrations. The numbers indicate the weight percentage of polymer in the sample.*

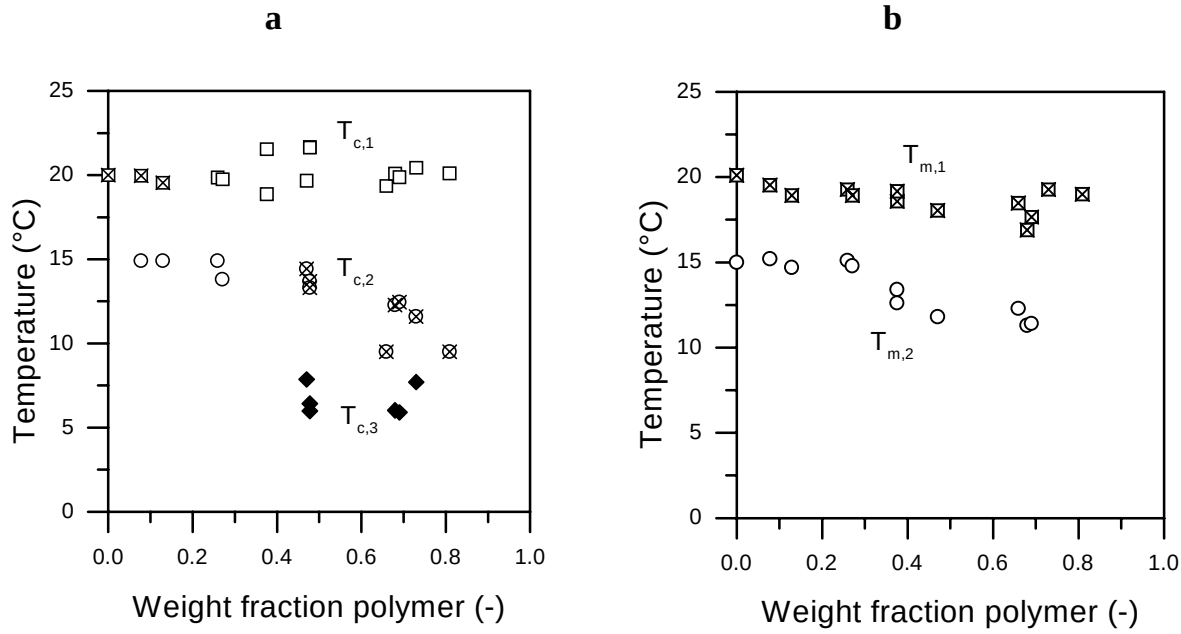

Figure 4. *Onset temperature observed in the cooling curves (4a) and heating curves (4b). A cross (x) within a data point represents the peak with the largest enthalpy.*

First of all, one can clearly observe in Fig. 3a and 3b that the peak sizes decrease with increasing polymer concentration. This is caused by the decreasing amount of solvent in the sample. This observation will be further quantified in §5.3. In the cooling curves (Fig. 3a), the location of the largest peak shifts to lower temperatures with increasing polymer concentration. Furthermore, a new small peak is formed ($T_{c,3}$ in Fig. 2) at polymer concentrations above 47 wt.%. The heating curve (Fig. 3b) hardly shows any shift of the peaks. Fig. 4a and 4b summarize the onset temperatures observed in the cooling curves (Fig. 3a) and the heating curves (Fig. 3b), as a function of the polymer concentration.

A cross in the data point denotes the onset temperature with the largest enthalpy change as observed in the DSC-curve. This indicates that the peak with the onset temperature $T_{m,1}$ remains the largest peak in the heating curve (Fig. 4b). The location of $T_{m,1}$ is constant over the entire polymer concentration range. $T_{m,2}$ shifts slightly to lower temperatures with an increasing polymer concentration.

Also during crystallization (Fig. 4a), $T_{c,1}$ remains constant over the entire concentration region. The enthalpy of the peak belonging to $T_{c,1,}$ however, decreases relatively faster with increasing concentration than the second peak with onset temperature $T_{c,2}$. Therefore, at low polymer concentrations (<13 wt.%) the largest peak belongs to $T_{c,1}$, while the largest peak is located at $T_{c,2}$ at polymer concentrations higher than 47 wt.%. Since the shift of the largest peak from location $T_{c,1}$ to $T_{c,2}$ is gradual, no datapoint for $T_{c,2}$ is observed for the experiment at 38 wt.%. For this concentration, one diffuse peak is observed because of an overlap of the peaks belonging to both $T_{c,1}$ and $T_{c,2}$. Furthermore, at a concentration of 27 wt.%, the magnitude of the enthalpies of peak $T_{c,1}$ and $T_{c,2}$ were equal, so no largest peak could be defined. $T_{c,3}$ is observed at polymer concentrations above 47 wt.% and its value is independent of polymer concentration.

An explanation for the observed crystallization and melting behavior will be discussed in the next paragraphs.

5.2.4 Influence of the experimental conditions on the DSC results

In this paragraph the influence of the experimental conditions on the DSC results will be discussed. This paragraph aims to establish a sound experimental basis for further discussion of the physical phenomena. The cooling or heating rate can influence the crystallization or melting behavior. It is, for example, known that the difference between the melting and crystallization point of polymers can be in the

order of magnitude of 10 K and that it strongly depends on the cooling rate [3]. For low molecular substances it is less common to observe such a large difference between the melting and crystallization point. The crystallization of a 48 wt.% aPS – 1-dodecanol solution is characterized at different cooling rates and heating rates to study the influence of the cooling and heating rate in my system. Furthermore, a second cooling experiment was carried out in the solid phase of 1-dodecanol to study transitions where no crystallization of 1-dodecanol is expected to occur.

5.2.4.1 Influence cooling and heating rate

Experiments with cooling rates up to 50 K·min^{-1} show that the onsets of the observed peaks slightly shift to lower temperatures (see Fig. 5). This is an indication that supercooling only has a small effect. The peak belonging to $T_{c,3}$ is not observed at a cooling rate of 50 K·min^{-1}, probably because of the overlap with the large peak belonging to $T_{c,2}$.

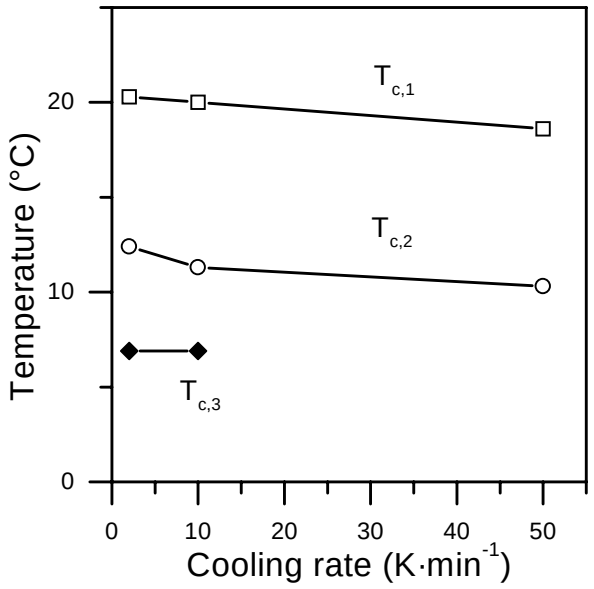

Figure 5. *Onset temperatures of crystallization peaks of a 48 wt.% aPs in 1-dodecanol solution. Lines are drawn to guide the eye.*

Heating curves (not shown) showed no difference in onset temperatures between the experiments at 2 and 10 K·min^{-1}. The experiment with a heating rate of 50 K·min^{-1} showed the same peaks as the 2 K·min^{-1} and 10 K·min^{-1} experiments. However, the onset temperatures were about 1 K higher. From these experiments it can be concluded that the influence of the cooling or heating rate is negligible for the first

peaks ($T_{c,1}$ and $T_{m,2}$) and the second peaks ($T_{c,2}$ and $T_{m,2}$). The peak belonging to $T_{c,3}$ is not observed when applying a cooling rate of 50 K·min^{-1}. This is explained by the overlap of the peak belonging to $T_{c,2}$ and $T_{c,3}$.

5.2.4.2 Results second cooling run between 20 and –10°C.

Subsequent to the normal cooling run, an experiment was carried out in which after a cooling trajectory (down to –10°C), the sample was heated up to 20°C, just below the melting point and cooled down again. The results are plotted in Fig. 6.

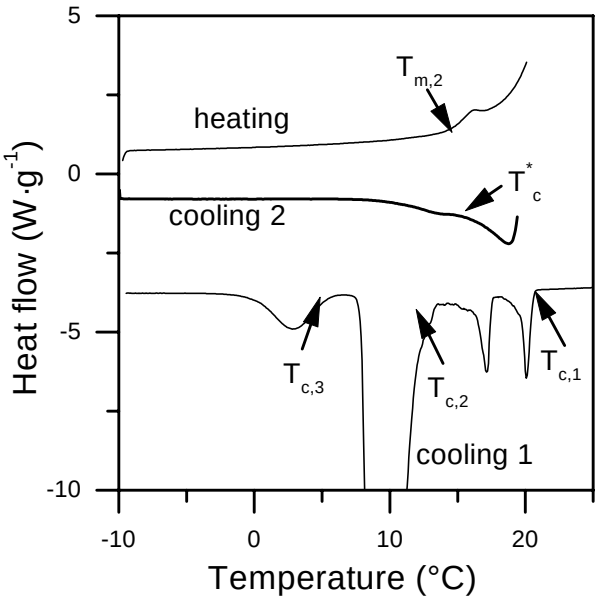

Figure 6. *DSC curves of a solution of 48 wt.% aPS in 1-dodecanol. The first and second cooling curve are plotted as well as the heating curve.*

The locations of the onsets (defined in Fig.2) are plotted in Fig. 6: $T_{c,1}$, $T_{c,2}$ and, $T_{c,3}$ in the first cooling curve, and $T_{m,2}$ in the subsequent heating curve. In the first cooling curve, an extra transition is observed between $T_{c,1}$ and $T_{c,2}$. This can be explained by the difference in the DSC instruments which were used. Both peaks belong to the first peak in Fig. 2 having the onset temperature $T_{c,1.}$ The resolution of the PE-DSC experiment is better, resulting in the observation of two peaks.

The second cooling curve only shows a small transition at about T^*_c = 15°C. The location of T^*_c is the same as $T_{m,2}$ in the heating curve. The enthalpies of both peaks are comparable as well. This is an indication of a reversible transition at said temperature. An explanation of this small peak can be the presence of impurities in

the diluent. This seems unlikely because literature states that the main impurity in 1-dodecanol is 1-decanol having a melting point of 7°C. There is no apparent heat effect at 7°C and it can be concluded that the peaks at 15°C are not from an impurity with a smaller concentration than the major impurity.

The peak appearing at $T_{c,3}$ in the first cooling curve does not show a melting peak with a comparable size in the subsequent heating curve. Hence there is no $T_{c,3}$ in a second cooling run. However, $T_{c,3}$ appears in a second cooling run after heating well above $T_{m,1}$ (data not showed).

5.3 Enthalpy of crystallization and melting of 1-dodecanol in the demixed domains

5.3.1 Theory and results

In the case of liquid-liquid demixing of a binary system of polymer and diluent, a polymer- rich part and a polymer-lean part are obtained. The absolute magnitude of the enthalpy of crystallization or melting is an indication of the fraction of diluent that undergoes the solid-liquid phase transition. For the theoretical calculation of the total enthalpy in relation to the initial concentration of 1-dodecanol, two possible explanations can be proposed. In model 1 it is assumed that a linear relationship exists between the measured melting enthalpy and the overall diluent concentration. Model 2 proposes a linear relation between the melting enthalpy and the diluent concentration in the polymer-lean phase only. From the slope and intersection of the linear fit of the measured enthalpy versus polymer concentration (w_0), the most appropriate physical model can be deduced.

Model 1

The crystallization or melting enthalpy depends linearly on the total concentration of diluent in the sample. Eq. 1 implies that both the diluent in the polymer-lean phase and polymer-rich phase will crystallize upon cooling. This can be written as:

$$\Delta H_m = \Delta H_{dil} - \Delta H_{dil} w_0 \qquad (1)$$

where ΔH_m is the measured enthalpy of melting, ΔH_{dil} the melting enthalpy of the pure diluent and w_0 the polymer weight fraction. To use the crystallization data instead of the melting data, the enthalpy of melting has to be replaced by the enthalpy of crystallization. Plotting ΔH_m versus w_0 would result in a line in which $\Delta H_m = 0$ at $w_0 = 1$. Fig. 7b shows that $\Delta H_m = 0$ at $w_0 = 0.84$. This experimental observation is sufficient to exclude model 1.

Model 2

The crystallization or melting enthalpy depends linearly on the concentration of diluent in the polymer-lean phase. Diluent in the polymer-rich phase forms a homogeneous phase with the polymer and is not able to crystallize. By assuming a mono-disperse polymer, the lever rule can be used to determine the mass of both the polymer-rich phase (m_{rich}) and polymer-lean phase (m_{lean}):

$$m_{tot} \cdot \frac{w_2 - w_0}{w_2 - w_1} = m_{lean} \tag{2}$$

$$m_{tot} = m_{lean} + m_{rich} . \tag{3}$$

w_1 and w_2 are the weight fractions of polymer in the polymer-lean phase and polymer-rich phase respectively, m_{tot} is the total mass of the polymer solution. The mass of diluent in the polymer-lean phase ($m_{diluent,lean}$) can be calculated according to:

$$m_{diluent,lean} = m_{lean}(1 - w_1) . \tag{4}$$

By substitution of m_{lean} in Eq. 3, Eq. 5 is obtained:

$$\frac{m_{diuent,lean}}{m_{tot}} = \frac{w_2 - w_0}{w_2 - w_1}(1 - w_1) . \tag{5}$$

Multiplying both the left and right hand side of Eq. 5 with the melting enthalpy of the pure diluent (ΔH_{dil}) and assuming $w_1 = 0$, a relation is obtained between the measured melting enthalpy and the concentration of the different phases:

$$\Delta H_m = \Delta H_{dil} - \frac{\Delta H_{dil}}{w_2} w_0 . \qquad (6)$$

Plotting ΔH_m versus w_0 gives the values of ΔH_{dil} and w_2.

The total crystallization enthalpy (obtained from Fig. 3a) as a function of the weight fraction of polymer is plotted in Fig. 7a. The melting enthalpy (obtained from Fig. 3b) is plotted in Fig. 7b

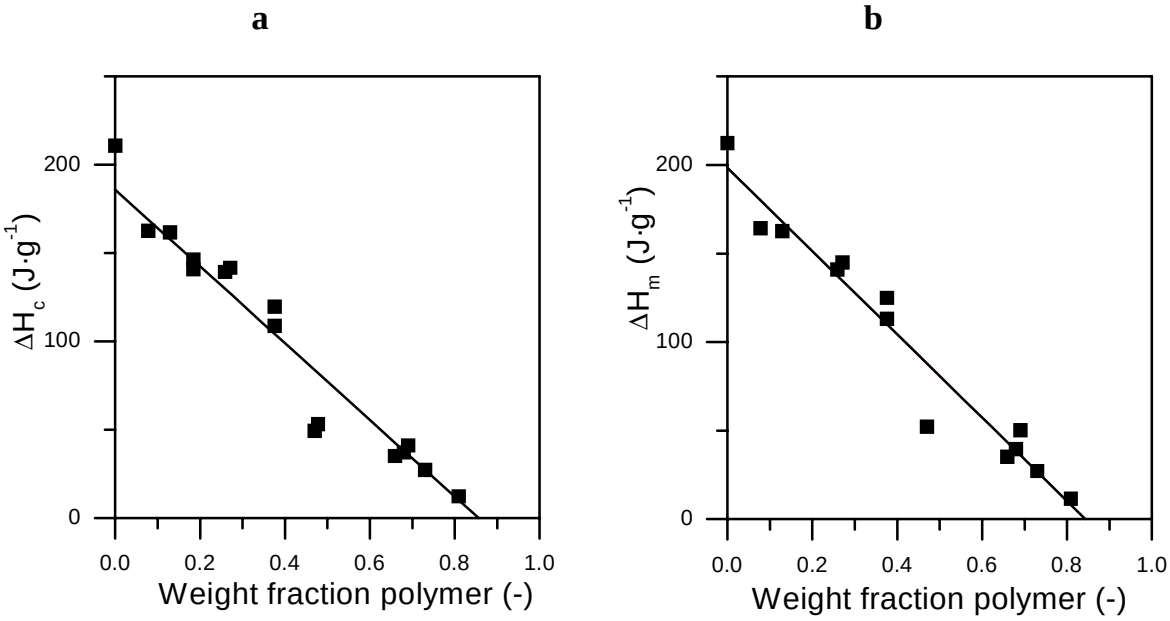

Figure 7. *Enthalpy of crystallization (7a) and melting (7b) of aPs in 1-dodecanol.*

Fig. 7a and 7b show that no crystallization or melting occurs for polymer weight fractions higher than $w_2 \approx 0.85$. The value of w_2 can also be determined from the intersection of the binodal with the glass transition temperature depression (Berghmans point [4]). Chapter 4 quantified this to be $\phi_2 = 0.83$ or $w_2 = 0.88$. The extrapolated value of w_2 from model 2 (= 0.86 for crystallization and 0.84 for melting) is in good agreement with the value of the Berghmans point deduced from the phase diagram.

5.3.2 Conclusions

From the results presented above, it can be concluded that the shift of the peaks with the largest enthalpies (peaks belonging to $T_{m,1}$ and $T_{c,1}$ or $T_{c,2}$ in the heating and cooling curves respectively) stem from the diluent in the polymer-lean phase. The

amount of diluent able to crystallize is determined by the Berghmans point. Diluent in the polymer-rich phase, molecularly dispersed in the polymer, causes a glass transition temperature depression but does not crystallize. This conclusion is valid assuming equilibrium concentrations in both the polymer-lean phase and polymer-rich phase. In Chapter 4 however, it is hypothesized that the equilibrium concentrations are not reached. Hence, it is possible that an additional small amount of 1-dodecanol is present in the polymer-rich phase leaving it supersaturated. Whether the enthalpy of the small peak in the crystallization curve (peak $T_{c,3}$) is caused by the diluent in the polymer-lean phase or polymer-rich phase can not be deduced from this paragraph.

5.4 Crystallization and melting temperature depression of 1-dodecanol confined in inorganic porous materials

§5.2 showed a difference between crystallization peaks of 1-dodecanol in a polymer-rich matrix and the crystallization peaks of pure 1-dodecanol. One of the possible reasons for such a temperature depression may be the confinement of 1-dodecanol inside a porous material. In this paragraph the crystallization and melting behavior of 1-dodecanol in a confinement will be systematically studied using inorganic porous materials with well defined pore sizes.

5.4.1 Theoretical background

The melting point depression of a confined substance can be described with the Gibbs-Thomson equation:

$$\Delta T_m = \frac{2\gamma_{S-L} T_m v_l}{r \Delta H_m} \qquad (7)$$

with $\gamma_{S\text{-}L}$ being the interfacial tension of the diluent between solid and liquid, r the cell radius , ΔH_m the enthalpy of melting, T_m the melting point, and v_l the specific liquid volume at the melting point. Eq. 7 can also be used to describe the crystallization point depression.

Experimentally, a linear dependency of the inverse of the pore radius with the melting point depression has been observed for water [5-7] and organics [8]. Brun *et al.* [9] derived equations for the temperature depression of water and benzene and used this concept to characterize pores and pore size distributions of porous materials. This experimental technique is called thermoporometry. Appendix 5 describes the comparison of the Gibbs-Thomson model (Eq. 7) with other models and reported experimental data. In the following paragraphs, the melting and the crystallization behavior will be studied of 1-dodecanol impregnated into inorganic porous materials with known pore sizes.

5.4.2 Experimental

Inorganic α-Al_2O_3 and γ-Al_2O_3 membranes, with average pore radii of 80, 40 (α-Al_2O_3) and 8.7 nm (γ-Al_2O_3) [10] (kindly supplied by A. Nijmeijer and S. de Lint of the Inorganic Material Science group of the University of Twente), and Vycor glass with a pore radius of 2 nm (kindly supplied by Dow Corning) were used as reference material. The inorganic films were broken and immersed in 1-dodecanol at T = 30°C for at least one day to fill the pores. This direct way of filling the pores appeared to be sufficient because the melting and crystallization peaks at large temperature depressions were observed in the reference materials with a pore radius of 2 and 9 nm. Furthermore, Rennie *et al.* [6] observed no difference between direct filling and filling after evacuation with experiments of water in silica gel.

The materials were analyzed using a Perkin Elmer DSC7. About 10 mg of the sample (inorganic material + 1-dodecanol) was placed in an aluminum closed sample pan. The sample pan was heated to a temperature of 35°C and cooled to -15°C. Subsequent cooling and heating runs were carried out with different temperatures rates (2 and 10 $K \cdot min^{-1}$). The extrapolated onset of the first cooling and heating run is used to characterize the pore sizes. No difference was observed in the onset temperatures in comparison with the subsequent runs.

5.4.3 Results of 1-dodecanol confined in inorganic materials

Fig. 8 shows the results of cooling experiments for 1-dodecanol in inorganic porous reference materials. The DSC curve belonging to the cooling of the pure unconfined 1-dodecanol is denoted with r = infinite. The term ‘pore’ will be used in this paragraph instead of ‘cell’ which is used to describe the morphology of the demixed

polymer solution. The reason is that the inorganic reference materials have a percolating porous structure which allows convection of liquid. Furthermore, the inorganic material is built from small inorganic particles in contrast to the demixed polymer solution, which consists of a continuous polymer-rich phase hosting spherical shaped diluent droplets (cells).

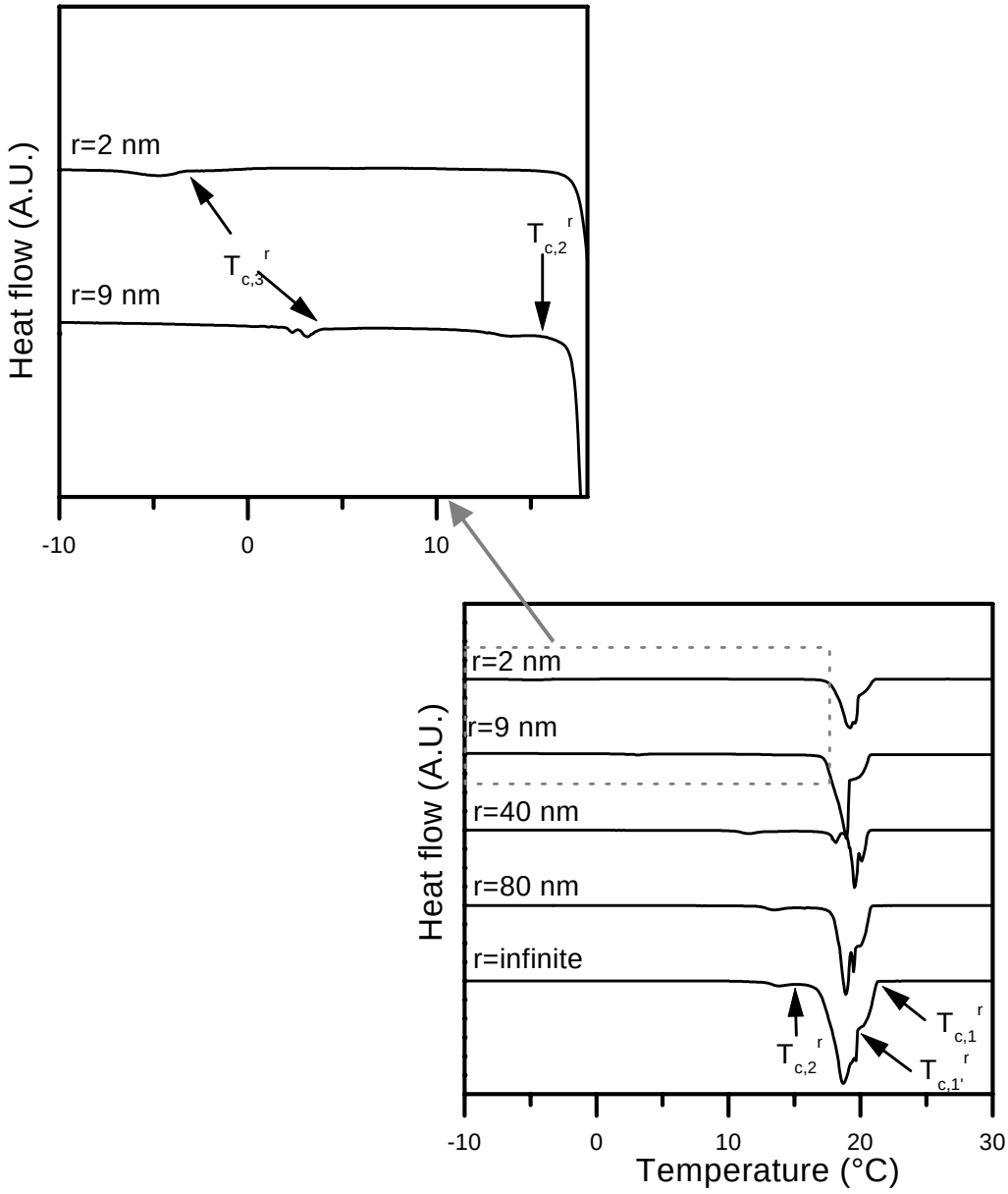

Figure 8. *Crystallization curves of 1-dodecanol. The different observed onset temperatures ($T_{c,1}^{r}$, $T_{c,1'}^{r}$, $T_{c,2}^{r}$ and $T_{c,3}^{r}$) are denoted in the figure.*

Fig. 8 shows that pure 1-dodecanol does not reveal one smooth peak around T = 20°C, but a number of overlapping peaks. For the pure 1-dodecanol curves, three different onsets temperatures ($T^r_{c,1}$, $T^r_{c,1'}$ and $T^r_{c,2}$) are distinguished. A difference with the pure 1-dodecanol curve in Fig. 3a is observed, this is caused by the different DSC-mode and instruments used in both experiments. However, the onset temperatures $T^r_{c,1}$ and $T^r_{c,2}$ coincide well with the onset temperature $T_{c,1}$ and $T_{c,2}$ of pure 1-dodecanol in Fig. 3a.

The onset temperatures observed for pure 1-dodecanol are also observed for the experiments with the inorganic matrix due to the immersion procedure. 1-dodecanol at the outside of the inorganic material is able to melt or crystallize like pure 1-dodecanol. The free 1-dodecanol peaks differ in size due to the amount of free 1-dodecanol in the sample. The location on the temperature axes of the maximum peak can differ significantly for each experiment. However, the onset temperature is always the same, and this quantity is used to characterize the peaks. The onset temperatures observed in Fig. 8 are plotted in Fig. 9a.

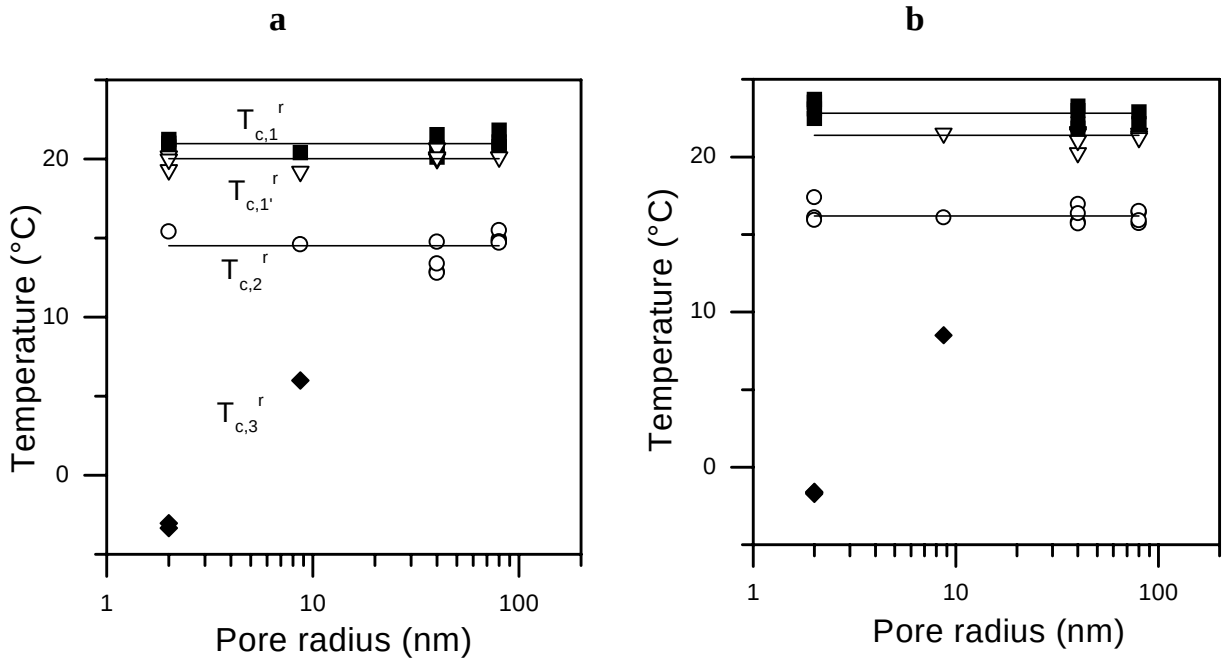

Figure 9. *Onset temperature of crystallization (9a) and melting (9b) of 1- dodecanol. The lines belonging to* $T^r_{c,1}$, $T^r_{c,1'}$, *and* $T^r_{c,2}$ *are also observed in the pure unconfined 1-dodecanol.*

The heating curves showed comparable results as the cooling curves. The locations of the onset temperatures of the heating curves are plotted in Fig. 9b. Fig. 9a and b show that only materials with pore sizes of 2 and 9 nm have a temperature depression. It is possible that the inorganic materials with larger pore size (40 and 80 nm) show a temperature depression as well. However, this will be observed in the region where the free 1-dodecanol gives also a crystallization or melting peak.

5.4.4 Conclusions

From the results with inorganic porous structures, it can be concluded that small pore sizes indeed result in a distinct crystallization and melting point depression of 1-dodecanol in the inorganic materials. Only very small pores can be observed from the crystallization or melting temperature depression because the peaks of the free 1-dodecanol overshadow any of the hypothetical present depression phenomena at larger pore sizes.

5.5 Morphology of a liquid-liquid demixed and vitrified polymer solution studied with scanning electron microscopy

To compare the crystallization or melting curves obtained from DSC, with the morphology of the demixed solution, scanning electron microscopy (SEM) pictures were made of the liquid-liquid demixed polymer solution. The predominant question is whether the samples show any morphology on nanometer scale as suggested by the supersaturation of the polymer-rich phase (hypotheszed in Chapter 4) and the crystallization point depression present in the demixed polymer solution (peak $T_{c,3}$ in §5.2.2).

5.5.1 Experimental

SEM (JEOL JSM-T220A, sputtering time: 3 min at I = 13 mA, p = 0.1 bar in a Balzers SCD 040) was used to study the final structure of the demixed polymer solution. 1-Dodecanol from the demixed polymer solution was extracted with ethanol which was removed by drying in a vacuum-oven at 30°C. From SEM pictures, cell sizes were determined visually.

5.5.2 Results

Fig. 10 and 11 show examples of SEM pictures for a demixed solution of 48 wt.% and 73 wt.% aPS in 1-dodecanol.

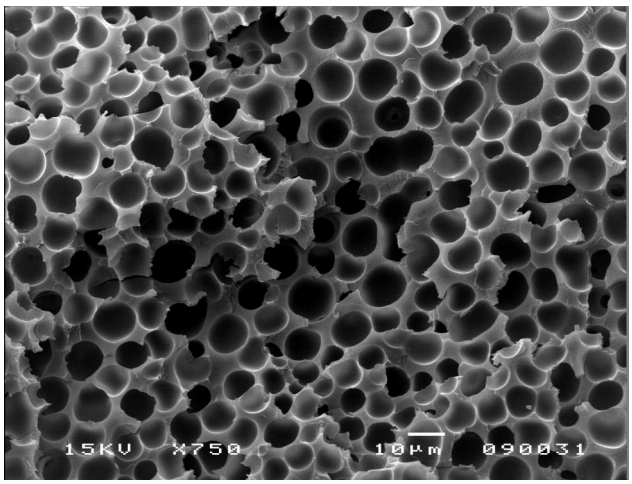

Figure 10. *SEM picture of a demixed solution of 48 wt.% aPS in 1-dodecanol, magnification x750.*

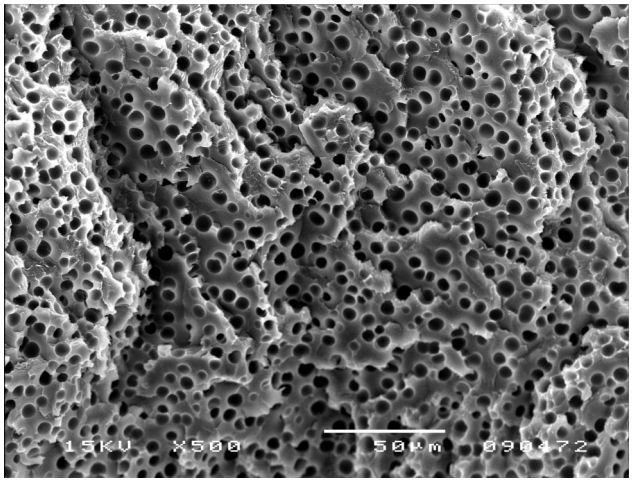

Figure 11. *SEM picture of a demixed solution of 73 wt.% aPS in 1-dodecanol, magnification x500.*

Cell radii were determined by measuring the cell radius of at least 60 cells and taking the average and standard deviation of the measured cells (Chapter 2). In Fig. 12, the cell radii determined from SEM pictures for concentrations of 27, 48, and 73 wt.% of polymer are plotted.

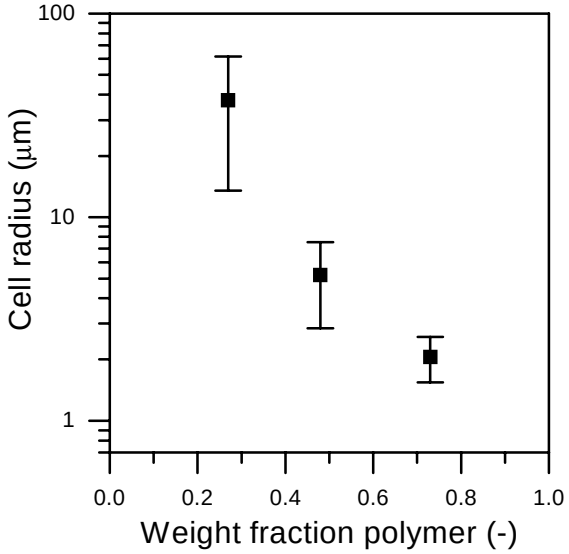

Figure 12. *Cell radii for different polymer concentrations determined with SEM. Error bars indicate the standard deviation. The data point at a concentration of 27 wt.% is obtained with a cooling rate of 1 K·min^{-1}. For the other data points a cooling rate of 2 K·min^{-1} was used.*

Cell sizes observed with SEM are in the order of micrometers. Such sizes cannot lead to a significant crystallization or melting point depression, as observed in the DSC experiments with the inorganic reference materials (§5.4). This implies that the observed shift of the largest peak in the cooling curve shown in Fig. 2 and 3a has to be caused by another mechanism.

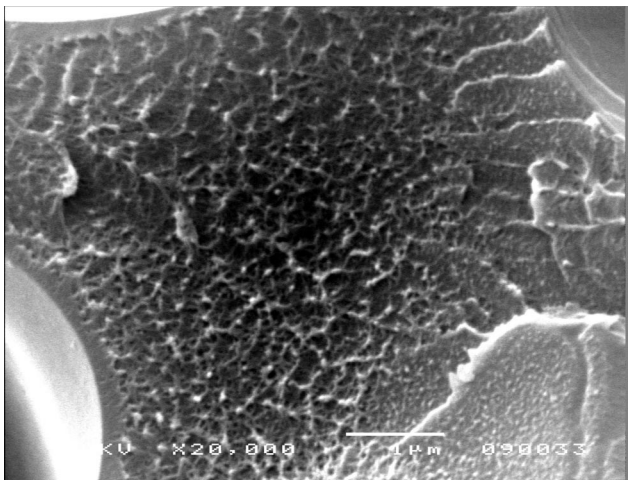

Figure 13. *SEM picture of a demixed solution of 48 wt.% aPS in 1-dodecanol, magnification x20000 (This picture is a magnification of Fig. 10).*

The small crystallization peaks at about 6°C (peak $T_{c,3}$ in Fig. 2 and 3a) were initially assumed to stem from a secondary cell formation which has its origin in the supersaturation of the polymer-rich phase forming the cell walls. If this supersaturation indeed can crystallize, one could expect some structure in the cell walls. Fig. 13 supports this hypothesis. Nevertheless, the relation between the observed nanopores in the cell wall and the DSC peak at a large temperature depression ($T_{c,3}$) is not proven yet. If the peak belonging to $T_{c,3}$ is present in a cooling curve, it should also be present in the heating curve, however, this is not the case in my experiments. From the study of Brun *et al.* [9] it is known that the temperature depression measured with melting and crystallization is different because of the shape of the pores. With cylindrical pores, the temperature depression for melting is two times smaller than with crystallization. If this is the case, a peak should be present with the same enthalpy as the peak belonging to $T_{c,3}$ in the melting curve in Fig. 2 and 3b. Furthermore in §5.2.4.2 an experiment was described in which no peaks at a large temperature depression are observed in a second cooling run (Fig.6). From this consideration, it is not probable that peak $T_{c,3}$ originates from confined 1-dodecanol.

5.5.3 Conclusions

The observation of the crystallization temperature depression of 1-dodecanol in the demixed and vitrified polymer solution can not be explained by a confinement because of the too large cell sizes. It is too preliminary to relate the crystallization peak observed at very large temperature depression (T_3 in Fig. 2 and 3b) to the confinement of 1-dodecanol in nanosized cells in the polymer-rich phase observed by SEM.

5.6 Polymorphism

5.6.1 Literature about polymorphism of 1-dodecanol

It has been suggested that almost all organic compounds exist in different solid phases [11]. Two different types of polymorphism are distinguished: monotropic and enantiotropic polymorphism. Enantiotropy is defined as the reversible change from one crystal form to another. Monotropy is defined as the irreversible transition from

a metastable form to a stable form [11, 12]. Meyer *et al.* [13] already showed in 1933 that long-chain alcohols show polymorphism. In his study he recorded the temperature versus time during the cooling of an alcohol. He observed that alcohols containing 13 carbon atoms or more show two transitions.

Table 1. *Reported transition temperatures data for 1-decanol, 1-dodecanol and 1-tetradecanol.*

Alcohol	**Transition**	**T_{tr} (K)**	**ΔH_m (kJ·mol)**	**Ref.**
1-decanol	s→l	280.1	37.6	[15]
	s→l	280.1	37.7	[16]
	s→l	280.2	28.8*	[17]
1-dodecanol	s→l	297.0	31.4	[15]
	α→l	294.8		[16]
	β→l	297.0	31.4	
	c→l	297.0	38.4*	[17]
1-Tetradecanol	α→l	310.8	25.1	[14, 15]
	β→l**	311	49.5	
	c→l	311.2	45.7*	[17]
	α→β	308.0		[16]
	α→l	311.0		
	γ→l	311.0	39.7	

s = solid phase; l = liquid phase; α, β, γ = different polymorphs

* Mosselman *et al.* and Eckert *et al.* discuss the reliability of this data [17, 18]

** A β-γ transition at 306±3 K (ΔH_{tr} = 1.8 kJ·mol^{-1}) has to take place theoretically in analogy with tridecanol [14]**

Later, Mosselman *et al.* [14] studied polymorphism from tridecanol (C13) to octadecanol (C18) with a more sophisticated calorimeter and they were able to show different solid-state structures in which the long chain alcohols could crystallize. They distinguished three different forms. In the high-entropic α-form, the chains are perpendicular to the hydroxy plane and they rotate around their long axis. In the β-form no rotation occurs and in the γ-form the molecules are tilted. In Table 1, transition data and heats of fusion are listed for decanol, dodecanol, and tetradecanol. The literature data are not complete in agreement with each other and the existence of polymorphism is not obvious for C10 and C12. The transition between two polymorphs in tetradecanol (C14) shows only a small transition enthalpy and furthermore some transitions occur within the melting region [14]. Studying polymorphism with DSC alone can not give a clear explanation, therefore X-ray diffraction experiments were carried out to study the crystal structure of 1-dodecanol at different temperatures for pure 1-dodecanol and 1-dodecanol in the polymer-rich matrix.

5.6.2 Experimental

X-Ray diffraction experiments were carried out on a Bruker D8 Advance in a temperature controlled chamber of Anton Paar, type TTK450. The cooling and heating rate between the isothermal temperatures were 6 $K \cdot min^{-1}$ and it took 1.5 hour to measure the X-ray pattern at one temperature. A kapton film was used to prevent leakage of the sample during the experiments with pure 1-dodecanol; with the experiments of 48 wt.% aPS in 1-dodecanol this precaution method was not necessary.

5.6.3 X-ray results

Fig. 14a shows the X-ray patterns of pure 1-dodecanol at different temperatures during a cooling run. The peaks between 2θ = 20° and 25° have a constant height over the complete temperature interval. The peak heights between 2θ = 2° and 16° increase with decreasing temperature. This observation of different behavior between two series of peaks can be explained by the existence of two crystal phases. The peaks between 2θ = 2° and 16° result from a different crystal phase then the peaks between 2θ = 20° and 25°.

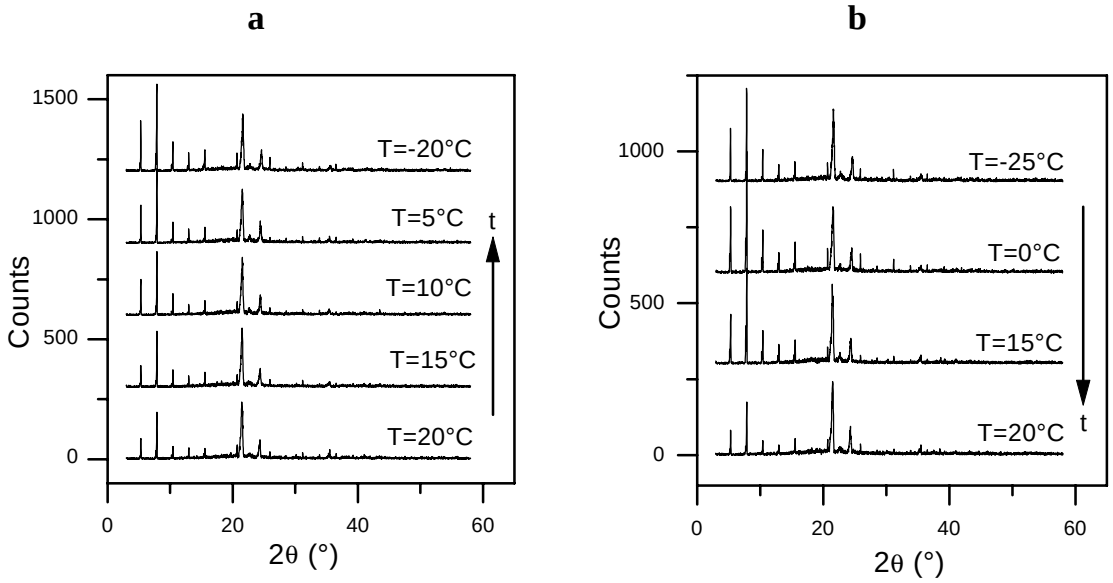

Figure 14. *X-ray pattern of cooling (14a) and heating (14b) of pure 1-dodecanol.*

The heating curve of pure 1-dodecanol, plotted in Fig. 14b, shows comparable X-ray patterns between T = –25°C and 15°C. For T = 20°C, smaller peaks are observed between 2θ = 2° and 16° in comparison with the X-ray patterns for the other temperatures. The crystal phase belonging to the peaks between 2θ = 2° and 16° disappears at a lower temperature than the phase belonging to the peaks between 2θ = 20° and 25°.

Fig. 15a shows the cooling curve of a sample of 48 wt.% of aPS in 1-dodecanol. A diffuse peak is observed between 2θ = 15° and 25° which is present even in the region of completely molten 1-dodecanol (at T = 30°C). Therefore, this diffuse peak has to be caused by the polymer-rich matrix. Peaks on top of the diffuse broad peak grow with decreasing temperature. There exists a large difference between the X-ray patterns between 20°C and 10°C. This is in agreement with the observation from the DSC experiment in which a large crystallization peak was observed at T = 12°C for a 48 wt.% aPS in 1-dodecanol solution (see Fig. 2) indicating that the influence of crystallization can be only observed at a temperature below T = 12°C.

The heating curves (Fig. 15b) show no significant difference as function of temperature. This is in agreement with the DSC experiments showing a melting temperature of 1-dodecanol in the aPS matrix of about 20°C for all polymer concentrations as well (Fig. 3b).

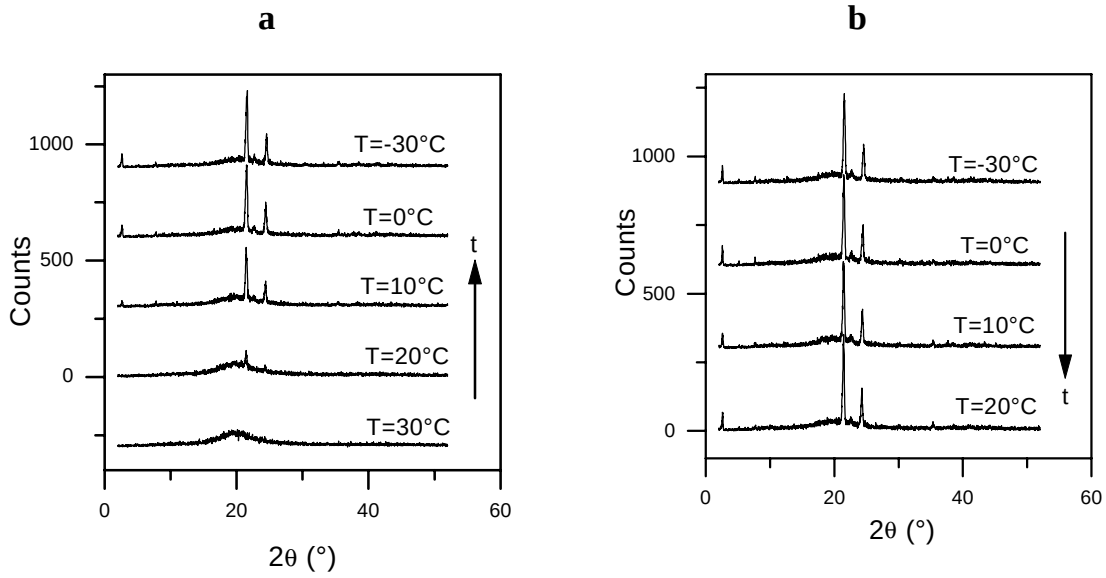

Figure 15. *X-ray pattern of cooling (15a) and heating (15b) of a 48 wt.% solution of aPS in 1-dodecanol.*

The relative low heights of the peaks between 2θ = 2° and 16° in the sample containing 48 wt.% aPS in comparison with the pure 1-dodecanol, indicates an influence of the polymer -rich matrix on the crystallization behavior of the 1-dodecanol. It can be hypothesized that the peaks between 2θ = 2° and 16° stem from a different crystal phase than the peaks between 2θ = 20° and 25° because of the difference in crystallization behavior.

5.6.4 Conclusions

The difference in crystallization and melting patterns between pure 1-dodecanol and 1-dodecanol in a polymer-rich matrix is evident. To quantify this difference however, a more detailed analysis of the X-ray patterns needs to be carried out. The trends observed between the X-ray patterns of 1-dodecanol in the polymer-rich phase upon cooling and heating coincide with observed DSC signals. X-ray peaks between 2θ = 2° and 16° show a different behavior than the peaks beween 2θ = 20° and 25° in the results of both the pure 1-dodecanol and the 1-dodecanol in the polymer-rich phase. This is an indication of the presence of two crystal phases of 1-dodecanol.

5.7 Discussion

Cooling curves of 1-dodecanol confined in a polymer-rich matrix show a large peak in DSC experiments, shifting to a higher temperature depression with increasing polymer concentration. In contrast, in heating curves, the largest melt peak is located at a constant temperature with changing polymer concentration. §5.3 showed that the origin of the large peak is the crystallization or melting of diluent in the polymer-lean phase.

Thermoporometry is able to measure cell sizes in the order of magnitude of nanometers, while the cell sizes in the demixed polymer solution are in the order of micrometers (§5.4). Therefore the concepts of thermoporometry can not describe the crystallization temperature depression of the 1-dodecanol

The observation of a crystallization peak at a very large temperature depression in the cooling runs of polymer solutions with a polymer content over 47 wt.%, was the direct reason to study the polymer-rich phase with SEM (see §5.5). Small cells were indeed observed in the polymer-rich phase. Hence, the hypothesis proposed in Chapter 4 that a supersaturated polymer-rich phase exists has been proven.

X-ray patterns of confined 1-dodecanol differ from the X-ray patterns of pure 1-dodecanol (§5.6). This indicates an influence of the polymer-rich phase on the crystallization behavior of 1-dodecanol.

I am not able yet to fully explain the observed cooling and heating curves of the diluent. The following physical interpretation is proposed. Cooling the polymer-rich matrix filled with a polymer-lean phase of almost pure 1-dodecanol below the crystallization temperature tends 1-dodecanol to crystallize. The density of pure 1-dodecanol in the liquid phase at T = 23.8°C is 830 kg·m^{-3} and the density of solid 1-dodecanol at that temperature is 950 kg·m^{-3} [15] resulting in a driving force for the shrinkage of the cells. However, the good contact of the crystallizing phase with the polymer-rich phase results in a restrictive/retarding force exerted by the polymer matrix on the crystallizing phase. This results in an increased supercooling, which strongly depends on the mechanical properties of the polymer-rich phase. With increasing polymer content, the retardation effect increases, hence, the crystallization peak shifts towards a larger temperature depression. The influence of the retarding force of the polymer-rich phase is even more distinct in the crystallization of 1-

dodecanol in the nanosized cells in the polymer-rich phase, because of the large contact of the diluent with the polymer-rich phase. Furthermore, two different crystallization structures of 1-dodecanol can be distinguished: the high melting temperature phase is defined as phase I, the low temperature is defined as phase II. These phases show an enantiotropic phase transition at $T_{m,2}$, because the transition is endothermic upon heating and reversible [11], which can be concluded by comparing the heating and second cooling curve in Fig. 8. Upon heating, phase II will first transform to phase I (at $T_{m,2}$) before melting occurs (at $T_{m,1}$). In general crystallization of a material is a kinetically determined process, nuclei have to be formed and these nuclei have to grow. On the other hand, melting is considered as an equilibrium process. Hence, the melting peaks will not be influenced as distinct by the polymer-rich phase as with crystallization. Maybe the transition between the two crystal structures of 1-dodecanol is influenced by the polymer-rich phase, because peak $T_{m,2}$ is decreasing with increasing polymer concentration.

To verify this physical picture, the influence of the mechanical properties of a solid matrix on the crystallization behavior of a liquid should be studied. However, it is hard to find experimental evidence to verify this physical explanation. The system considered is unique because of the formation method, resulting in a closed cell morphology in which the cells are filled with a liquid. Upon impregnating solid matrices with a liquid, the question always remains whether the structure is completely filled and how the liquid and solid matrix interact.

5.8 Conclusions

Crystallization peaks of 1-dodecanol in a liquid-liquid demixed and vitrified aPS - 1-dodecanol polymer solution show a strong dependency on polymer concentration. This is in contrast with the melting peaks in which the influence of polymer concentration is small. Only the 1-dodecanol belonging to the polymer-lean phase is able to crystallize, 1-dodecanol dissolved in the polymer-rich phase shows no contribution to the crystallization or melting enthalpy. However, a minor part of the diluent in the polymer-rich phase is present as clusters in the polymer-rich phase. These clusters are present because of supersaturation of the polymer-rich phase as observed in Chapter 4.

The location of the crystallization and melting peaks of 1-dodecanol are quantified with the concepts of temperature depression caused by confinements and polymorphism. Only confined 1-dodecanol in inorganic reference materials with pores sizes below 9 nm shows a distinct temperature depression peak in both the cooling and heating curve while the cell sizes in the demixed and vitrified polymer solution have magnitudes of micrometers. The absence of a melting peak and the absence of a crystallization peak in a second cooling run, both at a large temperature depression, rejects the possibility of crystallization of confined 1-dodecanol in the polymer-rich matrix.

From literature and X-ray experiments, there is a strong indication that different crystal structures of 1-dodecanol indeed exist and that the polymer-rich matrix influences the crystallization behavior of 1-dodecanol.

The total physical picture of the crystallization and melting behavior of 1-dodecanol in a polymer-rich matrix is not completely clear. An explanation which explains the observed behavior, based on the difference in volume of 1-dodecanol in the liquid and solid state, is difficult to verify because of the uniqueness of the considered system.

5.9 Acknowledgements

H. Koster (University of Twente) is acknowledged for carrying out the initial X-ray experiments and discussions. J. Baas en prof. T.Palstra (Groningen University) are acknowledged for carrying out the X-ray experiments described in this chapter.

5.10 List of symbols

ΔH_{dil}	Melting enthalpy of pure diluent	$J \cdot g^{-1}$
ΔH_m	Melting enthalpy of polymer solution	$J \cdot g^{-1}$
ν_l	Temperature	$m^3 \cdot g^{-1}$
$\gamma_{L\text{-}S}$	Interfacial tension of diluent between solid and liquid form	$N \cdot m^{-1}$
$m_{diluent,lean}$	Weight of diluent in the polymer-lean phase	g
m_{lean}	Weight polymer-lean phase	g

m_{rich}	Weight polymer-rich phase	g
r	Cell radius	m
$T_{c,i}$	Onset temperature crystallization peak i	°C
$T^{r}_{c,i}$	Onset temperature reference crystallization peak i	°C
$T_{m,i}$	Onset temperature melting peak i	
w_0	Weight fraction of polymer in polymer solution	-
w_1	Weight fraction of polymer in the polymer-lean phase	-
w_2	Weight fraction of polymer in the polymer-rich phase	-

5.11 References

1. Tsai, F.J., and Torkelson, J.M., *Roles of phase separation mechanism and coarsening in the formation of poly(methyl methacrylate) asymmetric membranes*, Macromolecules, 23, p. 775-784 (1989)
2. Mathot, V.B.F., *Calorimetry and thermal analysis of polymers*. , Munich: Hanser Publishers (1994)
3. Lloyd, D.R., Kinzer, K.E., and Tseng, H.S., *Microporous membrane formation via thermally-induced phase separation. I. Solid-liquid phase separation*, Journal of Membrane Science, 52, p. 239-261 (1990)
4. Arnauts, J., and Berghmans, H., *Amorphous thermoreversible gels of atactic polystyrene*, Polymer Communications, 28, p. 66-68 (1987)
5. Sliwinska-Bartkowiak, M., Gras, J., Sikorski, R., Radhakrishnan, R., Gelb, L., and Gubbins, K.E., *Phase transitions in pores: Experimental and simulation studies of melting and freezing*, Langmuir, 15, p. 6060 (1999)
6. Rennie, G.K., and Clifford, J., *Melting of ice in porous solids*, Journal of Chemical Society, Faraday1, 73, p. 680-689 (1977)
7. Morishige, K., and Kawano, K., *Freezing and melting of water in a single cylindrical pore: The pore-size dependence of freezing and melting behavior*, Journal of Chemical Physics, 110, p. 4867-4872 (1999)
8. Jackson, C.L., and McKenna, G.B., *The melting behaviour of organic materials confined in porous solids*, Journal of Chemical Physics, 93, p. 9002-9011 (1990)
9. Brun, M., Lallemand, A., Quinson, J.-F., and Eyraud, C., *A new method for the simultaneous determination of the size and the shape of pores: The thermoporometry*, Thermochimica Acta, 21, p. 59-88 (1977)
10. Nijmeijer, A., *Hydrogen-selective silica membranes for use in membrane steam reforming*, PhD thesis Universiteit Twente, Enschede (1999)

11. Giron, D., *Thermal analysis and calorimetric methods in the characterization of polymorphs and solvates*, Thermochimica Acta, 248, p. 1-59 (1995)
12. Souillac, P., and Rytting, J.H., *Characterization of delivery systems, differential scanning calorimetry*, in *Encyclopedia of controlled drug delivery*, Editor: Mathiowitz, E., New York: John Wiley & Sons Inc. p. 212-227 (1999)
13. Meyer, J.D., and Reid, E.E., *Isomorphism and alternation in the melting points of the normal alcohols, acetates, bromides, acids and ethyl estser from C10 to C18*, The Journal of the American Chemical Society, 55, p. 1574-1584 (1933)
14. Mosselman, C., Mourik, J., and Dekker, H., *Enthalpies of phase change and heat capacities of some long-chain alcohols. Adiabatic semimicrocalorimeter for studies of polymorphism*, J. Chem. Thermodyn., 6, p. 477-87 (1974)
15. Daubert, T.E., Danner, R.P., Sibul, H.M., and Stebbins, C.C., *Physical and thermodynamic properties of pure chemicals. Data compilation*. , Pennsylvania: Taylor&Francis (1989)
16. Thermodynamics Research Center, *TRC thermodynamic tables non-hydrocarbons*. , Texas: College Station (1985)
17. Eckert, T., and Müller, J., *Zur Schmelzenthalpie und schmelzentropie von Fettalkoholen*, Arch. Pharm. (Weinheim, Ger), 311, p. 31-34 (1978)
18. Mosselman, C., *On the polymorphism and the enthalpies of phase transition of 1-decanol, 1-dodecanol, 1-tetradecanol, 1-hexadecanol and 1-octadecanol*, Arch. Pharm. (Weinheim, Ger.), 314, p. 279-281 (1981)

Appendix 5

Comments on the concept of thermoporometry

Abstract

Thermoporometry is a technique to determine small pore sizes based on crystallization point depression of a liquid phase in a porous system. The temperature shift can be measured by Differential Scanning Calorimetry. A physical model is necessary to relate the experimental temperature depression data to a pore size. This study compares existing models to reported experimental data on melting and crystallization of pure water. A linear fit between the inverse pore size and the temperature depression according to the Gibbs-Thomson equation, describes the reported experimental results sufficiently accurate. Modifications on the Gibbs-Thomson equation do not give any further improvement.

A5.1 Introduction

The pore size in a porous matrix can be determined by measuring the crystallization point depression caused by confinement of a liquid inside this matrix. This method is called thermoporometry [1]. Generally, a porous system is filled with a liquid and is subsequently cooled down until crystallization occurs. Also the melting of the confined crystallites can be used to calculate pore sizes. For water and benzene, relations have been derived to calculate the pore size as a function of the temperature depression [1]. With this method many organic and inorganic porous structures have been characterized [2-4].

Besides the description with the Gibbs-Thomson equation or modifications of this equation, another model has been proposed by Shi [5, 6]. The model considers the difference in thermal fluctuations of atoms at the surface and in the bulk of a crystallite to relate the temperature depression to a pore size. This study compares the various models and a final relation will be proposed to describe the temperature depression caused by a confinement.

A5.2 Models to describe the melting and crystallization point depression

Different macroscopic models have been proposed to quantify melting and crystallization point depression. These models will be summarized briefly in the paragraphs below.

A5.2.1 Gibbs-Thomson model

The temperature depression has been described with the Gibbs-Thomson equation (eg. Ref. [7, 8]):

$$\Delta T = T^{\infty} - T^{R} = -\frac{2\gamma_{ls} T^{\infty} v_l}{R_n \Delta H_m} \qquad \text{(A1)}$$

where T^R is the melting temperature in a confinement, T^∞ the melting temperature of the bulk, γ_{ls} the interfacial tension between the solid and the liquid, R_n the nucleus size which is assumed to be equal to the pore size, ΔH_m the enthalpy of melting, and v_l the specific volume.

A linear dependency between the inverse pore radius with the temperature depression has experimentally been observed for water [9] and organics [7]. This is also expected according to Eq. A1, assuming constant physical properties of the liquid and the porous medium. However, this assumption may not hold in general. For example, Rennie *et al.* [10] observed a temperature dependency of the interfacial tension and Jackson *et al.* [7] observed a dependency of the interfacial tension on the type of porous material. Furthermore, the size dependency of the heat of fusion has been studied by Sliwinska-Bartkowiak *et al.* [9]. Nevertheless, in this study I am not interested in the behavior of the different variables, but I want to identify the most realistic equation to use for thermoporometry. Hence, by assuming constant physical properties, the equation obtained by using the Gibbs-Thomson relation can be further simplified:

$$\Delta T = \frac{c}{R_p} \tag{A2}$$

with:

$$c = -\frac{2\gamma_{ls} T^\infty v_l}{\Delta H_f}. \tag{A3}$$

A5.2.2 Modifications of the Gibbs-Thomson equation according to Brun *et al.*

In the model of Brun *et al.* [1] the influence of temperature on the specific volume of the liquid and the entropy change has been included in the Gibbs-Thomson equation:

$$\frac{2\gamma_{ls}}{R_n} = \int_{T^\infty}^{T^R} \frac{\Delta S_f}{v_l} \partial T \tag{A4}$$

where ΔS_f is the entropy of fusion. By assuming constant variables and by replacing ΔS_f with $\Delta H_f/T^\infty$ at T^∞, Eq. A1 is obtained.

Furthermore, Brun *et al.* proposed a temperature dependency of the interfacial tension. Eq. A4 was solved with the help of known values for the temperature dependency on the entropy and specific volume and they used experimental data to fit the temperature dependency of the interfacial tension. They also included a transition layer (t) between the nucleus (R_n) and the pore wall (R_p), which is due to an adsorbed layer of liquid. The transition layer of water is 0.8 nm and the transition layer of benzene is 1.33 nm [1]. The relation between the temperature depression and the pore size for crystallization is [1]:

$$R_p = \frac{64.67}{\Delta T} + 0.57 \qquad \text{(A5)}$$

and for melting:

$$R_p = \frac{32.33}{\Delta T} + 0.68\,. \qquad \text{(A6)}$$

The difference between the melting and crystallization behavior is caused by the shape of the pore. With spherical pores, the crystallization and melting temperature depression relations are the same because both the processes are dealing with a spherical crystal. In cylindrical pores, a spherical nucleus has to be formed in case of crystallization, therefore the same equations apply. In case of melting however, an equation has to be derived to describe melting in a cylindrical pore, which differs from equations applying for spherical pores. Brun *et al.* [1] used this concept to characterize the pore shape of a material as well. Because of his rather complex derivation procedure it is hard to give a physical explanation for the coefficients of Eq. A5 and A6.

By neglecting the temperature dependency of the entropy, specific volume, and the interfacial tension, and with introducing the transition layer, the following equation can be derived from Eq. A4:

$$\frac{2\gamma_{ls}}{R_p - t} = -\frac{\Delta S_f}{v_l}\Delta T\,. \qquad \text{(A7)}$$

To compare the different models, this equation is rewritten in the same mathematical form as Eq. A5:

$$R_p = \frac{c}{\Delta T} + d \qquad \text{(A8)}$$

with:

$$c = -\frac{2\gamma_{ls} v}{\Delta S_f} \qquad \text{(A9)}$$

$$d = t\,. \qquad \text{(A10)}$$

An equation with the same mathematical form as Eq. A8 can also be obtained by introducing a temperature dependent interfacial tension as proposed by Brun *et al.* [1]:

$$\gamma_{LS} = a + b\Delta T \qquad \text{(A11)}$$

and substitute this in the original Gibbs-Thomson equation (Eq. A1) or in the Gibbs-Thomson equation with a transition layer (Eq. A7).

By fitting Eq. A8 through the experimental data of Brun *et al*., the values of *c* and *d* have been determined, and are very similar to the values Brun *et al.* originally derived in Eq. A6: $c = 68.2 \pm 4.5$ and $d = 0.3 \pm 0.4$. In order to compare the various equations, Eq. A8 has to be slightly changed to a form as given in Eq. A12, because the reported literature data has been plotted as the inverse pore radius against the temperature depression:

$$\Delta T = \frac{c}{R_p - d} = \frac{c\frac{1}{R_p}}{1 - d\frac{1}{R_p}}\,. \qquad \text{(A12)}$$

A5.2.3 Model of Shi

Shi [5] derived a model for the size-dependent amplitude of the atomic thermal vibrations of a nanocrystal. Atoms at the surface of a crystal show large amplitudes in comparison with bulk atoms; by decreasing the crystal size the contribution of the vibrations of the surface molecules increases. On the base of this model and

Lindemann's criterion, an equation has been derived to relate the temperature depression to a pore size [5]. The Lindemann's criterium states that a crystal will melt when the root-mean-square displacement of the atoms in the crystal exceeds a certain fraction of the interatomic distance. Originally this model was derived to describe the melting point depression of melting metals. Jiang [6] generalized the model to organic compounds.

$$\frac{T^R}{T^\infty} = \exp\left(-\frac{\alpha - 1}{R_n / 3h - 1}\right) = \exp(x) \tag{A13}$$

with:

$$\alpha = \frac{\sigma_s(\infty)}{\sigma_v(\infty)}. \tag{A14}$$

$\sigma_s(\infty)$ is the mean-square-displacement of atoms at the surface of the crystal, $\sigma_v(\infty)$ is the mean-square-displacement of atoms at the interior of the crystal and h is the atomic diameter. The value of h can be calculated from the bond lengths of the molecule, the mean-square-displacements can be calculated from the entropy of melting.

The value of the term $T_m(r)/T_m(\infty)$ is approximately 1, so the term within the exponent of Eq. A13 (x) is close to 0. By using a Taylor expansion around $x = 0$ and truncation after the second term, the following expression is obtained:

$$\Delta T = T^\infty - T^R = \frac{3T^\infty(\alpha - 1)h}{R_p - 3h}. \tag{A15}$$

Eq. A15 can be rewritten in a form such as Eq. A12, with the parameters c and d:

$$c = 3T^\infty(\alpha - 1)h \tag{A16}$$

$$d = 3h. \tag{A17}$$

It is straightforward to show that the model based on the Gibbs-Thomson equation and a Taylor expansion of the model of Shi obey the same mathematical form. The fitting parameters however have different meanings.

A5.2.4 Comparison of the models and verification with literature data

Table 1 summarizes the different models and corresponding equations as described in previous paragraphs.

Table 1. *Proposed models to describe melting and crystallization behavior of water. The question marks belonging to the model of Brun et al. mean that the parameters c and d are only emperical parameters.*

Eq.	Model	Ref.	$\Delta T=f(R_p)$	c	d
A2	Gibbs-Thomson	[7, 8]	$\Delta T = \frac{c}{R_p}$	$-\frac{2\gamma_{ls}T^{\infty}v_l}{\Delta H_f}$	-
A12	Brun *et al*.	[1]	$\Delta T = \frac{c}{R_p - d}$	?	?
A12	Shi	[5]	$\Delta T = \frac{c}{R_p - d}$	$3T^{\infty}(\alpha - 1)h$	$3h$

A5.2.5 Comparison models with experimental data of water

Reported literature data were used to compare the relations from Table 1 with experimental data. Three data series from literature were used. Brun *et al*. [1] carried out crystallization experiments with water in Vycor glass and porous aluminum plugs with a pore radius between 2.4 and 10.5 nm. Ishikiriyama *et al.* [11] carried out both crystallization and melting experiments of distilled and deionized water in sillica gel with pore sizes between 1.8 and 29.1 nm. The scanning rate of their DSC experiments was 0.31 $K \cdot min^{-1}$. Rennie *et al.* [10] carried out melting experiments with water in CPG (Controlled Pore Glass) with a pore size of 7 to 200 nm (scanning rate: 4 $K \cdot min^{-1}$). It is unknown what quality of water Brun *et al*. and Rennie *et al*. used for their experiments. The data points are plotted in Fig. 1 and 2.

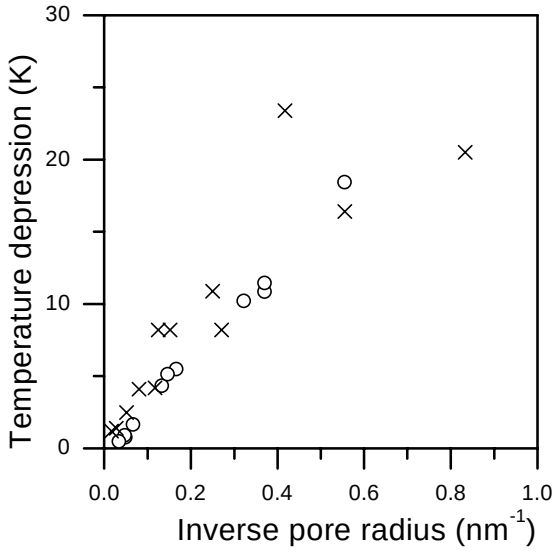

Figure A1. *Melting temperature depression of water as a function of the inverse pore radius. Data of Ishikiriyama et al. [11] (o), data of Rennie et al. [10] (x).*

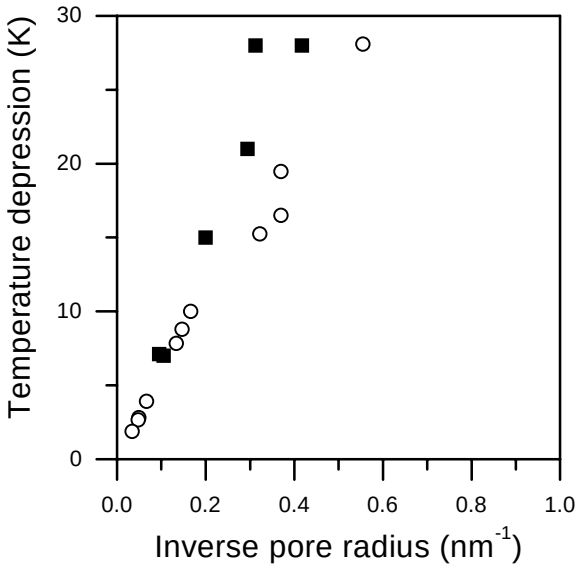

Figure A2. *Crystallization temperature depression of water as a function of the inverse pore radius. Data of Ishikiriyama et al. [11] (o), data of Brun et al. [1] (■).*

From Fig. A1 and A2, it can be concluded that the data points scatter significantly and in particular at a large temperature depression. The experimentally sensitive data are in the low temperature depression region, since the inverse pore size is plotted and small errors in temperature can cause a large error in the cell size.

Fig. A3 and A4 show the melting and crystallization points of Fig. A1 and A2 again, and Eq. A2 and A12 are used to fit these data points with a least squares method.

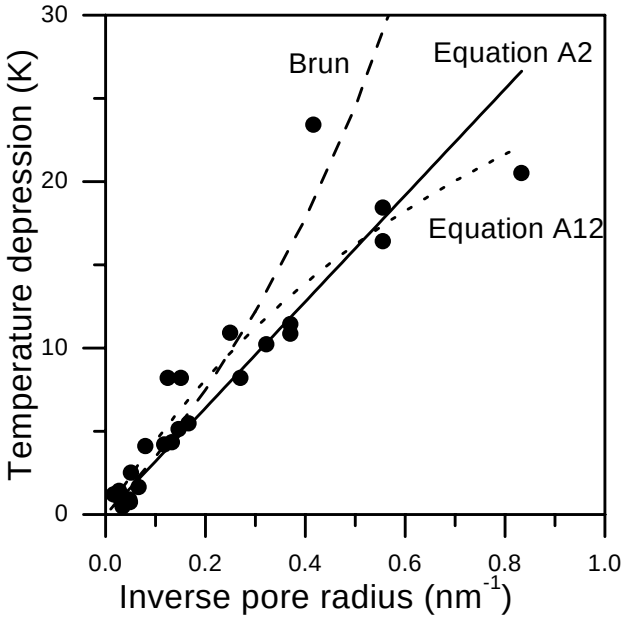

Figure A3. *Melting results with equation of Brun et al., best fit of Eq. A2 and best fit of Eq.A 12.*

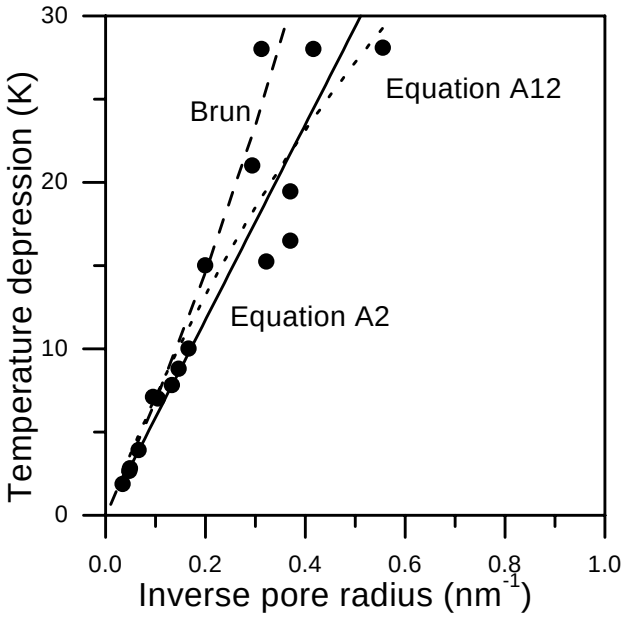

Figure A4. *Crystallization results with equation of Brun et al., best fit of Eq. A2 and best fit of Eq. A12.*

Furthermore the equation derived by Brun et al. (Eq. A5 and A6) are added to Fig. A3 and A4. The resulting fitting parameters are listed in Table A2.

Table 2. *Fit parameters for crystallization and melting of water.*

	Eq. A2: $\Delta T = \frac{c}{R_p}$		**Eq. A12:** $\Delta T = \frac{c}{R_p - d}$	
Fit parameters	**Melting**	**Crystallization**	**Melting**	**Crystallization**
c	32.0 ± 2.0	58.7 ± 3.3	48.5 ± 7.9	77.0 ± 14.7
d	-	-	1.0 ± 0.5	0.8 ± 0.7

Because of the scattering it is difficult to conclude which model is the best. The Gibbs-Thomson equation with constant variables as proposed in Eq. A1 is sufficient to describe the temperature depression. Only one fit parameter is necessary for this equation, the two parameters fit (Eq. A12) and the equation proposed by Brun *et al.* (Eq. A5 and A6) show no improvement. The linear relationship between the temperature depression and the inverse pore radius has also been found for organic materials [7] with pore radii between 2 and 25 nm, as already mentioned in the introduction of this appendix.

A5.3 Conclusions

From melting and crystallization experiments with water in porous materials with pore radii of 1.2 to 200 nm, it appeared that various literature data do not agree well. The best way to obtain reliable results from thermoporometry is to make a calibration curve with the liquid, which will be used in the experiment. By using previous reported literature data to obtain a calibration curve, a simple Gibbs-Thomson equation is sufficient to describe the data, modifications proposed by Brun *et al.* and the model of Shi do not show any improvement.

A5.4 List of symbols

ΔH_m	Enthalpy of melting	$J \cdot g^{-1} \cdot K^{-1}$
v_l	Specific volume	$m^3 \cdot g^{-1}$

γ_{ls}	Solid-liquid surface energy	$N \cdot m^{-1}$
$\sigma_s^2(\infty)$	Mean-square-displacement of atoms at the surface of the crystal	m^2
ΔS_m	Entropy of melting	$J \cdot g^{-1}$
ΔT	Temperature depression	K
$\sigma_v^2(\infty)$	Mean-square-displacement of atoms at the interior of the crystal	m^2
a,b,c,d	Empirical parameters	
h	Atomic diameter	m
R_n	Nucleus size	nm
R_p	Pore size	nm
t	Transition layer	nm
T^{∞}	Melting temperature in bulk	K
T^R	Melting temperature in confinement	K

A5.5 References

1. Brun, M., Lallemand, A., Quinson, J.-F., and Eyraud, C., *A new method for the simultaneous determination of the size and the shape of pores: The thermoporometry*, Thermochimica Acta, 21, p. 59-88 (1977)
2. Eyraud, C., Quinson, J.F., and Brun, M., *The role of thermoporometry in the study of porous solids*, in *IUPAC symposium (COPS 1)*. 1987, Elsevier: Bad Soden a. Ts, West Germany.
3. Nakao, S., *Determination of pore size and pore size distribution 3. Filtration membranes*, Journal of Membrane Science, 96, p. 131-165 (1994)
4. Cuperus, F.P., Bargeman, D., and Smolders, C.A., *Critical points in the analysis of membrane pore structures by thermoporometry*, Journal of Membrane Science, 66, p. 45-53 (1992)
5. Shi, F.G., *Size dependent thermal vibrations and melting in nanocrystals*, J. Mater. Research, 9, p. 1307-1313 (1994)
6. Jiang, Q., Shi, H.X., and Zhao, M., *Melting thermodynamcs of organic nanocrystals*, Journal of Chemical Physics, 111, p. 2176-2180 (1999)
7. Jackson, C.L., and McKenna, G.B., *The melting behaviour of organic materials confined in porous solids*, Journal of Chemical Physics, 93, p. 9002-9011 (1990)
8. Morishige, K., and Kawano, K., *Freezing and melting of water in a single cylindrical pore: The pore-size dependence of freezing and melting behavior*, Journal of Chemical Physics, 110, p. 4867-4872 (1999)
9. Sliwinska-Bartkowiak, M., Gras, J., Sikorski, R., Radhakrishnan, R., Gelb, L., and Gubbins, K.E., *Phase transitions in pores: Experimental and simulation studies of melting and freezing*, Langmuir, 15, p. 6060 (1999)
10. Rennie, G.K., and Clifford, J., *Melting of ice in porous solids*, Journal of Chemical Society, Faraday1, 73, p. 680-689 (1977)
11. Ishikiriyama, K., Todoki, M., and Motomura, K., *Pore size distribution (PSD) measurements of silica gels by means of differential scanning calorimetry*, Journal of Colloid and Interface Science, 171, p. 92-102 (1995)

Chapter 6

Determination of a binary phase diagram with one single temperature modulated differential scanning calorimetry experiment

Abstract

This chapter describes the possibility to use a single temperature modulated differential scanning calorimetry (TMDSC) experiment to determine the complete phase diagram of a binary polymer-diluent system. From a TMDSC experiment the liquid-liquid demixing temperature and the corresponding heat capacity shift will be quantified and used as input to calculate the binodal. The observed glass transition temperature and the crystallization enthalpy of the diluent are used as input to calculate the intersection between the binodal and the glass transition temperature (the Berghmans point).

6.1 Introduction

A binary phase diagram of an amorphous polymer-diluent system consists of a cloud point curve for a poly-disperse polymer and the glass transition temperature depression curve. For mono-disperse polymers the cloud point curve coincides with the binodal. The point of intersection between both lines is called the Berghmans point [1]. The Berghmans point is an important characteristic of the phase diagram and it is important for making the first estimation on the porosity of a demixed polymer-diluent solution via the lever rule. In Chapter 4, it was shown that the heat capacity shift due to liquid-liquid demixing, experimentally observed in a TMDSC experiment, can be predicted on the basis of the Flory-Huggis theory. By only using both the experimental data of the liquid-liquid demixing temperature ($T_{L\text{-}L}$) and the heat capacity shift from one experiment at one concentration, the Flory-Huggins interaction parameter can be calculated and hence the binodal can be predicted. The aim of this procedure is to obtain a new and simple method to calculate the complete binodal for binary polymer solutions. In addition, information will be extracted from the glass transition temperature and, if available, the crystallization and melting behavior of the diluent.

Chapter 5 showed that the Berghmans point determines the amount of free diluent in the demixed solution. By measuring the crystallization or melting enthalpy at a certain polymer concentration, the Berghmans concentration can be extrapolated as well. The concept of the use of one TMDSC experiment to determine the phase diagram will be discussed for three polymer-diluent systems: atactic polystyrene in diisodecylphthalate, cyclohexanol, and 1-dodecanol.

6.2 Experimental

6.2.1 Materials

Two types of atactic polystyrene (aPS) were used: commercial aPS (Styron* 686E) was kindly supplied by Dow Benelux NV (M_w and M_w/M_n: $2.3\cdot10^5$ g.mol^{-1} and 2.1 respectively, determined with GPC) and aPS synthesized in our own laboratory (M_w = $6\cdot10^4$, M_w/M_n =1.05) (see Chapter 3). The diluents used, 1-dodecanol (purity >98%, Merck-Schuchardt), diisodecylphthalate (DIDP, purity > 99%, Merck-

Schuchardt) and cyclohexanol (purity>99%, Merck-Schuchardt) were used without further purification. The commercial aPS was used to prepare solutions with cyclohexanol and DIDP. The narrow-disperse polymer was used to prepare a solution with 1-dodecanol. A homogeneous solution of aPS and diluent was prepared in a three-neck flask under nitrogen at elevated temperatures. After dissolution, the homogeneous solution was poured into a Petri-dish and quenched in air.

6.2.2 TMDSC

The TMDSC used is a DSC 2920 of TA Instruments. Calibration with indium and high density polyethylene (HDPE) (for calibration of the heat capacity) has been carried out. Approximately 5 mg of the quenched sample of a polymer-diluent system was used for TMDSC analysis. The TMDSC was heated up to a temperature within the homogeneous region, at least 30 K beyond the $T_{L\text{-}L}$. The cooling rate was set to 2 $K \cdot min^{-1}$ and continued to a final temperature of 273 K. In the experiment with aPS in 1-dodecanol a subsequent heating run was measured to determine the melting enthalpy of 1-dodecanol. The amplitude of the superimposed sine wave was 1 K with a period of 60 s. The glass transition temperature (T_g) and the liquid-liquid demixing temperature ($T_{L\text{-}L}$), the heat capacity shift at $T_{L\text{-}L}$ and when possible (only for 1-dodecanol) the enthalpy of crystallization and melting were determined with the TA Universal Analysis software.

6.2.3 Cloud point measurements

A cloud point meter, based on the transmission of laser light (wavelength = 670 nm) light transmission apparatus developed in our group, has been used to determine the cloud points of aPS in DIDP. A NMR-tube filled with the demixed solution was heated up to T = 353 K and afterwards it was water cooled at a rate of 1 $K \cdot min^{-1}$ down to T = 293 K while recording the transmission of the laser light. Fig. 1 shows a typical light-transmittance versus temperature diagram of aPS in DIDP. The cloud point is defined at the onset of the sharp decrease in light transmission.

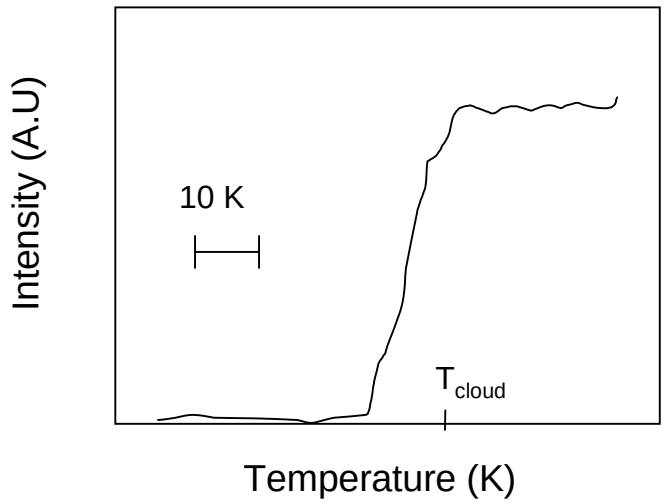

Figure 1. *Example of light transmission experiment.*

6.3 Methodology

Fig.1 and 2 in Chapter 3 show cooling curves, plotting the complex heat capacity as a function of the temperature for the polymer-diluent system atactic polystyrene in 1-dodecanol. The data extracted from these figures in this chapter are the:

- Liquid-liquid demixing temperature ($T_{L\text{-}L}$).
- Heat capacity shift at the liquid-liquid demixing temperature ($\Delta cp_{L\text{-}L}$).
- Glass transition temperature (T_g).
- Crystallization temperature of the diluent (T_c).
- Melting temperature of the diluent (T_m).
- Enthalpy of crystallization and melting of the diluent (ΔH_c and ΔH_m).

These data will be discussed in the following paragraphs.

6.3.1 Onset liquid-liquid demixing temperature and heat capacity shift

Chapter 3 showed that the onset temperature of the observed heat capacity shift ($T_{L\text{-}L}$) upon cooling coincides well with optical cloud point data for concentrated polymer-diluent systems. The heat capacity shift belonging to this temperature ($\Delta cp_{L\text{-}L}$) has been quantified and modeled in Chapter 4. It was derived that the $\Delta cp_{L\text{-}L}$ is directly related to the slope of the binodal. Below, I show that this slope and one

data point ($T_{L\text{-}L}$) is sufficient to quantify the Flory-Huggins interaction parameter of the empirical form:

$$\chi = a + \frac{b}{T}. \tag{1}$$

Hence, with a single TMDSC experiment at one fixed polymer concentration, the experimental values of $T_{L\text{-}L}$ and $\Delta cp^*_{L\text{-}L}$ are determined and the values for a and b can be calculated from Eq. 2 and 3, both derived from the Flory-Huggins theory for polymer solutions:

$$T_{L-L} = T_{bin} = \frac{b\phi_0^2}{\ln(1-\phi_0) + \left(1 - \frac{1}{N}\right)\phi_0 + a\phi_0^2} \tag{2}$$

$$\Delta cp^*_{L-L} = \Delta cp_{bin} = \frac{R}{M} \frac{\{\ln(1-\phi_0) + \phi_0\}(\phi_0 - 1)\{\ln(1-\phi_0) + \phi_0 + a\phi_0^2\}}{2\ln(1-\phi_0)\phi_0 - 2\ln(1-\phi_0) - 2\phi_0 + \phi_0^2}. \tag{3}$$

In Eq. 2 and 3, ϕ_0 is the polymer concentration of the homogeneous polymer-diluent solution, N is the ratio between the polymer and diluent molecular weight, R is the gas constant, and M is the molecular weight of a lattice site (in my case the molecular weight of the diluent is used). In Eq. 2 the term T_{bin} (binodal temperature) is used to make a clear distinction between the experimentally measured liquid-liquid demixing temperature of a poly-disperse system ($T_{L\text{-}L}$) and the theoretical calculated binodal temperature (T_{bin}) for a mono-disperse system. In this chapter, T_{bin} is assumed to be equal at $T_{L\text{-}L}$. A justification for this assumption can be found in Chapter 4. For the same reason the terms Δcp_{bin} and $\Delta cp^*_{L\text{-}L}$ are used, and they are also assumed to be equal. This procedure will be applied to two polymer-diluent systems: aPS in diisodecylphthalate and aPS in cyclohexanol.

6.3.2 Crystallization or melting enthalpy of diluent

Chapter 5 showed that the amount of diluent able to crystallize in the demixed solution is determined by the amount of diluent present in the polymer-lean phase.
The linear relationship between the measured enthalpy of crystallization or melting and the polymer concentration was observed in Chapter 5 and can be rewritten as:

$$w_B = \frac{\Delta H_{dil} w_0}{\Delta H_{dil} - \Delta H_m}. \qquad (4)$$

Extrapolation of the pure component enthalpy of crystallization or melting (ΔH_{dil} at $w = 0$) and the measured enthalpy at a certain concentration (ΔH_m at $w = w_0$) towards the concentration belonging to $\Delta H(w) = 0$ results in $w = w_B$, with w_B the Berghmans concentration. In §6.4.3 an example will be given for the polymer-diluent system aPs (with a poly-dispersity = 1.05) in 1-dodecanol.

6.3.3 Glass transition temperature

In the phase diagram of a polymer-diluent system comprising an amorphous polymer (see for example Fig 3. in Chapter 3), one can distinguish two different regions of the glass transition.

- The region of a homogeneous solution of the polymer and diluent, where an increased diluent concentration results in a decrease in T_g.
- The region below the liquid-liquid demixing gap, where the T_g is independent of the concentration.

By systematically measuring the glass transition temperature of different polymer concentrations, the Berghmans point can be directly determined experimentally. The glass transition temperature is independent of the polymer concentration after passing the binodal. Passing the glass transition temperature without prior liquid-liquid demixing gives a concentration dependent glass transition. However, this procedure requires measurements at different concentrations. In addition, it is possible to use predictive models for describing the glass transition point depression like the models of Chow [2] or Kelley-Bueche [3]. The intersection of the glass temperature of the demixed solution and the calculated glass transition temperature depression gives the concentration of the Berghmans point.

6.3.4 Construction of the Berghmans point

The aim of this chapter is to derive the Berghmans point from information obtained from a single TMDSC experiment, so additional information from the other TMDSC signals have to be used. The Berghmans point can be determined in three ways as visualized in Fig. 2:

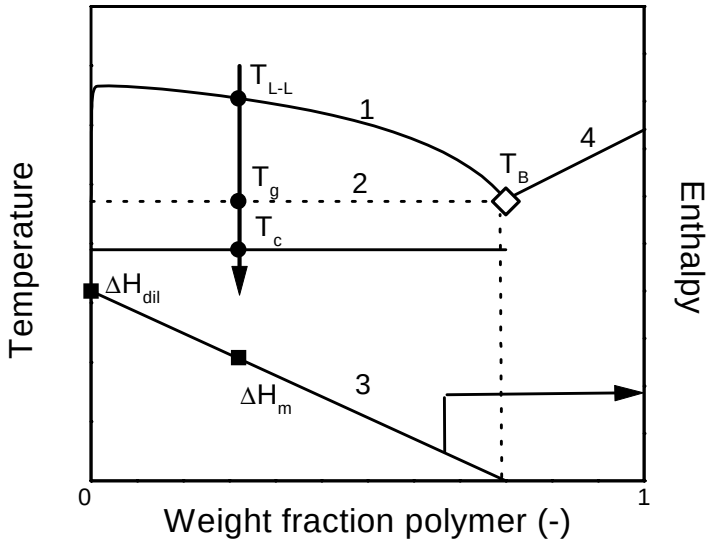

Figure 2. *Schematic representation of the three methods to determine the Berghmans point (T_B). Line 3 and the black squares belong to the enthalpy axis, the remaining lines and black circles belong to the temperature axis.*

1- By the intersection of the binodal calculated using $T_{L\text{-}L}$ and $\Delta cp^*_{L\text{-}L}$ (line 1) and the measured glass transition temperature below the liquid-liquid demixing gap (line 2).
2- By the intersection of the extrapolated melting or crystallization enthalpy (ΔH = 0, line 3) and the measured glass transition temperature below the liquid-liquid demixing gap (line 2).
3- By the intersection of the combined binodal calculated using $T_{L\text{-}L}$ and $\Delta cp^*_{L\text{-}L}$ (line 1), and extrapolated melting or crystallization enthalpy (ΔH = 0, line 3).

Line 4 can be predicted by using a model describing the glass temperature depression. It is possible to use such a model together with one of the data obtained from a TMDSC experiment to calculate the Berghmans point. It is known that the Kelley-Bueche or Chow models have good predicting capabilities. Since the Kelley-

Bueche method has been demonstrated in Chapter 4, it is mentioned only for completeness.

The three prediction methods will be applied to determine the Berghmans point for aPS (poly-dispersity of 1.05) in 1-dodecanol. The method to determine the binodal within one experiment will be used for aPs (poly-dispersity = 2.1) in DIDP and cyclohexanol.

6.4 Results and discussion

6.4.1 Calculation of the binodal for aPS in DIDP and aPS in cyclohexanol

Fig. 2 of Chapter 3 showed the complex heat capacity of aPS in DIDP and aPS in cyclohexanol for polymer concentrations of 30 wt.%. The measured $T_{L\text{-}L}$ and corresponding heat capacity shift are listed in Table 1.

Table 1. *Measured and input variables for the prediction of the empirical constants a and b in the interaction parameter for aPS in DIDP and aPS in cyclohexanol.*

Variable	Property	aPS in DIDP	aPS in cyclohexanol
Input	ρ (kg·m^{-3})	954	895
	M (g·mol^{-1})	447	100
Measured	w_0 (-)	0.30 ± 0.01	0.30 ± 0.01
	$T_{L\text{-}L}$ (K)	318 ± 1	355 ± 1
	$\Delta cp^*_{L\text{-}L}$ (J·g^{-1}·K^{-1})	0.0045 ± 0.002	0.083 ± 0.002
Calculated	ϕ_0 (-)	0.28 ± 0.01	0.27 ± 0.01
	a (-)	-0.14	-2.58
	b (T^{-1})	245	1136

To relate weight fractions to volume fractions a linear interpolation between the pure component density is assumed. The density of the diluent [4] must be calculated at $T_{L\text{-}L}$, the polymer density (= 1050 kg·m^{-3}) is assumed to be constant. Fig. 3 shows the cloud point curve of the aPS in DIDP determined with light transmission for different polymer concentrations, and the binodal calculated from the TMDSC

experiment, based on the method specified in §6.3.1. To draw the binodal curve, the Flory-Huggins equation (Eq. 4 in Chapter 4) is solved numerically.

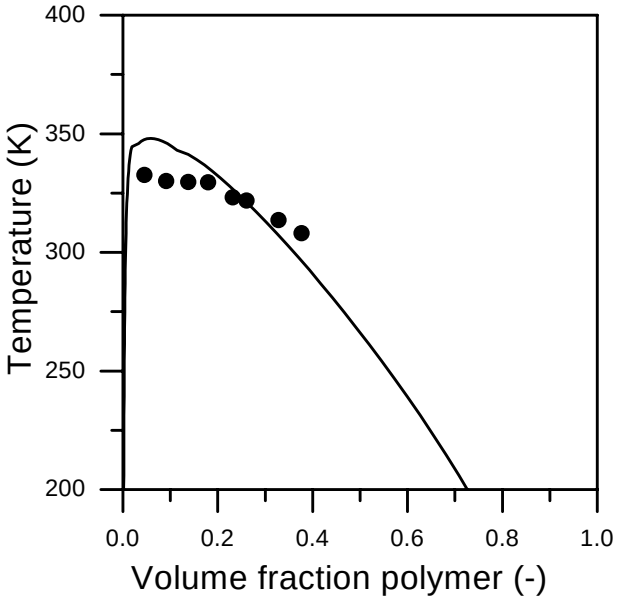

Figure 3. *Experimentally determined cloud points and calculated binodal (solid line) of aPS in DIDP. The input and experimental parameters to calculate the binodal are listed in Table 1. The ratio between the molecular weight of the polymer and the molecular weight of the diluent is 260.*

At low concentrations the predicted binodal overestimates the cloud points and at higher concentrations it underestimates the cloud points. This trend also was observed in previous work with aPS in 1-dodecanol in which optical microscopy data was used to determine the cloud points (see Chapter 3). The error in the prediction method of the binodal will be studied in §6.4.2.

Furthermore, no glass transition temperature was observed within the temperature interval of the TMDSC experiment. The reason is the large glass temperature depression of the system aPS in DIDP. Hence, it is not possible to determine the Berghmans point for this system.

6.4.2 Error analysis binodal

To quantify the error in the resulting interaction parameter and to find the optimal experimental conditions, the sensitivity of the procedure will be described below. Three experimental variables contribute to the error: ϕ_0, $T_{L\text{-}L}$ *and* $\Delta cp^*_{L\text{-}L}$. The errors

in the *a* and *b*, *ε(a)*, and *ε(b)* can be calculated as function of the experimental parameters from Eq. 5 and 6:

$$\varepsilon(a) = \left|\frac{\partial a}{\partial \Delta cp^*_{L-L}}\right|_{\phi_0} \cdot \varepsilon(\Delta cp^*_{L-L}) + \left|\frac{\partial a}{\partial \phi_0}\right|_{\Delta cp^*_{L-L}} \cdot \varepsilon(\phi_0) \qquad (5)$$

$$\varepsilon(b) = \left|\frac{\partial b}{\partial T_{L-L}}\right|_{\phi_0, a} \cdot \varepsilon(T_{L-L}) + \left|\frac{\partial b}{\partial \phi_0}\right|_{T_{L-L}, a} \cdot \varepsilon(\phi_0) + \left|\frac{\partial b}{\partial a}\right|_{T_{L-L}, \phi_0} \cdot \varepsilon(a). \qquad (6)$$

These equations can be solved analytically and the individual contribution of the three variables can be quantified. The absolute values of the partial derivatives of Eq. 5 and 6 are quantified for the system aPS in DIDP. The results are listed in Table 2 and 3. These tables indicate that the error in *a* is mainly caused by the measurement of the heat capacity shift. Furthermore, the main error in *b* is caused by the error in *a*. The conclusion of this analysis is that reducing the error in the determination of $\Delta cp_{L\text{-}L}$ reduces the error both in *a* and *b* to its largest extent.

Table 2. *Values of the absolute partial derivatives from Eq. 5 and 6 to calculate the absolute error in a. The values of aPS in DIDP from Table 1 are used.*

Partial derivative	**Value**	**Error**	**Total contribution to error**
$\left\|\frac{\partial a}{\partial \Delta cp_{L-L}}\right\|$	168	0.002 $J \cdot g^{-1} \cdot K^{-1}$	0.33
$\left\|\frac{\partial a}{\partial \phi_0}\right\|$	1.3	0.01 vol.-	0.01
Total error in a			0.34

Table 3. *Values of the absolute partial derivatives from Eq. 5 and 6 to calculate the absolute error in b. The values of aPS in DIDP from Table 1 are used.*

Partial derivative	Value	Error	Total contribution to error
$\left\|\frac{\partial b}{\partial a}\right\|$	318	0.34	108
$\left\|\frac{\partial b}{\partial T_{L-L}}\right\|$	0.48	1 K	0
$\left\|\frac{\partial b}{\partial \phi_0}\right\|$	172	0.01 vol.-	2
Total error in b			110

In fact to decrease this error, conditions must be identified where the partial derivative $\partial a / \partial \Delta cp^*_{L-L}$ is minimal. From Eq. 4, it can be concluded that the concentration is the only variable to optimize. Fig. 5 shows the derivative of a with respect to $\Delta cp^*_{L\text{-}L}$ as a function of $\phi_{0.}$ The derivative of a with respect to $\Delta cp^*_{L\text{-}L}$ only depends on M and ϕ_0:

$$\left(\frac{\partial a}{\partial \Delta cp^*_{L-L}}\right) = \frac{M\left[2\ln(1-\phi_0)\phi_0 - 2\ln(1-\phi_0) - 2\phi_0 + \phi_0^2\right]}{R\phi_0^2\left[\ln(1-\phi_0)\phi_0 - \ln(1-\phi_0) + \phi_0^2 - \phi_0\right]}. \qquad (7)$$

Hence, the shape of the curve of Fig. 4 is valid for all interaction parameters. The minimum is found at 55 vol.%, and it is therefore preferred to do the experiment at this concentration. But even at this optimal concentration, the error in a is very sensitive to the error in $\Delta cp_{L\text{-}L}$. To calculate the absolute error of the interaction parameter, the absolute error of the coefficients a and b have to be summed. By using errors in the measured data of aPS in DIDP listed in Table 1, the interaction parameter becomes $\chi = (-0.14 \pm 0.34) + (245 \pm 110)\cdot T^{-1}$.

In Fig. 5, an example will be given by plotting the binodals for extreme values of the interaction parameter. Combining a positive and negative deviation from either of the average values of a and b results in a reasonable data fit. However both positive or both negative deviations in a and b result in an unrealistic over or under estimation to such an extent that even $T_{L\text{-}L}$ is not in agreement with the predictions.

Therefore, these extreme interaction parameters will not be taken into account. The cloud points measured with the optical method fit very well with the binodal calculated for the interaction parameter: $\chi = -0.48+355T^{-1}$.

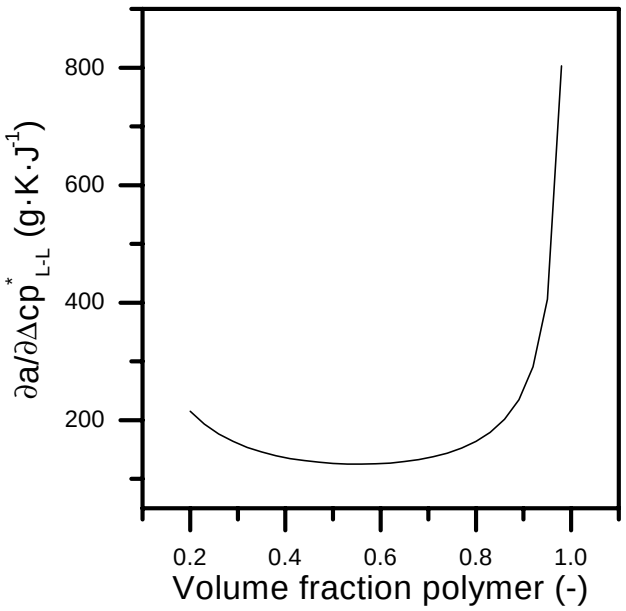

Figure 4. $\partial a / \partial \Delta cp^{*}_{L-L}$ *versus the volume fraction calculated for M = 446 g·mol*$^{-1}$.

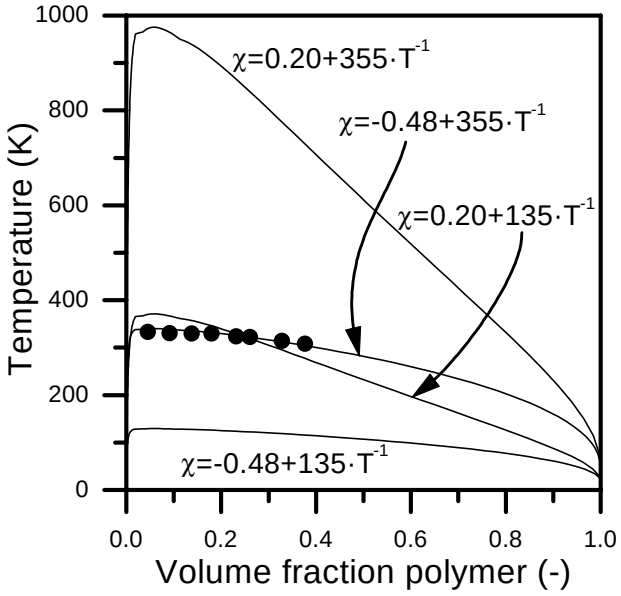

Figure 5. *Binodals of aPS inDIDP calculated from extreme values of the interaction parameter.*

6.4.3 Comparison of methods to determine the Berghmans point

The binodal will be determined as well as the Berghmans concentration with the help of the melting and crystallization behavior of the diluent. Only one TMDSC experiment was carried out for aPS with a poly-dispersity of 1.05 in 1-dodecanol. The results of that experiment and other input parameters are listed in Table 4. To determine the density of the solution, again a constant polymer density was assumed, the density of the diluent is estimated at $T_{L\text{-}L}$.

Table 4. *Input, measured and calculated parameters of aPS in 1-dodecanol. The poly-dispersity of aPS is 1.05.*

Variable	Property	aPS in 1-dodecanol
Input	ρ ($kg \cdot m^{-3}$)	739
	M ($g \cdot mol^{-1}$)	186
	ΔH_{dil} ($J \cdot g^{-1}$)	203.8
Measured	w_0 (-)	0.4±0.01
	$T_{L\text{-}L}$ (K)	422.3±1
	T_g (K)	335.6
	$\Delta cp_{L\text{-}L}$ ($J \cdot g^{-1} \cdot K^{-1}$)	0.0673±0.002
	ΔH_c ($J \cdot g^{-1}$)	98.8±2
	ΔH_m ($J \cdot g^{-1}$)	101.3±2
Calculated	ϕ_0 (-)	0.32
	a	-3.67
	b	1824
	w_B (-)	0.80

The enthalpy of melting of 1-dodecanol is 203.8 $J \cdot g^{-1}$ and obtained from Chapter 5. The Berghmans concentration extrapolated from the melting enthalpy of the diluent in the polymer matrix and the pure component is 80 wt.%, (= 76 vol.% when calculating the density of the diluent for $T = T_{L\text{-}L}$). Table 5 summarizes the resulting Berghmans points estimated by the three methods described in §6.3.

Table 5. *Result determination procedures of Berghmans point.*

Method	Description	ϕ_B (vol.%)	T_B (K)
1	T_g +Binodal	90	336
2	$\Delta H_m + T_g$	76	336
3	Binodal+ΔH_m	76	357

Figure 6 summarizes the results of the three prediction methods.

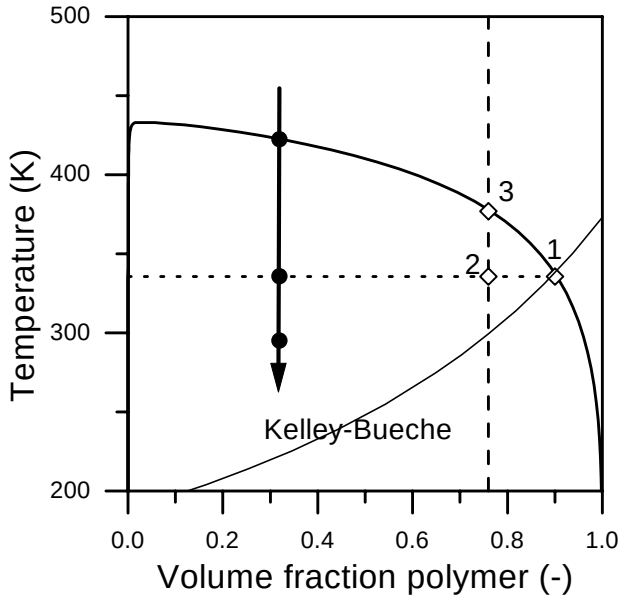

Figure 6. *Experimentally determined glass transition temperature, calculated binodal and calculated Berghmans concentration with the help of the melting enthalpy. Solid line: calculated binodal for N = 600. Dotted line: experimental glass temperature. Dashed line: calculated Berghmans concentration with melting enthalpy.*

The Kelley-Bueche prediction intersects with the measured glass transition temperature at a Berghmans point close the prediction of method 1. This is an indication that the predicted Berghmans point according the method 1 obtaines the best results. A difference in Berghmans temperature of about 20 K and a difference in Berghmans concentration of 14 vol.% between the three methods is significant. This difference is mainly caused by the error in the input parameters and the experimental results.

6.5 Conclusions

With one single TMDSC experiment in the concentrated region of a polymer solution, the binodal can be determined by using only liquid-liquid demixing data and the Flory-Huggins theory. The glass transition temperature and crystallization or melting data of the diluent can be used to calculate the Berghmans point. The accuracy of the measurements of the signals obtained from TMDSC is a critical step in the determination of the Berghmans point, in particular the error in the shift of the heat capacity at the liquid-liquid demixing temperature to the quality of the binodal prediction.

6.6 List of symbols

χ	Flory Huggins interaction parameter	-
$\varepsilon(...)$	Error in ...	
ϕ_0	Volume fraction polymer in solution	-
ϕ_2	Volume fraction of polymer in polymer-rich phase	-
ϕ_B	Volume fraction of polymer at Berghmans point	-
$\Delta cp^*_{L\text{-}L}$	Heat capacity shift at the liquid-liquid demixing temperature	$J \cdot g^{-1} \cdot K^{-1}$
Δcp_{bin}	Heat capacity shift at the binodal temperature	$J \cdot g^{-1} \cdot K^{-1}$
ΔH_c	Crystallization enthalpy of the diluent	$J \cdot g^{-1}$
ΔH_{dil}	Melting enthalpy pure diluent	$J \cdot mol^{-1}$
ΔH_m	Melting enthalpy of the diluent	$J \cdot g^{-1}$
a	Empirical parameter	-
b	Empirical parameter	K^{-1}
M	Molecular weight diluent	$g \cdot mol^{-1}$
T_{bin}	Binodal temperature	K
T_c	Crystallization temperature of the diluent	K
T_g	Glass transition temperature	K
$T_{L\text{-}L}$	Liquid-liquid demixing temperature	K
T_m	Melting temperature of the diluent	K

w_0	Weight fraction polymer in solution	-
w_B	Weight fraction of polymer at Berghmans point	-

6.7 References

1. Arnauts, J., and Berghmans, H., *Amorphous thermoreversible gels of atactic polystyrene*, Polymer Communications, 28, p. 66-68 (1987)
2. Chow, T.S., *Molecular Interpretation of the Glass Transition Temperature of Polymer-Diluent Systems*, Macromolecules, 13, p. 362-364 (1980)
3. Kelley, F.N., and Bueche, F., *Viscosity and glass transition temperature relations for polymer-diluent systems*, Journal of Polymer Science, 50, p. 549-556 (1961)
4. Daubert, T.E., Danner, R.P., Sibul, H.M., and Stebbins, C.C., *Physical and thermodynamic properties of pure chemicals. Data compilation*. , Pennsylvania: Taylor&Francis (1989)

Chapter 7

Evaluation and outlook

7.1 Introduction

In this chapter the most important conclusions of this thesis are evaluated. Furthermore, alternative experimental techniques to study the formation process of porous structures with the thermally induced phase separation method are presented.

7.2 DSC experiments

DSC experiments were used to follow the cooling trajectory of an initially homogeneous solution to a demixed and vitrified polymer-rich phase enclosing solidified diluent. This trajectory consists of three transitions: liquid-liquid demixing of the polymer solution, vitrification of the polymer-rich phase, and crystallization of the polymer-lean phase. These transitions will be evaluated separately in the next paragraphs.

7.2.1 Liquid-liquid demixing

At the liquid-liquid demixing temperature, a heat capacity shift is observed with TMDSC experiments, and a TMDSC curve only shows a small phase angle shift. The phase diagram of atactic polystyrene in 1-dodecanol can be determined with the help of experimental liquid-liquid temperatures determined with TMDSC. Furthermore, Chapter 4 shows that the heat capacity shift at the liquid-liquid demixing temperature can be predicted with the Flory-Huggins theory with the interaction parameter obtained from a fit through liquid-liquid demixing temperature data. This observation is used to predict the binodal with a single TMDSC

experiment in Chapter 6. However upon cooling deeper into the demixing gap, a growing deviation is observed between the theoretical and experimental heat capacity shift, and the heat capacity shift even disappears before reaching the glass transition temperature. From this observation it is concluded that upon cooling, equilibrium concentrations (according to the phase diagram) can not be reached anymore within a modulation period of 60 s. This is explained by the mass transfer process of diluent from the polymer-rich phase to the polymer-lean phase. With an increasing polymer concentration in the polymer-rich matrix, the mass transfer decreases because of the high viscosity of the polymer-rich phase and hence the mass transfer will be too slow to follow the temperature modulation. This results in a polymer-rich phase containing too much diluent in comparison with the equilibrium concentrations. This hypothesis on the supersaturated polymer-rich phase is proven by the observation of nanosized cells in the polymer-rich phase as discussed in Chapter 5. Only diluent in the polymer-lean phase is able to crystallize according to the phase diagram. The observed linear relation between the crystallization or melting enthalpy and the diluent concentration is valid for equilibrium concentrations of the polymer-rich and polymer-lean phase. The presence of cells in the polymer-rich phase has to be caused by diluent in the supersaturated polymer-rich phase.

From the TMDSC experiments carried out in this research, conclusions can be drawn with respect to the thermodynamics of a binary polymer solution because in a simple way the binary phase diagram can be composed. From the difference between the predicted heat capacity shift and the measured heat capacity shift, it can be concluded that the liquid-liquid demixing process is delayed and even stops at higher temperatures than expected. This observation gives information about the kinetics of liquid-liquid demixing. A more detailed study to the kinetics of liquid-liquid demixing is carried out in Chapter 2 in which the growth of demixed domains is studied. The growth rate exponent decreases when the temperature reaches the glass transition temperature. Together with isothermal quench data obtained from literature in which an increase in growth rate exponent is observed with increasing quench depth, a model between growth rate exponent and quench depth is proposed. At small quench depths close to the binodal and at quench depths close to the glass transition temperature, the growth rate exponent is smaller than in the intermediate region. This model obtained from isothermal quench experiments is compared with non-isothermal quench experiments and it can be concluded that other physical

processes influence the growth of the demixed domains besides the quench depth. Besides the increase of the growth exponent caused by the hydrodynamic flow regime, a growth rate limiting process is observed. According to Tanaka [1] the entanglements of polymers in the polymer-rich phase reduces the growth rate exponent in concentrated solutions.

Summarizing theoretical models describing liquid-liquid demixing in concentrated polymer solutions shows that models based on binodal or spinodal demixing results in comparable cell sizes. To have a better understanding in the liquid-liquid demixing process, it is more important to study the growth of the demixed domains than to discuss whether spinodal or binodal demixing takes place. As shown in Chapter 2, growth of demixed domains is a coupled function of a variety of physical phenomena. The stage between the initial formation of demixed domains either by binodal or spinodal demixing of a size smaller than 10 nm towards experimentally observed sizes of about 1 μm is still an area of investigation. Questions to be answered are:

- Is only diffusive mass transfer responsible for the growth between the initially formed demixed domains and the final observed cells?
- What is the influence of relaxation effects of the polymer chains during liquid-liquid demixing?
- What is the time scale of the demixed polymer solution to reach equilibrium concentrations, and what are the important parameters influencing this?

These questions can not be answered with the help of DSC experiments because of the small time scales involved in these processes. Computer simulations and models can be a useful tool to understand the liquid-liquid demixing process, but the attention should be focussed on the growth of the domains in the region between 10 nm and 1 μm.

7.2.2 Vitrification

The main emphasis in this work is related to liquid-liquid demixing because it is the main structure-determining step in the formation process of porous structures for amorphous polymers. Although the glass transition temperature and the region just above the glass transition temperature appears to have an influence on the growth rate exponent (Chapter 2), and the decreased heat capacity shift during liquid-liquid demixing (Chapter 4) as well. It should be of much interest to distinguish the

influence of vitrification and gelation of the polymer solution in more detail. In Chapter 4, it is observed that the heat capacity shift disappears at higher temperatures than the onset temperature of the glass transition of the investigated polymer-diluent system aPS in 1-dodecanol. The structure of the polymer-diluent system aPS in diisodecylphthalate (DIDP) is fixed by gelation. aPS in DIDP shows a gelation temperature of approximately T = 30°C (according to the falling bal method [4]) at polymer concentrations above 15 wt.%. The question arises whether the gelation mechanism, responsible for the fixation of aPS in DIDP, is valid for aPS in 1-dodecanol, just above the glass transition temperature. The TMDSC signal at the liquid-liquid demixing temperature of aPS in DIDP (see Fig. 4 in Chapter 3) is very small, so the experiment does not show whether the heat capacity shift disappears as result of gelation. Therefore, the question can not be answered from this study.

7.2.3 Crystallization and melting behavior of the diluent

In Chapter 5 the crystallization and melting behavior of the diluent shows a strong dependency on the polymer concentration of the polymer solution. It has not been possible so far to quantify this crystallization and melting behavior in detail. The only hard conclusion is that the DSC signals originate from diluent crystallizing in the polymer-lean cells. By understanding the relation between the crystallization or melting behavior, and the morphology of the polymer-diluent system, DSC can be a tool to obtain information about the morphology of a demixed polymer solution.

Another direction which can be studied is the influence of the polymer matrix on the crystallization behavior of a diluent. Chapter 5 gives a strong indication of the influence of the polymer-rich matrix on the crystallization behavior of the diluent. Confinement in a matrix may be a method to control the polymorph of a crystallizing diluent.

7.3 Alternative techniques

In this thesis, DSC is used to study liquid-liquid demixing and the structure fixation step of a polymer solution. By analyzing the observed signals in detail, it is possible to draw conclusions with respect to the formation process of porous structures. By using the same methodology with other, preferably well-established experimental

techniques, detailed information about the TIPS process can be obtained. Viscometry, rheology and acoustic time reflectometry experiments were carried out on the polymer-diluent system aPS-diisodecylphthalate (DIDP). In the following paragraphs the additional value of these techniques will be pointed out.

The reason to study the mentioned polymer-diluent system aPS-DIDP is the following. The high vapor pressure of diluents in relation to the liquid-liquid demixing temperature is often a problem studying liquid-liquid demixing experimentally. Special care has to be taken to prevent evaporation of the diluent during an experiment. The diluent DIDP shows a cloud point with the polymer of about 50°C and has a very low vapor pressure. (For comparison, the vapor pressure of water at T = 20°C is $2 \cdot 10^3$ Pa and the vapor pressure of DIDP at T = 100°C is 0.1 Pa [2].)

7.3.1Viscometry and rheology

The viscosity of the polymer diluent system aPS-DIDP was measured at a Brabender Viscotron, Mod. Nr 8024.

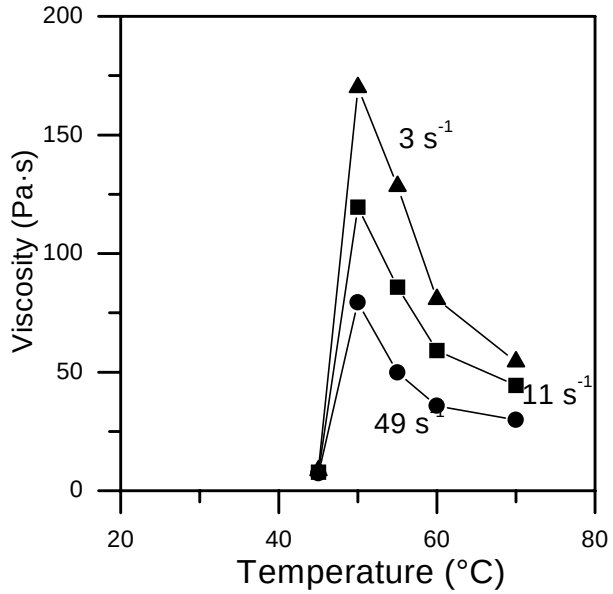

Figure 1. *Viscosity of a 30 wt.% solution of aPS in DIDP as a function of the temperature upon cooling for different shear rates (indicated in the figure).*

At a fixed temperature the viscosity was measured for different shear rates. Subsequently the temperature was lowered and the complete procedure was repeated. Results of this experiment are visualized in Fig. 1. The observation of an

increasing viscosity upon cooling as the temperature approaches the liquid-liquid demixing temperature is in agreement with the work of Wolf *et al.* [3]. In fact, the location of the sharp decrease in viscosity (between T = 45 and 50°C) is in good agreement with cloud point experiments of this polymer-diluent system described in Chapter 6 (Fig. 2, T = 49°C). The observation of the sudden decrease at lower temperatures inside the liquid-liquid demixing gap is not in agreement with the physical expectation. Upon cooling a polymer solution, the viscosity increases. At the liquid-liquid demixing temperature, a polymer-rich matrix is formed enclosing the polymer-lean phase. The viscosity is determined by the major phase of the system and is influenced by the dispersed phase to a lower extent. Therefore, it should be expected that upon liquid-liquid demixing the viscosity increases further. An explanation of the sharp decrease in viscosity can be the formation of a slip layer of DIDP between the rotating cone in the viscometer and the polymer. To apply less mechanical force on the polymer solution, an oscillating rheometer was used instead of the rotating viscometer.

Polymer solutions of aPS in DIDP were studied in a Bohlin Rheometer, CS50. Upon cooling with a cooling rate of 2 $K \cdot min^{-1}$ the complex viscosity was measured (at a constant frequency of 0.1 Hz) for different strains. As can be observed from Fig. 2, a sharp decrease in complex viscosity is observed at a large strain (0.1). The reason is probably the same as in the viscosity experiments. Diluent is pushed out of the demixed solution and forms a slip layer. Upon lowering the strain, an increase in the complex viscosity can be observed as expected. When using rheology or viscometry experiments to determine the liquid-liquid temperature, a lot of mechanical force should be applied on the polymer solution to observe a significant signal. However, this observation will destroy the structure of the polymer-diluent system. For studying the mechanical properties of the demixed solution, very small strains are recommended to minimize the influence of the experiment. It should be of much interest when rheological experiments can be carried out with a polymer solution at different frequencies to obtain information about the time scale of liquid-liquid demixing and the subsequent growth.

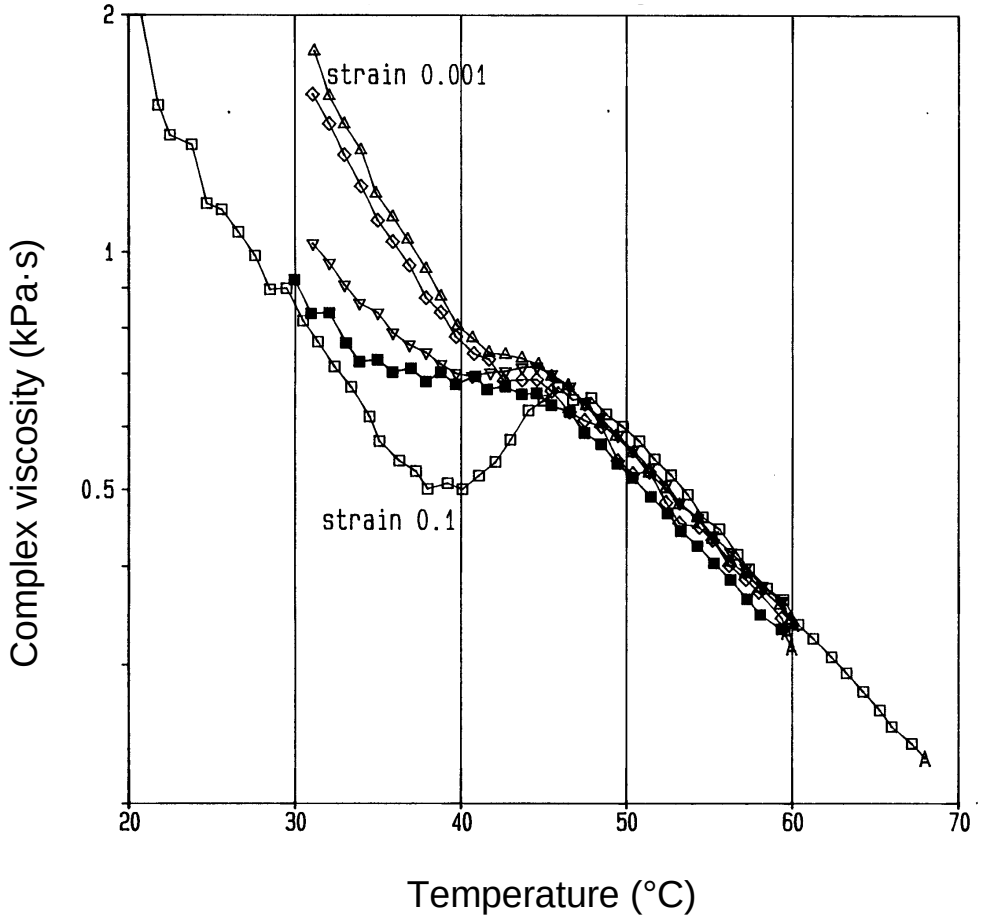

Figure 2. *Complex viscosity for a 30 wt.% solution of aPS in DIDP. The frequency is 0.1 Hz. The strain varies from 0.1 to 0.001 in steps in order of magnitudes. The cooling rate is 2 K·min^{-1}.*

Furthermore, rheological experiments can be very suitable to study the mechanical behavior of the polymer-diluent system at a temperature in the region of the glass transition. Maybe an answer can be found on the question whether gelation or vitrification is responsible for the fixation of the structure of aPS in 1-dodecanol (see §7.2.2)

7.3.2 Ultrasonic Time Domain Reflectometry (UTDR)

A different method to study the mechanical properties of a demixing polymer-diluent system is UTDR. The propagation of a sound wave through a material depends on the mechanical properties of the material. An interface between two phases causes partial reflection of a sound wave. During heating a liquid-liquid demixed solution from only one side, an interface is formed between the homogeneous and the

demixed solution. Furthermore it is possible that the acoustic velocity changes during liquid-liquid demixing. Upon quantifying acoustic reflection or transmission patterns, information about the mechanical properties of both the homogeneous and demixed phase can be obtained as well as information about the interface. An initial experiment was carried out in which a liquid-liquid demixed aPS in DIDP solution at room temperature is heated from one side, and the acoustic reflection pattern was recorded during time.

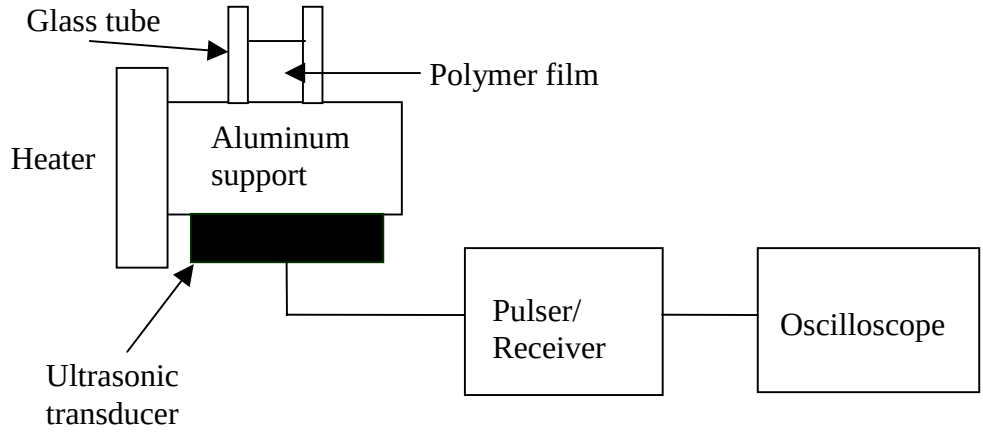

Figure 3: *Schematic set-up UTDR.*

The schematic setup is plotted in Fig. 3. The pulser / receiver (Panametrics, Ultrasonic Pulser / Receiver Model 5072 PR) sends a signal of 500 Hz to the transducer (Panametrics) which generates an ultrasonic wave toward the aluminum support. Reflections of the ultrasonic wave are recorded by the transducer and amplified by the pulser / receiver to a digital oscilloscope (LeCroy, 1GHz Digital Oscilloscope, LC534 AM). The height of the polymer solution enclosed by the glass tube was 2.0 cm, the diameter of the glass tube was about 3 cm. During heating of the demixed polymer solution, a demixing front is formed between the homogeneous and demixed solution. A reflection peak is indeed observed in the acoustic reflection signal, which agrees with the visually observed demixing front. The temperature at the interface between the demixed and homogeneous solution is by definition the liquid-liquid demixing temperature, and by calculating a heat profile over the polymer solution, heat transfer properties of the polymer solution can be studied in time. Furthermore by quantifying the obtained reflection patterns and by comparing these results to existing acoustic models related to emulsions, information can be obtained about the morphology of the demixed solution. Unfortunately this

experimental technique is not very useful to study liquid-liquid process at very small length scales because the resolution of the experiments is in the order of microns [5].

7.4 Acknowledgements

M. van Egmond, University of Twente is acknowledge for carrying out the viscosity, the UTDR experiments, and for the discussions. B. Reuvers, Akzo Nobel in Arnhem, is acknowledged for carrying out the rheological experiments and for the discussions as well.

7.5 References

1. Tanaka, H., *Critical dynamics and phase-separation kinetics in dynamically asymmetric binary fluids: New dynamic universally class for polymer mixtures or dynamic crossover?*, Journal of Chemical Physics, 100, p. 5323-5337 (1994)
2. Daubert, T.E., Danner, R.P., Sibul, H.M., and Stebbins, C.C., *Physical and thermodynamic properties of pure chemicals. Data compilation*. Pennsylvania: Taylor&Francis (1989)
3. Wolf, B.A., and Sezen, M.C., *Viscometric determination of thermodynamic demixing data for polymer solutions*, Macromolecules, 10, p. 1010-1014 (1977)
4. Brandrup, J., and Immergut, E.H., *Polymer Handbook*. 3th. ed, New York: John Wiley & sons (1989)
5. Kools, W.F.C., Konagurthu, S., Greenberg, A.R., Bond, L.J., Krantz, W.B., Boomgaard, T.v.d., and Strathmann, H., *Use of ultrasonic time-domain reflectometry for real-time measurement of thickness changes during evaporative casting of polymeric films*, Journal of applied polymer science, 69, p. 2013-2019 (1998)

Summary

Porous polymer structures can be prepared with thermally induced phase separation (TIPS). The polymer is dissolved at elevated temperature and upon cooling the homogeneous solution demixes in a polymer-rich phase and a polymer-lean phase. Afterwards, the structure of the obtained demixed polymer solution is fixed by crystallization, vitrification, or gelation. In this thesis, differential scanning calorimetry (DSC) is used to study the transitions in the cooling trajectory of a polymer-diluent system, which are: liquid-liquid demixing, vitrification of a polymer-diluent system, and crystallization of diluent.

Chapter 2 summarizes models and experimental data with respect to liquid-liquid demixing to describe the formation and growth of demixed domains. A homogeneous polymer solution is quenched to a constant temperature in the liquid-liquid demixing gap, and the domain growth is recorded during time. It can be concluded that a large difference exists in time and length scales between models and simulations which describe the formation of demixed domains (~10^{-5} s) and experimental data describing the growth of these domains (> 1 s). Furthermore the frequently proposed growth rate exponent of 1/3 is only valid in a limited region of quench depths.

In Chapter 3, temperature modulated differential scanning calorimetry (TMDSC) results are presented for the polymer – diluent system atactic polystyrene in 1-dodecanol. With TMDSC, a temperature modulation (sine wave) is superimposed on the linear cooling trajectory, and from the resulting heat flow the heat capacity (independent on cooling rate) can be calculated directly. The conclusion of this chapter is that liquid-liquid demixing, vitrification, and crystallization of diluent can be observed with TMDSC with a modulation period of 60 s.

The obtained TMDSC signals for liquid-liquid demixing are quantified in Chapter 4 with the help of the Flory-Huggins theory (F-H). The observed heat capacity shift at the liquid-liquid demixing temperature can be predicted with the help of the F-H theory with an interaction parameter obtained from liquid-liquid demixing temperatures. The contribution of liquid-liquid demixing in the TMDSC curve disappears at a higher temperature than the onset of the glass transition

temperature. Therefore, the hypothesis is proposed that during liquid-liquid demixing deep in the demixing gap, equilibrium concentrations (according to the phase diagram) are not reached anymore and that a supersaturated polymer-rich phase is present.

In Chapter 5 the crystallization and melting behavior of the diluent is examined. Crystallization curves differ significantly from melting curves and they strongly depend on the polymer concentration. The concepts of thermoporometry and polymorphism have been studied, however no satisfactory explanations for the observed results have been obtained. The enthalpy of crystallization and melting is quantified and related to the diluent present in the polymer-lean phase. Small cells observed in the polymer-rich phase with scanning calorimetry are caused by diluent present in the supersaturated polymer-rich phase. This is a proof of the hypothesis proposed in Chapter 4 in which it was stated that the polymer-rich phase is supersaturated.

In Chapter 6 an application of the insights obtained from Chapter 3 to 5 are used to predict a phase diagram containing a binodal and the glass temperature with the help of one single TMDSC experiment. It appears that the measurement of the heat capacity shift is a very critical step in this procedure to determine the binodal.

Chapter 7 summarizes the physical phenomena one could learn from this thesis. Furthermore, alternative experimental techniques are proposed to study the formation of porous structures with the TIPS method.

Samenvatting

Poreuze polymeerstructuren kunnen worden gemaakt door middel van thermisch geïnduceerde fasenscheiding (TIPS). Het polymeer wordt opgelost en tijdens het koelen ontmengt de homogene oplossing in een polymeer-rijke fase en een polymeer-arme fase. Daarna wordt de structuur vastgelegd door kristallisatie, vitrificatie of gelering. In dit proefschrift is differential scanning calorimetry (DSC) gebruikt om de overgangen te bestuderen die plaatsvinden tijdens het koeltraject van een systeem bestaande uit polymeer en een verdunningsmiddel. Deze overgangen zijn vloeistof-vloeistof ontmenging van de oplossing, het vitrificeren van de polymeer-rijke fase en kristallisatie van de polymeer-arme fase.

In hoofstuk 2 zijn modellen samengevat die de formatie en groei van ontmengde gebieden beschrijven tijdens vloeistof-vloeistof ontmenging. Een homogene polymeeroplossing is gequenchd tot een constante temperatuur in het vloeistof-vloeistof ontmenggebied en de groei van ontmengde gebiedjes is gevolgd in de tijd. Het blijkt dat er een groot verschil zit in lengte- en tijdschalen tussen simulaties en modellen die de formatie van ontmengde gebieden beschrijven (~10^{-5} s) en de resultaten van groeiexperimenten (>1 s). Bovendien is de veel gebruikte groeiexponent van 1/3 alleen geldig voor een beperkte quenchdiepte.

In hoofdstuk 3 zijn de experimentele resultaten gepresenteerd die verkregen zijn met temperature modulated differential scanning calorimetry (TMDSC) met het polymeer-verdunningsmiddel systeem atactisch polystyreen in 1-dodecanol. Met TMDSC wordt een temperatuur modulatie (in de vorm van een sinusgolf) opgelegd over het koeltraject. Met behulp van de gemeten warmtestroom kan direct de warmtecapaciteit bepaald worden, die onafhankelijk is van de gebruikte koelsnelheid. De conclusie van deze experimenten is dat zowel vloeistof-vloeistof fasenscheiding, vitrificatie en kristallisatie van het verdunningsmiddel geobserveerd kunnen worden met TMDSC met een temperatuurmodulatie van 60 s.

De verkregen TMDSC resultaten met betrekking tot vloeistof-vloeistof ontmenging zijn gekwantificeerd in hoofdstuk 4 met behulp van de Flory-Huggins theorie. Het blijkt dat de warmtecapaciteitssprong op de vloeistof-vloeistof ontmengtemperatuur voorspeld kan worden met behulp van de interactieparameter die verkregen is uit een fit door vloeistof-vloeistof ontmengtemperaturen. Verder is

de hypothese voorgesteld dat tijdens vloeistof-vloeistof ontmenging diep in het ontmenggebied evenwichtsconcentraties niet meer bereikt kunnen worden en dat de polymeer-rijke fase oververzadigd is met verdunningsmiddel.

In hoofdstuk 5 is het kristallisatie- en smeltgedrag van het verdunningsmiddel onderzocht. Het kristallisatiegedrag verschilt van het smeltgedrag en is sterk afhankelijk van de polymeerconcentratie. De concepten van thermoporometry en polymorfisme zijn gebruikt om een verklaring te vinden voor de gevonden experimentele resultaten, maar tot dusver is die nog niet gevonden. De smelt- en kristallisatie-enthalpy is gekwantificeerd en gerelateerd aan de hoeveelheid verdunningsmiddel aanwezig in de polymeer-arme fase. Verder zijn er kleine cellen geobserveerd met Scanning Electron Microscopy die veroorzaakt zijn door verdunningsmiddel in de oververzadigde polymeer-rijke fase. Dit is een bewijs voor de hypothese voorgesteld in hoofdstuk 4.

In hoofdstuk 6 zijn de inzichten die verkregen zijn in hoofstuk 3 t/m 5 gebundeld en het blijkt mogelijk te zijn om het fasendiagram, bestaande uit de binodaal en de glasovergang, te bepalen met de hulp van één TMDSC experiment. Het blijkt dat het meten van de warmtecapaciteitssprong de cruciale stap is in de procedure om de binodaal te bepalen.

Hoofdstuk 7 vat de observaties samen die gevonden zijn in dit werk. Verder zijn er alternatieve experimentele technieken voorgesteld voor vervolgonderzoek.

Dankwoord

Als u dit proefschrift in de juiste volgorde hebt gelezen bent u nu bijna aan het eind en kunt u zien wie er allemaal een bijdrage hebben geleverd aan de tot standkoming hiervan. Uiteraard zijn dat veel meer mensen dan ik nu op ga noemen. Dus wil ik iedereen alvast bedanken die op één of andere manier een steentje bijgedragen heeft aan dit proefschrift. Allereerst moet ik natuurlijk de persoon bedanken die het mogelijk gemaakt heeft dat ik aan deze opdracht kon beginnen: prof. Heiner Strathmann. Na ongeveer twee jaar nam prof. Matthias Wessling zijn taak over en ik moet toegeven dat ik erg moest wennen aan jouw ideeën over ‘het verkopen’ van wetenschappelijk onderzoek, maar ik heb er veel van geleerd. Prof. Marcel Mulder was gedurende de gehele periode mijn dagelijkse begeleider. Ondanks je zeer volle agenda was er regelmatig de mogelijkheid om te discusseren over veel verschillende zaken.

In het begin van mijn promotieperiode heb ik veel geleerd over de formatie van poreuze structuren met het TIPS proces tijdens mijn bezoeken aan de polymeer exploratiegroep van dr. Elwin Schomaker bij Akzo Nobel in Arnhem. Later heb ik gebruik mogen maken van de TMDSC apparatuur die daar beschikbaar was. De aandacht voor de voortgang van mijn promotie en de steun als ik weer eens wat te vragen had van onder andere Johan, Laurens, Leo, Nel en Ruurd heb ik als zeer aangenaam ervaren.

I had the honor to visit the membrane group of prof. Li Shuguang of the Dalian Institute of Chemical Physics in China. Wang Lianjun. Li Wei, Li Xiang, Luan Ming Zhang, Cao Chun, all basketball, soccer, badminton, chess, and (table)tennis opponents: thanks for the great time.

Het is ondoenlijk om iedereen te bedanken die een bijdrage heeft geleverd aan dit proefschrift van de membraantechnologiegroep en andere groepen op de faculteit chemische technologie, maar ik moet bekennen dat onder meer door jullie toedoen het een onvergetelijke tijd is geweest. Willem, onder meer door jouw inspirerende begeleiding tijdens mijn afstudeerperiode wilde ik doorgaan met het doen van onderzoek. De koffiepauzes met mijn kabelvriendinnen en anti-kabelvrienden, de borrels en de groepsuitjes waren altijd erg leuk. Herman en Clemens worden bedankt voor hun steun aan het DSC werk, Erik en Lydia voor de goede zorgen in labzaal

2308, John voor de technische ondersteuning en Greet voor de papieren ondersteuning. Mijn kamergenoten, Ryo, Claudia, Nela voor een kortere tijd en Tao voor de gehele periode worden bedankt voor het dulden van mij in jullie buurt. Verder was het uitgenodigd worden voor het voetballen met het MT-team (Marcel, GH, Alberto, John) in de vakgroepcompetitie altijd weer een eer. Maarten en Thomas worden bedankt voor het geleverde werk tijdens hun respectivelijke afstudeer- en stageperiode. Verder waren de de Geus bezoekjes met de meer of minder regelmatige bezoekers (Antoine, Jonathan, Marcel (2x), Warner e.v.a) erg onderhoudend.

Jonathan, Bastiaan, Sybrand, Tao, Nela en Natasja worden bedankt voor het doorlezen en corrigeren van mijn thesis. Dr. van de Berg wordt eveneens bedankt voor de suggesties en de correcties die hij gaf tijdens het doorlezen van mijn manuscript. Verder stel ik het zeer op prijs dat Bastiaan en Tao mij ter zijde willen staan tijdens mijn verdediging.

Mijn huisgenoten van de afgelopen vier jaar, Corné, Paul, Tom, Otto Ger en Hans wil ik bedanken voor het gezelschap en de lekkere maaltijden die zo nu en dan op tafel kwamen. Een gezonde geest in een gezond lichaam is een uitdrukking waar ik geheel achter sta, daarom wil ik mijn teamgenoten van frisbeevereniging DDT bedanken voor de mogelijkheid om elke week weer lui zweet kwijt te raken (en het daarna net zo hard weer aan te aanvullen tijdens het evalueren).

Natasja, het afgelopen jaar met jou was geweldig!

Pa, Ma Carolien (Jan) en Henk, het is een heel fijne gedachte om te weten dat er altijd mensen zijn waar je onvoorwaardelijk op terug kan vallen.

Levensloop

Op 16 augustus 1973 ben ik geboren in Hooglanderveen. In 1991 behaalde ik mijn VWO diploma aan `t Hooghe Landt College in Amersfoort. Datzelfde jaar begon ik aan de studie Chemische Technologie aan de Universiteit Twente. Tijdens mijn studie liep ik in 1995 stage bij Dow Benelux in Terneuzen waar ik werkte aan het bepalen van de verblijftijdspreiding in het polymerisatieproces van styreen polymeren op produktie- en miniplantschaal. Mijn afstudeerwerk heb ik uitgevoerd in de membraantechnologiegroep onder leiding van prof. Strathmann, waarin ik het droogproces heb bestudeerd van polymeeroplossingen bestaande uit meerdere componenten. Na het behalen van het doctoraal diploma Chemische Technologie in juni 1997, ben ik in dezelfde vakgroep begonnen aan de promotieopdracht die beschreven staat in dit proefschrift.

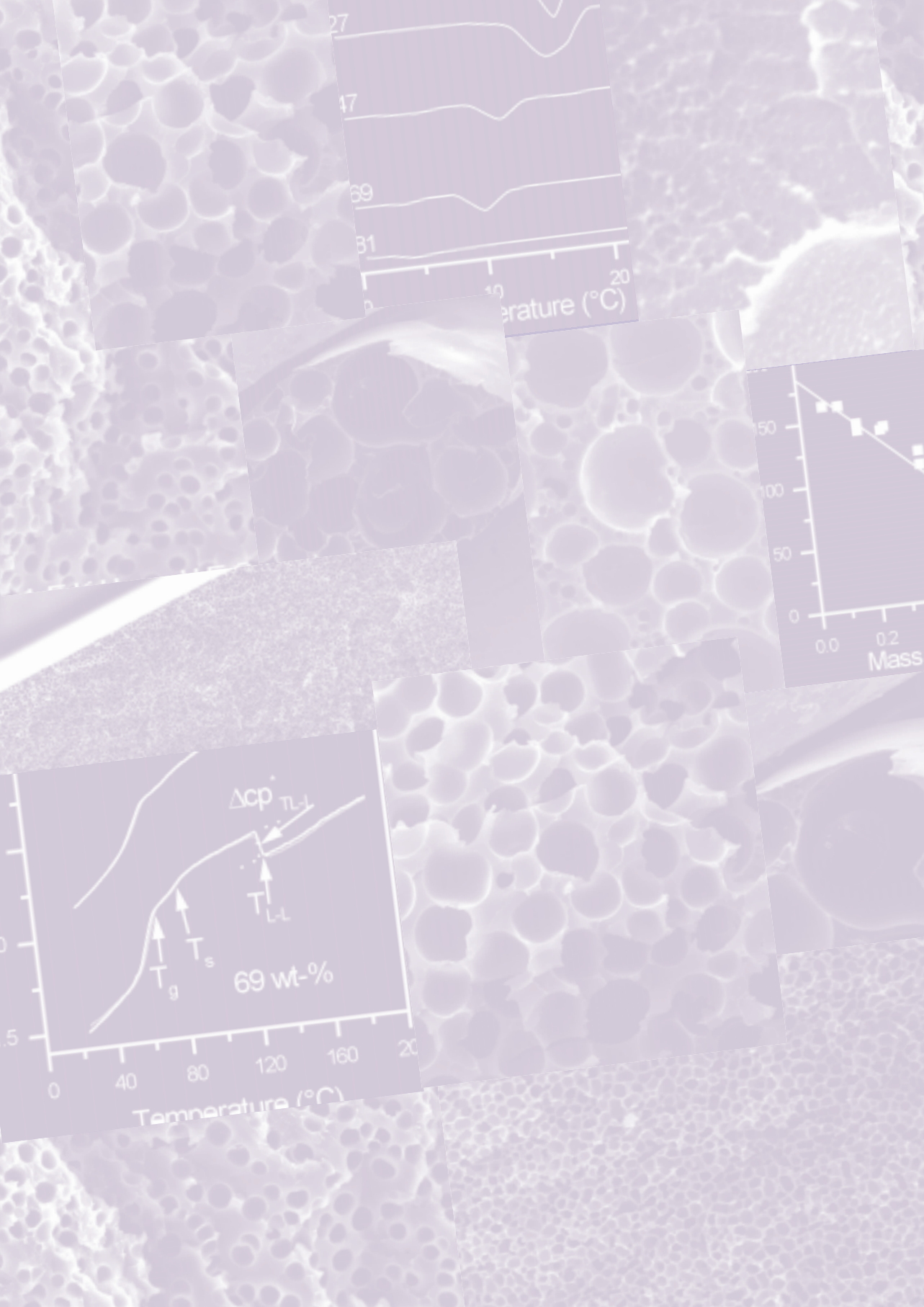
erature (°C)
Mass
Δcp
T
L-L
T
s
T
g
69 wt-%
0
40
80
120
160
Temperature (°C)